Ultrafast spin dynamics

a theoretical investigation of laser induced ultrafast spin dynamics in thin-film magnetic systems

de Mare, Koen A.

Award date:
2021

Eindhoven University of Technology
Department of Applied Physics
Physics of Nanostructures

Master Thesis

Ultrafast spin dynamics

A theoretical investigation of laser induced ultrafast spin dynamics in thin-film magnetic systems

K.A. de Mare
0955739

supervised by

Prof. dr. B. Koopmans
MSc. M. Beens

Eindhoven, March 17, 2021

Abstract

Magnetic state has been the basis for various, increasingly performant digital storage devices, supporting the stunning rise of the computer in recent history. The field of Spintronics studies how the electronic spin corresponding to magnetic state can be used and manipulated, improving our ability to exploit magnetism in future devices.

Recent experiments have shown that laser-induced ultrafast demagnetisation of thin-film ferromagnets can cause a spin transport between magnetic layers. The mechanism producing this spin current is not well understood, potentially preventing this effect from being applied in useful ways. One proposed explanation of the spin transfer is optical excitation creating "hot" electrons with ballistic trajectories, moving their spin angular momentum. A second hypothesis is the ultrafast demagnetisation causing a local spin accumulation that would drive a diffusive spin current.

In this thesis a model for ultrafast spin dynamics is proposed that includes both of these effects. This allows the behaviour of the two processes to be compared, potentially giving insight into their relative importance to the experimental observations. Approximations of this model are proposed to significantly simplify it, making it substantially simpler to interpret and apply. Applying this to models of experiments gives closed-form expressions of possible behaviour, this in contrast to the numerical approach used in other studies. These results are compared to the experimental results that motivated this study. The hot electron mechanism explaining the observed spin transfer seems to be unlikely, while the diffusion of a demagnetisation-driven spin accumulation might be consistent with the experimental observations.

Contents

Chapter 1

Introduction

This chapter will introduce the context of magnetism and spintronics. More specifically, ultrafast demagnetisation and femtomagnetism will be presented. This will lead into the current state of the field, and the study presented in this thesis attempted to advance this. Section 1.3 will lay out the structure of this thesis.

1.1 Context

1.1.1 Magnetism and spintronics

Magnetism is a fascinating and useful effect. An extremely valuable application of magnetism was found in digital data storage. In particular digital storage that does not need electricity to retain its information. Various types of digital storage rely on magnetism. Early computers made use of magnetic tape or magnetic core memory. Later advancements brought the hard disk drive and various improvements of this technology, which are still widely used today. These technologies have been some of the more important developments facilitating the stunning improvements of computers. The three types of magnetic digital data storage devices listed above rely on magnetic fields to read and write the magnetic state. The use of magnetic fields does however have some drawbacks regarding energy use and size.

The field of spintronics studies transport of electron spin. As magnetism is a consequence of the ordering of spin in a material, spin transport is closely tied to magnetisation. In particular, we can change the magnetic state of a material by pumping electron spin into the material using a so-called "spin current". These spin currents are simply moving electrons, but instead of looking at the charge they transport, we are interested in the electron spin carried and transported by these electrons. Spin transport and spin currents are the basis of various technologies and devices being developed by the spintronics field. Some of these devices show promise of being able to improve future computers, both by improved memory devices and other components[1, 2].

1.1.2 Magnetoresistance and the Valet-Fert model

Magnetism relates to the state of electrons in materials, while electric currents correspond to a movement of electrons. This makes it sensible that there is a fairly direct connection between the two. Various effects connecting magnetism with electric resistance have been discovered[3].

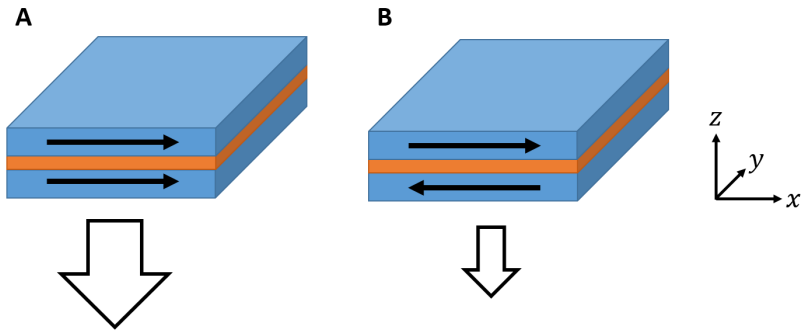

Figure 1.1: A cartoon of the giant magnetoresistance effect. A multilayer consisting of two magnetic layers (blue) and a conductive spacer (orange) has an out-of-plane voltage applied to it. Current flowing through the multilayer (drawn as the vertical arrow) changes substantially by the magnetisations of the magnetic layers being aligned in parallel or antiparallel. Subfigure (A) shows the parallel, low resistivity configuration, while (B) shows the antiparallel configuration which has relatively large resistivity.

In the late 1980s, the electric resistance in samples consisting of alternating layers of nonmagnetic metals and ferromagnetic metals was studied. It was found that the electrical conductivity is substantially smaller if the magnetisations of the ferromagnetic layers are parallel, compared to the case when the layers are antiparallel[4, 5]. Figure 1.1 shows these two configurations; subfigure A has the magnetisations parallel to give a relatively large charge current, while subfigure B has the magnetisation of the lower layer reversed to substantially decrease the charge current flowing through the multilayer. In fact, the change in resistance was substantially larger than previously observed magnetoresistance effects, so this effect was named giant magnetoresistance. It found application in magnetic field sensors such as the read head of hard disk drives, and in 2007 the Nobel prize in physics would be awarded to Albert Fert and Peter Grünberg for their discovery of the giant magnetoresistance effect.

It only took a few years for a satisfying explanation of this behaviour to be found[6]. In the Valet-Fert model, the conducting electrons are modeled as being either spin up or spin down with respect to the magnetisation of one of the ferromagnetic layers, though electrons can occasionally flip their spin to the opposite state. In a ferromagnetic layer, the conductivity related of spin up electrons can differ from the conductivity of spin down electrons. This imbalance in conductivity causes the electron current driven through the magnetic layers to have imbalanced spin; the currents are spin polarised. If the magnetisations of the two ferromagnetic layers are the same, the electron current leaving the first magnetic layer is equally spin polarised as the current entering the second magnetic layer. However if the magnetisations are opposite, most of the electrons leaving the first layer have the wrong spin to efficiently flow through the second layer, causing the electric resistance to be larger than in the aligned case.

1.1.3 Ultrafast demagnetisation

In 1996 the discovery was made that illuminating a thin-film ferromagnet by a femtosecond laser-pulse can lower the magnetisation substantially within picosecond time scales[7], as shown in Figure 1.2. The horizontal axis of the figure is the time interval between the laser pulse that excites the thin-film ferromagnet and the moment the magnetisation is probed. The vertical axis represents the magnetisation of the magnetic layer, measured using the magneto-optical Kerr effect (MOKE). The magnetisation is observed to decrease by as much as 40 % within a picosecond after optical excitation, with a small remagnetisation in the following picoseconds. The effect was dubbed as "ultrafast demagnetisation". Its discovery spawned a subfield of spintronics called femtomagnetism, where laser pulses are used to manipulate magnetic state at extremely short time scales.

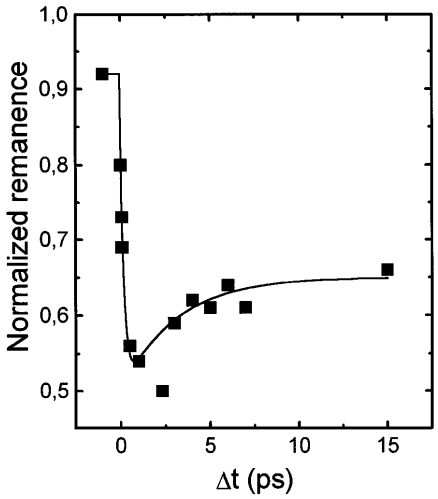

Figure 1.2: Ultrafast demagnetisation in thin film Ni samples. On the vertical axis the magneto optic Kerr effect signal measuring the magnetisation of the sample, with 1 corresponding to the room temperature equilibrium magnetisation and 0 to not being magnetised. The time interval between laser excitation and moment of probing on the horizontal axis, where $t = 0$ is the moment of laser excitation. The magnetisation is reduced by 40 % within a ps. Adapted from [7], Figure 2.

The observation of ultrafast demagnetisation spawned experimental and theoretical efforts to investigate the underlying physical process. In particular, the quenched magnetisation corresponds to a decrease in electron spin, which has associated angular momentum. The angular momentum corresponding to the magnetisation being dissipated on timescales of some 100 fs would require a particularly strong angular momentum dissipation channel. The paper that demonstrated ultrafast demagnetisation claimed that this angular momentum is dissipated locally [7].

1.1.4 Non-local spin dissipation

About ten years later a similar experiment[8] was performed, but like in the samples of giant magnetoresistance the sample consisted of two separate magnetic layers which could be aligned either parallel or anti-parallel relative to each other. The ultrafast demagnetisation of these samples was measured in both the parallel and anti-parallel configurations, and with versions of the sample where the layer between the magnetic layers is either electrically conducting or isolating. These four types of samples are shown in Figure 1.3.

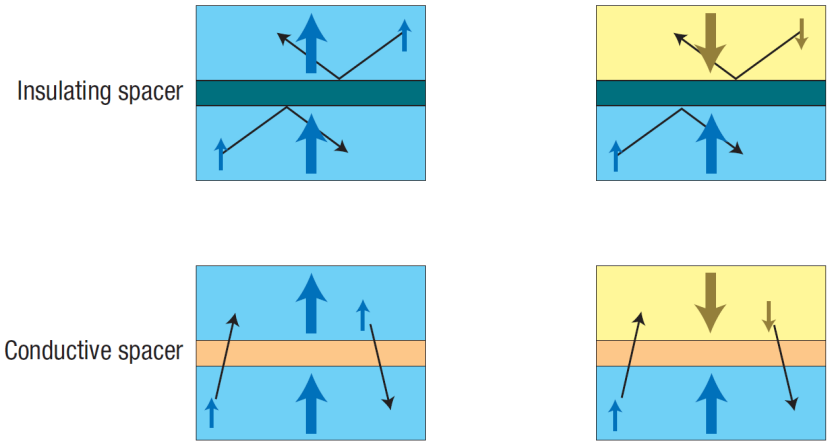

Figure 1.3: Sketch of the various samples studied in [8]. The samples consist of two ferromagnetic layers, which are either aligned (left) or anti-aligned (right). The spacer layer between the magnetic is either insulating (lower) or conducting (upper). Only when the spacer layer is conducting and the magnetisations are anti-aligned (lower right subfigure) can transport of spin contribute to the demagnetisation of the magnetic layers. Adapted from [8].

It was observed that if the spacer layer between the ferromagnetic layers is a conductor, the anti-parallel magnetic configuration shows a stronger peak demagnetization than the parallel configuration. The interpretation of this effect is that the conducting spacer allows electrons to be transported between the magnetic layers. The laser excitation causing demagnetisation would also cause electrons to move between the layers. This movement would slightly mix the spin angular momentum between the layers. If the magnetic layers have opposite magnetisation this mixing decreases the magnetisation of both layers, causing the stronger peak magnetisation. Figure 1.3 sketches how spin transport would only contribute to demagnetisation in multilayers with a conducting spacer layer and the magnetisations being anti-aligned. This showed that non-local effects may play a role in ultrafast demagnetisation, and suggests that ultrafast demagnetisation is able to cause a flow of electron spin; a spin current.

This observation inspired researchers to develop models of ultrafast demagnetisation where spin angular momentum is not locally dissipated at all[9]. Instead, electron movement would transport the spin corresponding to the magnetisation out of the magnetic film into an adjacent nonmagnetic layer, causing the measured loss of magnetisation. The basic idea is that the laser pulse optically excites electrons from the Fermi sea to states far above the Fermi level. These states are called "hot", as their energy is much more than the thermal energy above the Fermi level. Electrons in hot

states would have a large velocity, and move through the material on ballistic trajectories. They will occasionally scatter with electrons in the Fermi sea, transferring some energy such that both of these electrons are now in hot states. This would result in a cascade of many electrons transitioning from the Fermi sea to hot states, to start moving on ballistic trajectories. Such a cascade of hot electrons is shown in Figure 1.4. During this process the electrons would maintain their spin, such that the ballistic movement of hot electrons can transport electron spin. If the lifetime of hot electrons strongly depends on their spin, the hot electron current leaving the magnetic layer could even become quite spin polarised.

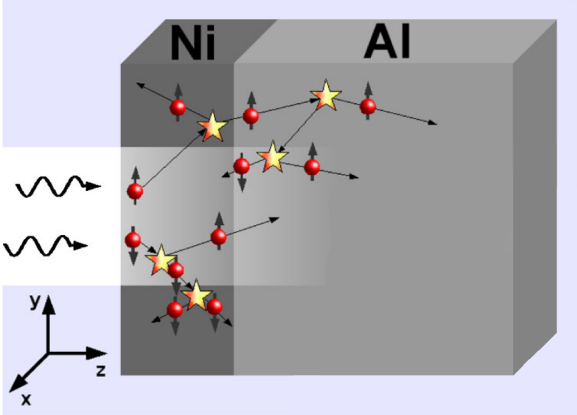

Figure 1.4: The hot electron cascade of the superdiffusive model of demagnetisation. A laser pulse incident on the nickel ferromagnetic layer excites electrons to "hot" states, which are the drawn electrons. These electrons take ballistic trajectories through the multilayer and will occasionaly scatter with other electrons, exciting them to hot states. Electrons conserve their spin during excitation, transport and scattering. The lifetime of hot electrons does depend on their spin. In the nickel layer, spin up electrons to have a longer lifetimes than spin down electrons. This causes most electrons leaving the nickel layer to be spin up, such that hot electrons cause a nett spin transfer. Adapted from [9].

This process of a hot electron cascade being created, and the difference in hot electron lifetimes causing a spin polarised hot electron current is shown in Figure 1.4. If hot electron movement transports enough spin out of the magnetic layer this process would cause a demagnetisation of the magnetic layer. As a side effect, the non-magnetic layer adjacent to the magnetic layer would have spin injected into it. Such a spin accumulation was observed in experiment shortly afterwards[10]. This demagnetisation model is named the "superdiffusive" model, in reference to the hot electrons being modelled to travel ballistic trajectories between scattering events. This would cause the hot electrons spread out more quickly than diffusive models would predict.

1.1.5 Spin-transfer torques

Moreover, this laser-induced spin current was successfully used to manipulate the magnetisation of a second magnetic layer[11, 12]. In these experiments, the angular momentum carried by the optically induced spin current is absorbed in a different magnetic layer, changing the magnetisation direction of the second layer. The relaxed state of the multilayer is as sketched in Figure 1.5 A. The samples used in these experiments are thin-film stacks consisting of two magnetic layers (drawn in blue and red) separated by a conducting spacer layer. One of the magnetic layers is oriented out of plane (by perpendicular magnetic anisotropy), drawn as the blue layer in the figure. The other layer, drawn in red, has in-plane magnetisation due to the shape anisotropy of thin layers. An in-plane magnetic field is applied to which the magnetisation orients itself. The optical excitation of this sample is sketched in Figure 1.5 B, it causes the magnetic layers demagnetise (not drawn) and exchange spin with each other. The magnetic layers absorbing spin of a different orientation than the magnetisation direction of the layer will cause the magnetisation direction to slightly change. This change of magnetic orientation due to absorbed spin is called a spin-transfer torque, its effect on the magnetisation direction of the layers in the discussed experiment is shown in Figure 1.5 C.

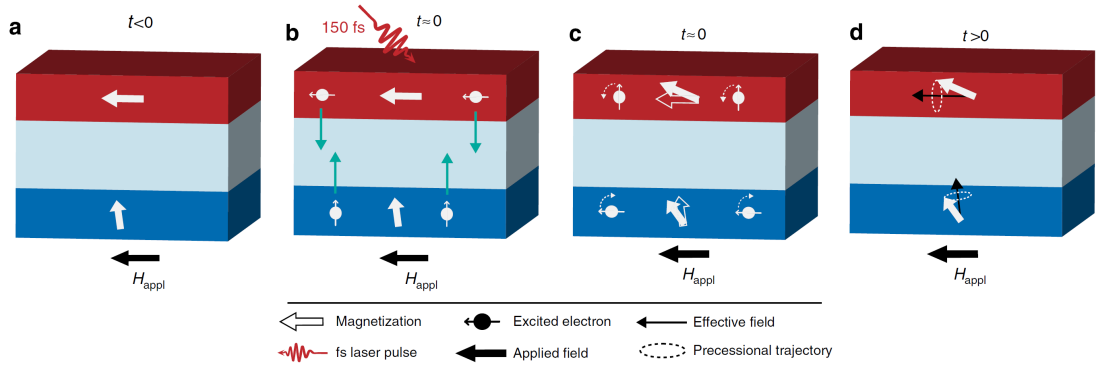

Figure 1.5: The structure of the sample used in spin-transfer torque experiment of [11]. The multilayers consist of two thin-film magnets, one with out-of-plane magnetisation, and another one with in-plane magnetisation, biased by an external magnetic field. (A) is the system at rest. On laser excitation, shown in (B), spin currents transfer angular momentum between the layers; a spin-transfer torque. This effect affects the magnetisation direction of both magnetic layers as shown in (C). The mechanisms pulling the magnetisation of both layers back to their equilibrium state provide a torque on the magnetisation of both layers, causing the magnetisation to precess as is shown in (D). Adapted from [11], Figure 1.

Most relevant to the observation of spin-transfer torques in these experiments is the in-plane magnetised layer (red) now having its magnetisation slightly canted out of plane, as is visible in the figure. The magnetisation now not being aligned to the external field will induce a torque on the magnetisation of the red layer. As magnetisation corresponds to an angular momentum, this torque does not cause the magnetisation to align to the external field, but will instead cause the magnetisation to precess around the external field direction[1]. This magnetic precession is sketched

[1]Magnetic precessions are exactly like gyroscopic precessions that one might be more familiar with. Both are

in Figure 1.5 D, where the dashed ellipse shows the various magnetisations that will materialise after allowing the precession to evolve.

The related change of magnetisation over time can be measured, and is shown in Figure 1.6. This figure shows the MOKE signal corresponding to the out of plane magnetisation of the sample, so the change in out of plane magnetisation of both magnetic layers contributes to the signal. The ultrafast demagnetisation of the out of plane layer gives a strong contribution to the signal, but in the 100 ps time-scale a clear precession of the MOKE signal can be observed. This oscillating signal indicates a precession of the magnetisation, indicating that magnetisation of the red layer had been canted out of plane, proving the effect of an optically induced spin-transfer torque altering the magnetisation of a magnetic layer[2].

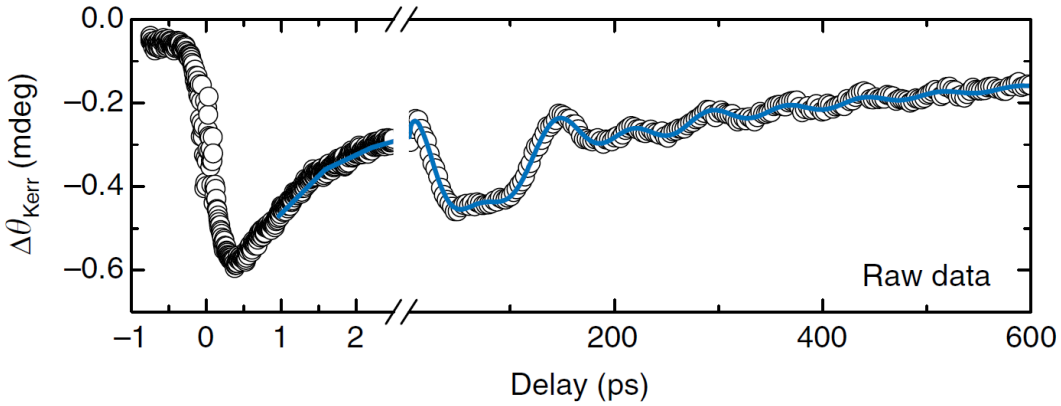

Figure 1.6: From the experimental set-up sketched in Figure 1.5, a MOKE time trace after laser excitation at $t = 0$. The MOKE signal measures the out of plane magnetisation of the sample. The ultrafast demagnetisation and subsequent remagnetisation of the out of plane layer is the dominant part of the signal. During the re-magnetisation we can see oscillations corresponding to the magnetic precession of both magnetised layers. Adapted from [11], Figure 2C.

It turns out that the electrons that transfer spin into the other layer have their spin absorbed fairly quickly, causing the absorption of spin angular momentum to only occur close to the interface where these electrons enter the layer. This makes the magnetisation of the magnetic layer non-uniform, exciting inhomogeneous spin waves. These spin waves can again be measured in a pump-probe setup for measuring the MOKE depending on the time since laser excitation[13]. These inhomogeneous modes have much larger frequencies than the homogeneous modes; up to 1 THz, in contrast to 10 GHz.

caused by a torque being applied to something win angular momentum, but this torque not being aligned with the angular momentum.

[2]In reality the experiment is somewhat more involved than this. In particular the out of plane layer also experiences a precession caused by an entirely different effect, but which causes an additional oscillation in the MOKE signal. This precession is drawn in Figure 1.5 d. Fortunately, the contributions of the two effects can be separated effectively, such that we can be sure that the IP magnetised layer does precess as spin transport would predict it to.

These experiments demonstrating spin-transfer torques caused by laser excitation were interesting to the field of spintronics. A novel way of manipulating magnetic state was found, in particularly one that works on extremely short time scales. This new effect would potentially provide a foundation for new kinds of technologies and devices. Furthermore, the excitation method being optical connects the fields of photonics to magnetism and spintronics. Already shortly afterwards a different type of magnetic multilayer was found to be able to switch between binary magnetic states using a laser-induced spin currents[14], a first step towards new digital storage devices based on laser induced spin currents.

1.1.6 Alternative models for demagnetisation and spin currents

The superdiffusive model for demagnetisation described before would indicate that hot electron movement would potentially cause a movement of spin, explaining the observed spin current. Around the time when the first spin-transfer torque measurements were performed, an alternative explanation for demagnetisation and spin currents was proposed in the "*s-d* model"[12, 15, 16]. This model is based on a separating the electrons in two groups; localised electrons and itinerant electrons. The localised electrons carry most of the spin corresponding to the magnetisation, but can not contribute to currents. In contrast, the itinerant electrons can move through sample, moving their spin angular momentum. This movement of itinerant electrons can even cross material interfaces, transporting spin between different layers. Through spin-orbit coupling the itinerant electrons may experience spin-flips, eventually dissipating their spin angular momentum into the crystal lattice.

The *s-d* model claims that laser excitation causes spin to be transferred between the localised electrons and the itinerant electrons. Initially most spin is tied to the localised electrons, so this spin transfer will reduce the amount of spin of localised electrons. The itinerant electrons however gain a substantial amount of spin. As the spin of itinerant electrons in the magnetic layer now is unbalanced, spin flips of itinerant electrons will start to dissipate this imbalance. Spin flips serve as a local process that dissipate spin angular momentum, causing part of the ultrafast demagnetisation.

This is not the only channel of spin dissipation in the *s-d* model. If the magnetic layer is adjacent to a conducting, nonmagnetic layer, the itinerant electrons in the magnetic layer can move into this second layer. The spin accumulation in itinerant electrons in the magnetic layer will therefore diffuse into the adjacent layer, transporting spin out of the magnetic layer. This transport of spin would reduce the magnetisation of the magnetic layer, aiding the ultrafast demagnetisation. These diffusive spin currents could potentially explain the spin currents observed in experiments.

Furthermore, a spin-dependent Seebeck effect has been proposed as being the cause of the spin currents[17]. While the superdiffusive, *s-d* and spin-dependent Seebeck models describe a spin current induced by laser excitation of thin-film magnets, the processes they describe are quite different. Which of these effects best describes spin currents in what experiment is still debated. Gaining a better understanding of the effect driving spin currents could lead to new improvements in our capability of manipulating magnetism.

1.2 Objective

The main interest of this study is to describe laser-induced ultrafast spin currents, in particular those relevant to experiments such as [11, 12, 13]. Based on the Valet-Fert model[6], we propose a model for ultrafast spin dynamics including both hot electron[9] and *s*-*d* model[15] contributions. Combining these effects in the same model allows the behaviour of spin currents produced by hot electrons and *s*-*d* effects to be compared more carefully, potentially yielding insight in their relative contribution to experimental observations. The proposed model for spin dynamics will be interpreted and simplified. Furthermore, it will be used to model the relevant experimental systems and their measurements.

1.3 Structure of this thesis

A model for spin transport is set up in Chapter 2. It is based on the Valet-Fert model, but is modified to include time dependence and the studied effects driving spin currents; an *s*-*d* spin source and hot electrons. Later chapters have the goal of simplifying the model. This simplification will also make it conceptually more clear what sorts of behaviour the model could show. In particular, the model set up in Chapter 2 contains the electric charge density caused by the electrons, the electric fields created and the resulting current of the thermal electrons. On the time-scales of spin diffusion this is approximately instantaneous, so in Chapter 3 we are able to simplify the model substantially by making this process exactly instantaneous.

Using some abstract mathematical properties of the model (linearity and time invariance), the time-dependence of the model can effectively be removed when studying some relevant measurements. With this, the model will appear like a steady-state model, hugely reducing its complexity. The justification of this change of perspective is discussed in Chapter 4. The model simplified using this perspective is shown and discussed in Chapter 5.

With this infrastructure build up, simple models of the studied experiments become tractable to solve in closed form. A variety of models based on *s*-*d* like spin sources and hot electrons are given in Chapter 6. These results are compared to measurements of the experiments they meant to describe, giving insight into which model more plausibly explains the true process causing the observed spin transfer.

Chapter 2

Model

To study spin currents induced by hot electrons and *s-d* spin sources, we need a model for the dynamics related to electrons that constitute the spin currents. This chapter will build such a model, based on the Valet-Fert model of magnetoresistance. Section 2.1 will describe the Valet-Fert model, to later generalise the model to introduce time-dependence, compatibility with the *s-d* model, and the the interaction with hot electrons. The resulting generalisation of the Valet-Fert model will be the foundation of the remainder of the thesis. The various processes of this model that are relevant to ultrafast spin currents will be explained in Section 2.2. Section 2.3 will introduce some notation for later convenience, and Section 2.4 derives conservation laws of the model. The way the proposed model relates to the experiments we are interested in is discussed in Section 2.5. Finally, Section 2.6 will discuss three sensible ways to parameterise the state of the model in preparation of the next chapter.

2.1 Generalised Valet-Fert model

This section is concerned with deriving the generalised Valet-Fert model that will be the basis of our efforts to describe ultrafast spin currents. The original Valet-Fert model will be introduced in Section 2.1.1. The later subsections will introduce some more structure of the model, and then extend it to make a model for electron currents related to ultrafast spin currents. The remainder of the thesis will be build on the model derived in this section.

2.1.1 The original Valet-Fert model

The Valet-Fert model was developed to describe the giant magnetoresistance effect in magnetic multilayers. Giant magnetoresistance (GMR) is the effect where an electric current is driven through a multilayer consisting of both ferromagnetic (FM) and non-magnetic (NM) layers in the out-of-plane (OOP) direction. Such configurations are shown in Figure 2.1. If the magnetisations of the FM layers are aligned (Figure 2.1 a), the electric resistivity of the multilayer is substantially smaller than if the FM layers have alternating magnetisations (Figure 2.1 b).

The Valet-Fert model describes this observed magnetoresistance by modelling the spin composition of the electron current flowing through the multilayer. Furthermore, the Valet-Fert model concerns thin-film magnetic systems and the currents flowing in the OOP direction. As the spin

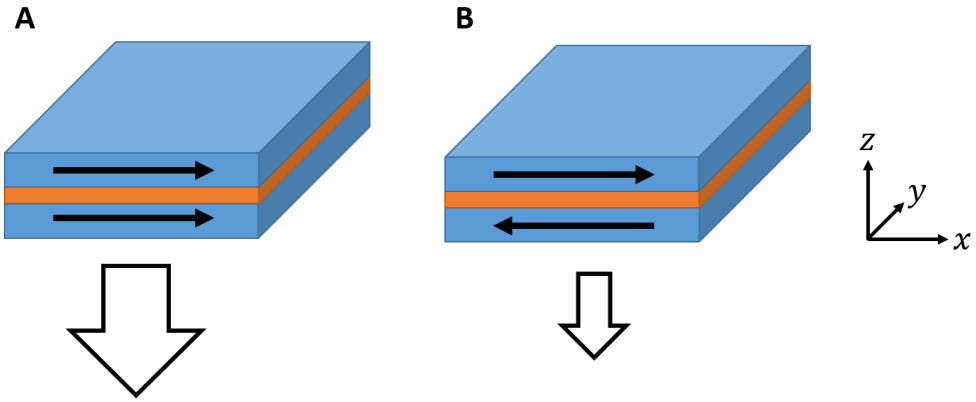

Figure 2.1: A cartoon of the giant magnetoresistance effect. A multilayer consisting of two ferromagnetic layers (blue) and a conductive spacer (orange) has an out-of-plane voltage applied to it. Current flowing through the multilayer (drawn as the vertical arrow) changes substantially by the magnetisations of the magnetic layers being aligned or not. Subfigure a shows the low resistivity configuration, while subfigure b shows the large resistivity configuration. The convention for coordinates are shown on the right of the figure.

transport experiments we are interested in also concern OOP spin currents through magnetic multilayers, this makes the Valet-Fert model a suitable foundation to base our study on.

Because we apply an OOP current to the multilayers and these multilayers are much wider than they are thick, the in-plane (IP) coordinates x and y are mostly unimportant. Furthermore, the Valet-Fert model is a steady state model, making it independent of the time t. This makes the model one-dimensional, only referencing the OOP coordinate. We use the convention that the OOP coordinate is written as z.

The goal of the Valet-Fert model is to calculate the OOP current through the magnetic multilayer when a potential is applied over it. We will write $J^t(z)$ for the current density flowing through the xy plane at coordinate z. We use number density currents, so the values of currents represent the number of electrons per area per time. The superscript t states that the quantity relates to thermal electrons, which are the only electrons present in these GMR measurements and the Valet-Fert model. We will later modify the Valet-Fert model by adding hot electrons to it, to make the model compatible with superdiffusive models for spin currents. Please do not confuse these t superscripts with the coordinate of time t, which will be written as function evaluation.

Every electron has a spin direction, which could potentially be oriented in any direction. The Valet-Fert model is a two-current model, which simplifies the problem by modelling spin to be only in one of two directions. A direction is chosen, and every spin must either be aligned with this direction or have the exact opposite spin direction. Spin being aligned to the quantisation direction is called "spin up", while the anti-aligned spin is called "spin down". The quantisation direction will always be chosen as the majority spin in one of the magnetic layers. For example in the multilayers shown in Figure 2.1), we would choose the quantisation direction as the $+x$ direction. Both layers in the low resistivity case would then be majority spin up, while in the large resistivity case only the upper layer is majority spin up, with the lower layer being majority spin down.

Quantities related to the spin up electron population will be labeled with a subscript +, while those related to spin down electrons are labeled with subscript −. Equations will be written using ± and ∓ to describe both the spin up and spin down populations simultaneously. For example, an equation $a_\pm = \pm b_\mp$ would be shorthand for the combination of the equation with the upper signs, $a_+ = +b_-$, and the equation with lower signs used; $a_- = -b_+$.

As electrons are labeled as being either spin up, +, or spin down, −, these subpopulations have an electron current of themselves. $J^t_\pm(z)$ is the current density of spin ± electrons flowing through the xy plane at z. J^t_+ and J^t_- are the two currents that are referenced by the name "two current model". These currents are related to the total electron current through simple addition of the spin populations;

$$J^t = J^t_+ + J^t_-. \tag{2.1}$$

The Valet-Fert paper derives a macroscopic transport equation describing the spin specific currents $J^t_\pm$, which is given as

$$J^t_\pm = -\sigma_\pm \frac{\partial \mu_\pm}{\partial z}. \tag{2.2}$$

$\sigma_\pm$ is a the conductivity related to the spin ± electron population, while $\mu_\pm$ is the electrochemical potential of spin ± electrons. The conductivities $\sigma_\pm$ and chemical potentials $\mu_\pm$ are functions of the OOP coordinate z, just like J^t and $J^t_\pm$ were. The conductivity $\sigma_\pm$ is a material property, so $\sigma_\pm(z)$ depends on the material at coordinate z. If the material at z is ferromagnetic, the local conductivity of spin + electrons, $\sigma_+(z)$, will in general differ from the conductivity of spin − electrons, $\sigma_-(z)$.

The electrochemical potential $\mu_\pm$ describes the energy of the spin ± Fermi level. More concretely, $\mu_\pm(z)$ is the energy required to add a single spin ± electron to the Fermi sea at coordinate z. Spatial gradients of the electrochemical potential imply that energy can be dissipated by electrons flowing from larger to smaller $\mu_\pm$, so will cause a flow of electrons. As is shown by Equation (2.2), this flow is proportional to the gradient of the relevant electrochemical potential and proportional to the relevant conductivity. The negative sign makes sure that electrons flow from large to small electrochemical potential, as the conductivity must be a non-negative number.

As the Valet-Fert model describes a steady state solution and electrons are conserved, the number of electrons flowing into some region $[z_1, z_2]$ must be the same as the number of electrons flowing out of it. This implies $J^t(z_1) = J^t(z_2)$. In this region some electrons may however flip their spin, so electrons that flow into the region with spin ± may flow out of the region with spin ∓, allowing the spin specific currents to change with z; $J^t_\pm(z_1) \neq J^t_\pm(z_2)$.

Like differences in electrochemical potential drive electron flow, it also drives electrons to change their spin; spin flips. In this case, the spin flips at z are driven by the difference between $\mu_+(z)$ and $\mu_-(z)$. This difference is an important enough quantity to give a name and symbol. We define the spin accumulation μ_s as

$$\mu_s = \mu_+ - \mu_-. \tag{2.3}$$

Besides the rate of spin flips being proportional to this energy difference, there again is a factor of proportionality involved. This factor of proportionality is written as r. This makes the rate of spin flips from spin + to spin − at z equal to $r(z)\,\mu_s(z)$. Using this with the continuity of spin ± electrons gives

$$J^{t\,\prime}_\pm = \mp r\,\mu_s. \tag{2.4}$$

For example; suppose we have a positive spin accumulation $\mu_s(z) > 0$, so $\mu_+(z) > \mu_-(z)$. This energy difference will push spins to flip from spin + to spin −, so the current of spin + electrons leaving z must be smaller than the current flowing into it, implying $J^{t\,\prime}_+ < 0$. As $r(z) \geq 0$ this

is consistent with the above equation. Also note that this equation is consistent with the total electron current being constant in space; $J^{t\prime} = J_+^{t\,\prime} + J_-^{t\,\prime} = -r\mu_s + r\mu_s = 0$.

Equations (2.2) and 2.4 form the system of equations defining the Valet-Fert model. Provided the material properties $\sigma_\pm$ and r, and the boundary conditions of the problem (the applied potential) we can use these equations to calculate the electrochemical potentials $\mu_\pm$ and the spin specific currents $J_\pm^t$. Adding the spin specific currents together gives the total electron current J^t. Comparing this to the potential applied by the boundary conditions the resistivity of the multilayer is calculated, allowing the Valet-Fert model to describe the GMR effect.

To illustrate the behaviour of the Valet-Fert model somewhat, we briefly study how it behaves in magnetic multilayers composed of a number of distinct, internally homogeneous layers. Within the homogeneous layers, the material properties $\sigma_\pm$ and r are constant in space (reducing from z-dependent functions to real numbers). This causes the solution of $\mu_\pm$ and $J_\pm^t$ within homogeneous layers to have the form

$$\begin{cases} \mu_\pm(z) & = a - \frac{J^t}{\sigma_{\text{tot}}} z \pm \sigma_\mp \left(b_1\, e^{+z/\lambda} + b_2\, e^{-z/\lambda} \right) \\ J_\pm^t(z) & = -\sigma_\pm \left(-\frac{J^t}{\sigma_{\text{tot}}} \pm \frac{\sigma_\mp}{\lambda} \left(b_1\, e^{+z/\lambda} - b_2\, e^{-z/\lambda} \right) \right) \end{cases} \tag{2.5}$$

where a, J^t, b_1 and b_2 are parameters of the solution, and we introduced the derived material properties

$$\sigma_{\text{tot}} = \sigma_+ + \sigma_-, \quad \lambda = \sqrt{\frac{\sigma_+ \sigma_-}{r\, \sigma_{\text{tot}}}}. \tag{2.6}$$

Given the material properties, the solution has four degrees of freedom; a, J^t, b_1 and b_2. As the notation suggests, J^t is exactly the total electron current, which corresponds to a slope of both spin specific electrochemical potentials $\mu_\pm$. The parameter a is related to a constant being added to both $\mu_\pm$ which does not effect spin specific electron currents, nor the rate of spin flips. The parameters b_1 and b_2 are related to a spin accumulation at large z, respectively small z. Diffusion of this spin accumulation will give a contribution to the spin specific currents. This spin accumulation and the related currents decay over distance with the length scale λ, which is called the spin diffusion length of the material. This is a material property that is well documented for magnetic materials[3, 16].

As an example of the Valet-Fert model describing multilayers, consider a space filled by a FM layer on $z < 0$, where the conductivity of spin + electrons is larger than that of spin − electrons; $\sigma_+ > \sigma_-$. The half space at $z > 0$ is filled by an NM material, such that symmetry forces the spin specific conductivities in this layer to be equal; $\sigma_+ = \sigma_-$. Within the $z < 0$ and $z > 0$ half-spaces, the solution of the electrochemical potentials and spin currents are described by Equation (2.5). On the interface between these homogeneous layers, both the spin specific electrochemical potentials and electron currents must be continuous. Applying a potential to this multilayer to drive electrons from negative to positive z would give a solution such as the one shown in Figure 2.2.

As is visible in Figure 2.2b, the imbalanced conductivity in the FM layer causes the spin current in it to be spin polarised, while far enough from the interface in the NM layer we have $J_+^t = J_-^t$. This difference in spin currents causes more spin + to flow towards the interface than leave it, while the opposite holds for spin − electrons. This causes a spin accumulation near the interface, which can be seen in Figure 2.2a. This spin accumulation is associated with diffusive currents away from the interface. Spin flips cause this diffusive current to decay with the spin diffusion length of the respective material.

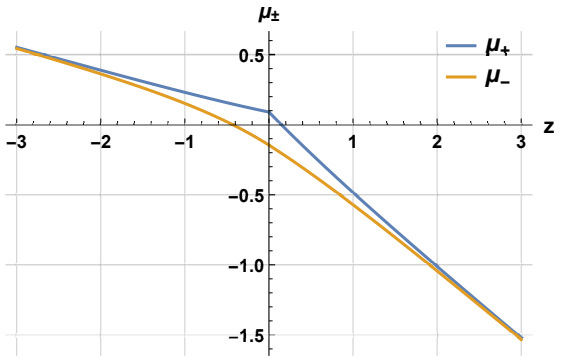

(a) The spin specific electrochemical potentials $\mu_\pm$ as function of z.

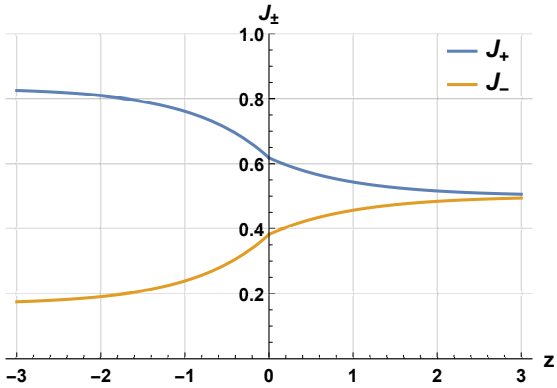

(b) The spin specific electron currents $J^t_\pm$ as function of z.

Figure 2.2: Example of the electrochemical potentials $\mu_\pm$ and spin specific electron currents $J^t_\pm$ as a function of z as modeled by the Valet-Fert model. All quantities are dimensionless. An external current source drives a particle current of $J^t = 1$ through a space consisting of a magnetic layer in the $z < 0$ half-space and a nonmagnetic metal in the $z > 0$ half-space. The two materials having different spin-specific conductivities causes μ_+ to differ from μ_- near the interface. Spin flips restore the balance between the spin + and spin − subpopulations far away from the interface.

In making this figure, total conductivity σ_{tot} of the NM layer was chosen to be smaller than that of the FM layer. This is the cause of the slope of the electrochemical potential to be steeper in the NM layer.

The GMR samples as shown in Figure 2.1 have multiple FM-NM interfaces. If the distance between these is small enough, this will cause the spin accumulations related to the individual interfaces to interact. Depending on the magnetisation of the FM layers this interaction will either increase or decrease the spin accumulation, affecting the current flowing through the multilayer.

2.1.2 The spin-specific electrochemical potential

To extend the Valet-Fert model we need to take a slightly closer look at it. Most importantly, introducing time dependence will allow the number of thermal electrons at some position to change over time.

We stated earlier that the electrochemical potential $\mu_\pm(z)$ is the energy required to add an electron with spin $\pm$ to some position z. There are two contributions to this energy. Firstly, we have to move the electron through the electric potential to z. As electrons have a charge $-e$, the energy required to do this is $-e\,V(z)$. Once this is done we still need to overcome the chemical potential, representing the orbital energy of the state we put the electron in. The chemical potential at z will be written as $\mu_{0,\pm}(z)$. As these two energies constitute the electrochemical potential, we have

$$\mu_\pm = \mu_{0,\pm} - e\,V. \tag{2.7}$$

This composition of the electrochemical potential is made visual in Figure 2.3, which shows that even if the electrochemical potential is constant there might be spatial differences in the Coulomb

energy of electrons, $-eV$, and the chemical potential. The figure also indicates that the density of electrons with spin $\pm$ is related to the chemical potential $\mu_{0,\pm}$, which we will use later.

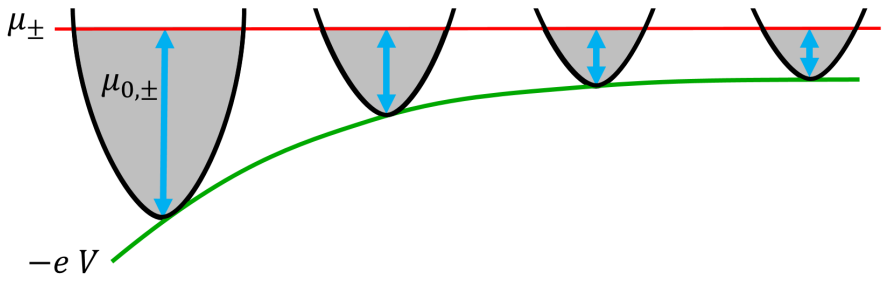

Figure 2.3: For either the spin + or − subpopulation, a constant electrochemical potential $\mu_\pm$ (red) composed by a spatially varying Coulomb energy $-eV$ (green) and chemical potential $\mu_{0,\pm}$ (blue arrows). On the vertical axis energy, and on the horizontal axis position. The black curves represent the density of states (width of the curves) at the locations where the chemical potential are drawn, with vertically the electron energy composed both of the Coulomb energy and the orbital energy. Drawing the figure as if in zero temperature, all electron states with smaller energy than the electrochemical potential are filled. These filled states are drawn as the shaded areas in the drawn densities of states. Note that the density of electrons depends only on the density of states and the chemical potential.

To calculate the electrical potential we resort to electrostatics[1]. As we deal with thin films, the electric fields and potentials are approximately independent of the IP coordinates x and y, and the electric field may not have an IP component. The laws of electrostatics then reduce to the scalar equations

$$\frac{\partial E}{\partial z} = \rho/\epsilon_0, \qquad \frac{\partial V}{\partial z} = -E. \tag{2.8}$$

$E(z)$ is the OOP electric field component at z, $V(z)$ is the electric potential and ϵ_0 the vacuum permittivity. The charge density ρ is specified by the density of electrons, which we will introduce and relate to the charge density shortly. Using these equations allows Equation (2.2) describing spin specific electron currents to be rewritten as

$$J^t_\pm = -\sigma_\pm \left(\frac{\partial \mu_{0,\pm}}{\partial z} + eE \right), \tag{2.9}$$

showing that there are two causes of electron currents; electric fields and gradients in the chemical potential. At this point we will depart from the original treatment of the Valet-Fert model and introduce some extensions for treating ultrafast spin dynamics.

2.1.3 Time dependence

In steady state, Equation (2.4) guaranteed that the number of electrons flowing into some region equals the number leaving it, where entering and leaving can be caused by either transport or

[1] We work with length-scales on the order of 10 nm, which takes the speed of light a mere $3.3 \cdot 10^{-2}$ fs to traverse. This is extremely short compared to the dynamics we will be studying, which last tens of femtoseconds or more.

the electron flipping spin. Allowing the state of the system to change over time, the continuity equations become substantially weaker. We now introduce the number density of electrons with spin $\pm$, written as $N_\pm^t$. It is a function of both space and time; $N_\pm^t(z,t)$ is the number density of spin $\pm$ electrons at position z and time t. This number density can only be changed by the processes of transport and spin flips. Thermal electron transport is $J_\pm^t$, while the rate of spin flips is still $r\,\mu_s$. Continuity then requires the time evolution of the electron density to conform to

$$\frac{\partial N_\pm^t}{\partial t} = -\frac{\partial J_\pm^t}{\partial z} \mp r\,\mu_s. \tag{2.10}$$

While hidden in this notation, the current $J_\pm^t$ and spin accumulation μ_s have become functions of both space and time, whereas they were only functions of space in the Valet-Fert model. r is a material property, so it still only a function of space. As a sanity check, setting the time derivative to zero reproduces Equation (2.4).

The chemical potential $\mu_{0,\pm}(z,t)$ and the number density $N_\pm^t(z,t)$ are related, as already was shown in Figure 2.3. If the number density of electrons changes, the number of orbitals that are filled changes, in turn changing the chemical potential. This relation is given by the spin specific density of states $D_\pm$, which is defined by

$$D_\pm = \frac{\mathrm{d}N_\pm^t}{\mathrm{d}\,\mu_{0,\pm}}. \tag{2.11}$$

Like the conductivities $\sigma_\pm$ and r, the density of states is a material property so will depend on position but not on time. In principle the density of states depends on the energy of the orbitals we are considering, which would be the chemical potential $\mu_{0,\pm}$. However, we approximate this as being constant to make our model linear.

We have freedom to choose the zero energy of the chemical potential. Also, all previous steps are insensitive to $N_\pm^t$ being shifted by a function that is constant in time. At this point it is most convenient to define zero chemical potential and zero electron density to be their respective equilibrium values if the system experiences no external influence. To first order, this would make the electron density $N_\pm^t$ depend on the chemical potential $\mu_{0,\pm}$ through

$$N_\pm^t = D_\pm\,\mu_{0,\pm}. \tag{2.12}$$

Furthermore, having the electron densities $N_\pm^t$ we can now make a statement about the charge density. If $N_\pm^t = 0$ the system is relaxed, so has zero charge density. Any additional electron contributes a charge $-e$, so the charge density must be

$$\rho = -e\left(N_+^t + N_-^t\right). \tag{2.13}$$

2.1.4 External spin source

Now that the Valet-Fert model is expanded to allow time dependence it is straight-forward to introduce the modification required to combine it with the *s-d* model. The *s-d* model claims that some electrons are localised, while other are itinerant. These electron populations can exchange spin on laser excitation. The Valet-Fert model and its extension to time dependence only describes electrons that can flow; the itinerant electrons. By adding an external spin source term to the time-dependent Valet-Fert model, we can model the itinerant electrons gaining or losing spin angular momentum by interaction with the localised electrons.

Such a spin source is is incorporated as simply introducing a second term driving spin flips, which will be written as S. We will choose the convention that these driven spin flips have positive sign if they increase the spin accumulation, so $S > 0$ corresponds to spin $-$ electrons flipping to spin $+$. Previously the rate of spin flips from spin $+$ to $-$ was $r\,\mu_s$, which now becomes $r\,\mu_s - S$. Regarding the equations describing the model, this only affects the time evolution of the spin density, which now becomes

$$\frac{\partial N_{\pm}^{t}}{\partial t} = -\frac{\partial J_{\pm}^{t}}{\partial z} \mp r\mu_s \pm S. \tag{2.14}$$

We attempt to build a model describing ultrafast spin currents. The s-d interactions causing the spin source S to be non-zero is outside the scope of this model, so we will use S as an input of the model. We do not provide equations describing it.

2.1.5 Hot electrons

The superdiffusive model of demagnetisation and spin transport relies on electrons in hot states moving through the multilayer, transferring their spin. The Valet-Fert model however only describes electrons in thermal states, which is why all previous electron densities and currents had been labeled with a superscript t. To include hot electrons to the model, we choose to model all electrons as either being thermalised or in a hot state, though in reality this distinction is admittedly not this binary. Figure 2.4 C provides a sketch of the states filled by electrons arranged by their energy, sketching the distinction between thermal electrons and hot electrons. The hot electron subpopulation will be labeled with superscript h, while the thermalised electrons have superscript t.

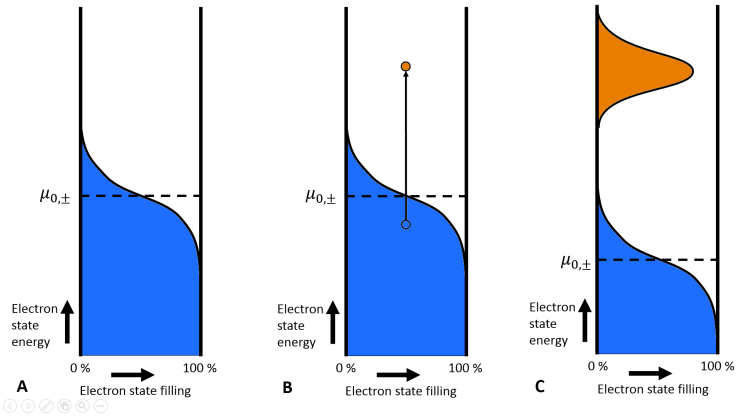

Figure 2.4: A sketch of laser excitation of electrons from thermal state to hot states. The filling of spin $\pm$ electron states at some position is shown before (A), during (B) and after (C) optical excitation. The blue area represents electron states filled by thermal electrons, while the orange area are electron states filled by hot electrons. The unshaded area represents empty electron states. Subfigure A shows the situation before laser excitation, where all electrons are thermalised such that state filling follows a Fermi-Dirac distribution. Subfigure B shows a single thermal electron being excited to a hot state by raising its energy. Subfigure C shows the situation after laser excitation of many electrons. Excited electrons leave their original state empty, reducing the effective chemical potential $\mu_{0,\pm}$related to the thermalised electrons.

The density of spin $\pm$ hot electrons is written as $N^h_\pm$, while the associated current is $J^h_\pm$. The convention for $N^h_\pm = 0$ is there not being any spin $\pm$ hot electrons[2]. Immediately, the equation for the charge density must be changed to account for the charge of hot electrons. The charge density now becomes

$$\rho = -e\left(N^t_+ + N^t_- + N^h_+ + N^h_-\right). \tag{2.15}$$

Laser excitation of thermal electrons to become hot is sketched in Figure 2.4. Optical excitation increases the energy of a number of thermal electrons, such that the original states they occupied have become empty. Having absorbed the photon energy, the hot electrons occupy states with larger energy than the states filled by thermal electrons. The figure also shows how electrons are conceptually split in the thermal and hot populations we label with superscript t, respectively h. Laser excitation is shown to move electrons from thermal states to hot states, increasing the number of hot electrons but decreasing the number of thermal electrons. The opposite happens during decay of hot electrons.

We introduce $R_\pm(z,t)$ as the local signed rate of electrons of spin $\pm$ transferring from a thermal state to a hot state at position z and time t. Excitation removes electrons from the thermal state, so corresponds to positive $R_\pm(z,t)$. Hot electron decay adds electrons to the thermal state, and has negative $R_\pm(z,t)$. This gives a new contribution to the time evolution of the thermal electrons, which now becomes

$$\frac{\partial N^t_\pm}{\partial t} = -\frac{\partial J^t_\pm}{\partial z} \mp r\,\mu_s \pm S - R_\pm. \tag{2.16}$$

Regarding the hot electron populations, the superdiffusive model assumes that hot electrons conserve their spin during excitation, transport and decay. If a spin $\pm$ thermal electron is excited, it becomes a hot spin $\pm$ electron. When this electron decays is has spin $\pm$ still, becoming a spin $\pm$ thermal electron again. The only things that affect the hot electrons density is hot electron transport and excitation/decay. Continuity then requires that the time evolution of the hot electron density follows

$$\frac{\partial N^h_\pm}{\partial t} = -\frac{\partial J^h_\pm}{\partial z} + R_\pm. \tag{2.17}$$

We assume that hot electron excitation/decay $R_\pm$ and hot electron currents $J^h_\pm$ to not depend on the state of the thermal electron system.

Like is done for the *s-d* spin source S, these functions describing the hot electrons are treated as an input to the model of the thermal electrons. As far as the model of the thermal electrons is concerned, it does not matter what procedure gives the excitation rates $R_\pm$, hot electron densities $N^h_\pm$ and hot electron currents $J^h_\pm$, as long as they are are consistent with above continuity equation.

To make a complete model for ultrafast spin dynamics, a model for the excitation rate and hot electron currents is required. Such a model is given in Appendix A. The provided model is linear and satisfies the continuity equation stated in Equation (2.17). While such a hot electron required to provide a complete model for ultrafast spin dynamics, the remainder of this thesis will focus mostly on the behaviour of the thermal electrons. The study will therefore not actually use the model presented in Appendix A, or be limited by the choices made in this model. Because of this independence on the used hot electron model, it is not discussed in the main text.

[2]This is in contrast to thermal electrons, where $N^t_\pm = 0$ implied that there as many thermal electrons as there would be if the system is not externally perturbed.

2.1.6 Final generalised Valet-Fert model

Because we introduced quite a few modifications to the original Valet-Fert model, let us summarise the equations governing the proposed generalisation of the Valet-Fert model. The equations governing the model can roughly be divided into three groups; the equations governing the state of the thermal electrons, the electric field equations, and the continuity equations. To simplify the notation beyond this point, we will use notation of primes for spatial partial derivatives, $f' = \partial f/\partial z$.

Equations governing thermal electrons

Thermal electron currents are governed by

$$J^t_\pm = -\sigma_\pm \, {\mu_\pm}', \tag{2.18}$$

which depends on the spin specific conductivity and the electrochemical potential,

$$\mu_\pm = \mu_{0,\pm} - eV. \tag{2.19}$$

In turn, the electrochemical potential depends on the electric potential discussed below and the chemical potential, which is related to the density of thermal electrons through

$$N^t_\pm = D_\pm \, \mu_{0,\pm}. \tag{2.20}$$

For convenience we introduced the spin accumulation

$$\mu_s = \mu_+ - \mu_-, \tag{2.21}$$

describing the energy difference that serves to drive spin currents.

Electric charge and field equations

The charge density that produces electric fields depends on the number densities of electrons through

$$\rho = -e \left(N^t_+ + N^t_- + N^h_+ + N^h_- \right). \tag{2.22}$$

We use Gauss' law to calculate the electric field as

$$E' = \rho/\epsilon_0, \tag{2.23}$$

which is used to calculate the electric potential

$$V' = -E. \tag{2.24}$$

Continuity equations

Having the state of thermal electrons and the resulting currents, continuity requires the time evolution of thermal electrons to conform to

$$\frac{\partial N^t_\pm}{\partial t} = -{J^t_\pm}' - R_\pm \mp r\mu_s \pm S. \tag{2.25}$$

Hot electrons densities are only changed through hot electron transport and excitation/decay, such that its time evolution must be

$$\frac{\partial N_{\pm}^{h}}{\partial t} = -J_{\pm}^{h\,\prime} + R_{\pm}. \tag{2.26}$$

These continuity equations describe the time evolution of the four electron subpopulations N_{+}^{h}, N_{+}^{t}, N_{-}^{t}, N_{-}^{h}. These populations can change by transport and excitation/decay of electrons. The thermal electron populations are additionally affected by spin flips. In Figure 2.5 these subpopulations are arranged, and the processes transferring electrons between them are drawn as arrows. This serves as a visual confirmation to show how electrons are never created or removed, but can only move spatially (drawn with horizontal arrows) or transition between different electron subpopulations (vertical arrows).

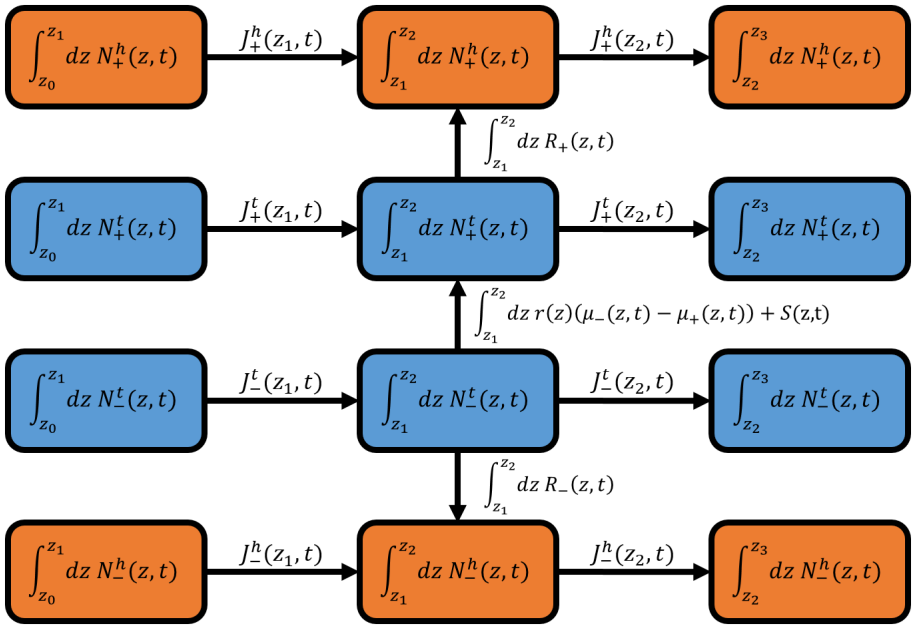

Figure 2.5: The four electron sub-populations and the processes that affect the subpopulations on the interval $z_1 < z < z_2$. The four electron subpopulations are arranged vertically, with the upper half corresponding to spin + and the lower half to spin −. The orange populations are hot electrons, while the blue populations are thermal electrons. Vertical arrows therefore correspond to processes moving electrons between different subpopulations. These are either excitation/decay or spin flips. The spatial OOP position is arranged horizontally with arbitrary values of $z_0 < z_1 < z_2 < z_3$, such that horizontal arrows represent spatial transport of electrons. The arrows represent the convention for flow when the associated quantity is positive. .

2.2 Modelled processes

The derivation of our proposed generalisation of the Valet-Fert model does show what effects are modelled, but not how they interact with each other to predict a spin current. To give a better feel for the various processes and how they relate to the spin currents that the model might predict, this section will discuss how the hot electron processes, the *s-d* effect and diffusion of electrons contribute to the spin current. This exposition is quite verbose and the connection to the model is somewhat indirect in places, but the next chapter will be able to make the processes described here substantially more concrete.

Before the optical excitation happens the system would be in equilibrium. The densities of thermal electrons $N_{\pm}^{t}$ would be zero, implying that the chemical potentials are zero, such that there is zero spin accumulation[3]. The charge is neutral such that there are no electric fields, and there would be no currents of thermal electrons. This equilibrium can be destroyed by an *s-d* source injecting spin into the thermal electron system, or hot electrons being excited and moved through the material.

2.2.1 s-d driven processes

The *s-d* model states that on laser excitation of ferromagnetic (FM) layers, localised electrons that carry most of the magnetic spin will transfer spin with the electrons that we call thermal electrons. The generalised Valet-Fert model was made capable of describing such an effect by having an external spin source S that can flip the spin of thermal electrons, exactly like the interaction with localised electrons would. On laser excitation, this spin source would momentarily become non-zero in any FM layer, causing thermal electrons in a FM layer to have their spins flipped. For concreteness, let us take the external spin source to increase the thermal spin density by flipping spin $-$ electrons to spin $+$ in the FM layer. In this FM layer, the local density of spin $+$ electrons is increased, while the density of spin $-$ electrons is decreased. This comes with an increase in the chemical potential of spin $+$ electrons, and the chemical potential of the spin $-$ electron population being lowered. This difference in chemical potential comes with a finite spin accumulation in the FM layer. This spin accumulation would immediately drive spin flips, working to lower the spin accumulation.

Such an external spin source is not present in nonmagnetic (NM) layers. The spin specific electric potentials will therefore have a gradient over FM - NM material interfaces. In the FM layer, the chemical potential of spin $+$ has become positive, while it has remained zero in the NM layer. This gradient pushes spin $+$ thermal electrons from the FM layer into the NM layer. The opposite happens for the spin $-$ thermal electron population, where electrons are pulled out of the NM layer into the FM layer. We have spin $+$ electrons moving in the opposite direction to spin $-$ electrons; a spin current.

A more intuitive way of thinking about this process is the spin accumulation in the FM layer diffusing into the adjacent NM layer. Figure 2.6 visualises the spatially imbalanced electrochemical potentials caused by an imbalanced spin accumulation. These imbalances in the electrochemical potential cause electron currents and spin flips, which are drawn in the figure as horizontal, respectively vertical arrows. This spin diffusion of the created spin accumulation is the sole manner in which the *s-d* process is able to induce a spin current.

[3]Remind that the density of thermal electron is taken relatively from equilibrium, so by definition in equilibrium $N_{\pm}^{t} = 0$.

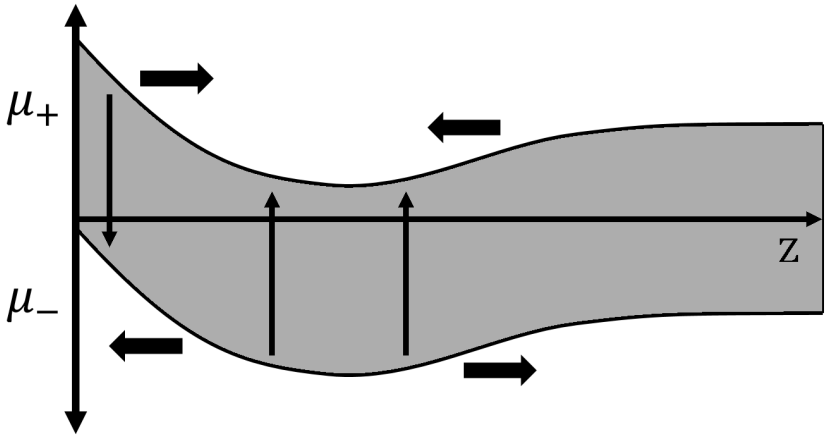

Figure 2.6: A cartoon of the electrochemical potential of spin $\pm$ electrons $\mu_\pm$. The spin + electrochemical potential is drawn above the horizontal axis, while the spin $-$ electrochemical potential is drawn below it. The shaded are corresponds to states with less energy than the electrochemical potential, so taking zero temperature these states would be filled. Gradients in electrochemical potential cause a net flow of electrons with the corresponding spin (horizontal arrows). A difference between μ_+ and μ_- causes electrons to flip spin (vertical arrows), transitioning between the spin populations.

2.2.2 Hot electron driven processes

The superdiffusive model models ultrafast demagnetisation to be caused by the laser pulse optically exciting electrons to hot states. These hot electrons would move through the multilayer, potentially excite other electrons to hot states and eventually decay back to a thermal state. Figure 2.7 visualises a single electron being excited to a hot state to be transported to a different layer and decay there. The hot electrons maintain their spin, so the movement of hot electrons may move spin through the material. Hot electron currents can directly contribute to the spin current, as is also clear from the equation for the total spin current; $J_s = J_s^t + J_s^h$. Furthermore, hot electron excitation and decay affect the density of thermal electrons. Excitation and decay can therefore induce spin accumulations, which cause diffusive currents as was sketched in Figure 2.6.

Furthermore, hot electrons are charged. Moving hot electrons will therefore move charge, and in turn create electric fields. These electric fields would drive thermal electron currents until charge neutrality is restored. Any hot electron current will therefore cause a thermal electron current in the opposite direction; a screening current. Such a screening current is represented by the green dots and the corresponding arrows in Figure 2.7. These screening currents may carry spin, and therefore contribute to spin currents. Screening currents transporting spin implies that they affect the spin accumulation, and again this spin accumulation can diffuse to cause spin transport.

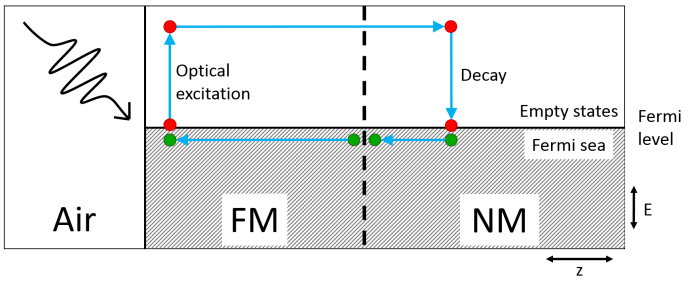

Figure 2.7: A cartoon of a multilayer composed of a ferromagnetic and nonmagnetic layer being optically excited to excite hot electrons. The horizontal axis represents the out of plane coordinate z, while the vertical axis represents electron energy. The red dot represents an electron that is excited in the ferromagnetic layer, which moves into the nonmagnetic layer to finally decay. The green dot represents electrons being moved in the opposite direction to the hot electron to compensate for the transport of charge. The spin polarisation of these screening currents depends on the material property, which is why it is drawn separately in the different layers.

2.3 Notation

For convenience of writing we will now introduce some variables. We already encountered the total thermal electron current $J^t = J^t_+ + J^t_-$, and the spin accumulation $\mu_s = \mu_+ - \mu_-$, and the total conductivity $\sigma_{\text{tot}} = \sigma_+ + \sigma_-$. These follow a pattern that we now extend to define many more variables.

The electrons we describe can be either spin + or spin −, and are either in a thermal or hot state. This gives four electron subpopulations. The number densities related to these are N^t_+, N^t_-, N^h_+, N^h_-, and their related current densities are J^t_+, J^t_-, J^h_+, J^h_-. Often we will use sums or differences of these terms. For example the thermal current J^t was the sum of the thermal currents of both spin species, while the spin accumulation μ_s is the difference between the two. The notation we use is to suppress a subscript or superscript to denote taking the sum over both subspecies; in J^t the spin subscript is suppressed, so $J^t = J^t_+ + J^t_-$.

We will also often take the difference between the spin subspecies, which is written with subscript s. The spin accumulation $\mu_s = \mu_+ - \mu_-$ is an example of this convention in action. All symbols related to electron densities and currents defined by these conventions are shown in Table 2.1.

	spin ±	thermal	hot	all electrons
density	$N_\pm = N^t_\pm + N^h_\pm$	$N^t = N^t_+ + N^t_-$	$N^h = N^h_+ + N^h_-$	$N = N^t_+ + N^t_- + N^h_+ + N^h_-$
current	$J_\pm = J^t_\pm + J^h_\pm$	$J^t = J^t_+ + J^t_-$	$J^h = J^h_+ + J^h_-$	$J = J^t_+ + J^t_- + J^h_+ + J^h_-$
spin density		$N^t_s = N^t_+ - N^t_-$	$N^h_s = N^h_+ - N^h_-$	$N_s = N^t_+ - N^t_- + N^h_+ - N^h_-$
spin current		$J^t_s = J^t_+ - J^t_-$	$J^h_s = J^h_+ - J^h_-$	$J_s = J^t_+ - J^t_- + J^h_+ - J^h_-$

Table 2.1: Symbols derived from the density and current of the four electron sub-populations, with their defining equation.

The spin accumulation μ_s is the only symbol following this pattern but is not in the table. We could also take the difference between the chemical potentials $\mu_{0,\pm}$, but from their relation with the electrochemical potential given in Equation (2.19) this is exactly the spin accumulation;

$$\mu_s = \mu_+ - \mu_- = \mu_{0,+} - \mu_{0,-}. \tag{2.27}$$

Some of the variables in the table are important enough to give a name. The goal of the model is study the amount of spin that is transported, which is done by J_s. We call J_s the (total) spin current. The total spin current is composed of the thermal electron spin current J_s^t, and the hot electron spin current J_s^h. The local amount of spin in the thermal system is reflected by N_s^t so it will be called the spin density of the thermal system. Despite the naming, currents are expressed in terms of number current densities (number of particles per area per time), while N_s^t is a number density (number of particles per volume).

This is a good moment to point out the difference between the spin accumulation μ_s and the thermal spin density N_s^t. Both specify a local imbalance between the spin populations, but the spin accumulation does so in terms of an energy and the spin density in terms of a density. The relation between the two will be revisited in Section 2.6.

As was done by introducing σ_{tot}, we will also introduce notation for the sum of material properties. Instead of suppressing the spin subscript we will write a subscript "tot" for total, such that we define

$$D_{\text{tot}} = D_+ + D_-, \qquad \sigma_{\text{tot}} = \sigma_+ + \sigma_-. \tag{2.28}$$

2.4 Conservation laws

With the new notation it becomes simpler to study combinations of electron subpopulations. In particular it is interesting to take a look at the spin $\pm$ electron density $N_\pm$, which includes both the thermal and hot electrons with spin $\pm$. Taking the sum of Equations (2.25) and (2.26) gives a continuity equation for spin $\pm$ electrons, as

$$\frac{\partial}{\partial t} N_\pm = -J'_\pm \mp r\mu_s \pm S. \tag{2.29}$$

This indicates that the density of electrons with spin $\pm$ is changed only by spin $\pm$ electron transport or spin-flips of thermal electrons, as was shown in Figure 2.5. Subtracting the spin down result from the spin up result gives

$$\frac{\partial}{\partial t} N_s = -J'_s - 2r\mu_s + 2S \tag{2.30}$$

relating the spin current J_s and spin accumulation μ_s with the evolution of the total spin density N_s densities of the four electron populations. Moreover, it is clear that spin flips are the only events that may change the total amount of spin. Looking instead at the time evolution of the density of all electrons

$$\frac{\partial}{\partial t} N = -J', \tag{2.31}$$

we see that the electrons density can only be changed by transport in a way that is consistent with continuity of electrons, verifying that the number of electrons is conserved. Equations (2.30) and (2.31) provide a sort of conservation law for spin, respectively electrons. These conservation laws will be useful in later chapters.

2.5 Application to experiments

We now have a model of optically excited ultrafast spin dynamics. We will focus on using this model to better understand experimental measurements of magnetic precessions excited by ultrafast spin currents, such as done in [11, 12, 13]. In this section we will describe these experiments, and how the proposed model can be used to describe them. First, the sample structure and processes occurring in the experiments are described. How our proposed model connects to these is discussed afterwards.

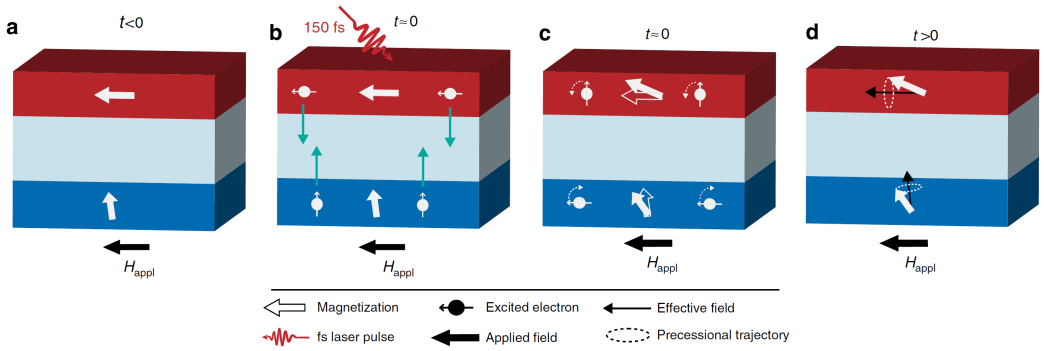

Figure 2.8: The structure of the sample used in the spin-transfer torque experiment of [11]. The multilayers consist of two thin-film magnets. One layer has out-of-plane magnetisation (blue). The other has in-plane magnetisation (red), biased by an external magnetic field. (A) is the system at rest. On laser excitation, shown in (B), spin currents transfer angular momentum between the layers; a spin-transfer torque. This effect affects the magnetisation direction of both magnetic layers as shown in (C). The mechanisms pulling the magnetisation of both layers back to their equilibrium state provide a torque on the magnetisation of both layers, causing the magnetisation to precess as is shown in (D). Adapted from [11], Figure 1.

The samples used in the experiments under consideration consist of thin films of two FM layers separated by a NM conducting spacer. One of the magnetic layers has out-of-plane (OOP) magnetisation, while the second is in-plane (IP) parallel to an externally applied magnetic field. This configuration is sketched in Figure 2.8 a. On laser excitation both layers demagnetise. A spin current between the layers will arise, causing spin to be transferred between the FM layers. This exchange of spin causes the magnetisation of both layers to change, tilting it slightly away from their relaxed orientation. Most relevant to the measurements is the spin from the OOP magnetised layer flowing into the IP magnetised layer, causing the magnetisation of the IP layer to cant slightly out of plane. The state of the multilayer at this moment is sketched in Figure 2.8 c. Because the magnetisation of the IP magnetised layer is now misaligned with the external field, the external field will apply a torque to its magnetisation. Spin being angular momentum, a torque acting on the magnetisation of a magnetic layer will not cause its magnetisation to align with the external field. Instead the magnetisation will experience a precession around the direction of the external field, with a small dampening causing this precession to decay over time. In Figure 2.8 d this path of precession of both the IP and OOP magnetisations are shown [4].

[4]There is a second precession contributing to the signal, which is the cause of the beating that can be seen in

The dynamics in such experiments are observed by the magneto optical Kerr effect (MOKE) in the "polar configuration". This signal is related to the OOP magnetisation of the multilayer. A time trace of a typical MOKE signal in such experiments is shown in Figure 2.9. In such a measurement we can see how the OOP magnetisation of the sample changes over time[5]. Indeed, on the time-scale of picoseconds we can see the ultrafast demagnetisation of the OOP layer quickly lowering the MOKE signal. On longer time-scales of tens to hundreds of ps we can see the remagnetisation of the OOP layer giving a gradual increase in the MOKE signal. Magnetic precessions of both layers gives the oscillating component of the signal. This oscillation is caused by the laser-induced spin currents between the layers, so is the most relevant component of the signal. By fitting the MOKE signal to a demagnetisation model with an additive dampened oscillation, we can calculate the amplitude of this oscillation. This amplitude can be compared to the amount of magnetisation that was lost in the initial demagnetisation. For this reason the experimental papers tend to quantify to what extend the precession is excited in terms of an efficiency; the precession amplitude per demagnetisation. Usually this can alternatively be thought of as the fraction of spin removed from the OOP layer that was absorbed by the IP layer [6].

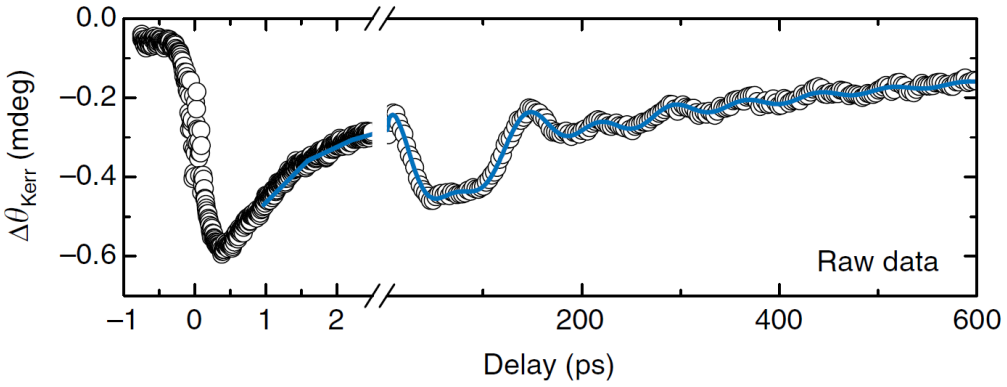

Figure 2.9: From the experimentel setup sketched in Figure 1.5, a MOKE time trace after laser excitation at $t = 0$. The MOKE signal measures the out-of-plane magnetisation of the sample. The ultrafast demagnetisation and subsequent remagnetisation of the out of plane layer is the dominant part of the signal. During the remagnetisation we can see oscillations corresponding to the magnetic precession of the in-plane magnetised layer. Adapted from [11], Figure 2C.

At this point the problem is applying the model introduced earlier in this chapter to such experiments. The goal is to calculate the excitation of the magnetic precession of the IP magnetised layer. This excitation is caused by an OOP polarised spin current being absorbed by the IP layer. To study the OOP component of the spin current we will chose spin up of our model as the OOP

the figure. This is an oscillation of the OOP magnetisation caused by the external magnetic field slightly canting it in-plane, and laser heating causing a demagnetisation and change in magnetic anisotropy. The two processions can effectively be separated from the data by a fit, such that it does not pose a problem to our discussion of spin currents.

[5]Technically, how the MOKE signal changes with the delay between the laser excitation and probing pulse.

[6]This interpretation of efficiency is only allowed when the transferred spin contributes to the excitation with approximately the same phase. Chapter 4 will further explore this situation.

direction, or alternatively the majority spin in the OOP magnetised layer. We write z_{IP} for the coordinate of the interface between the spacer and the IP magnetised layer, so the canting of the IP layer is then caused by the spin current over time $J_s(z_{\mathrm{IP}}, t)$.

Both theory and experiments suggest that in a ferromagnet, electrons with spin orthogonal to the majority spin are absorbed exceptionally efficiently [13]. Considering we have chosen spin up and down to be in the OOP direction, this causes the IP magnetised layer to quickly dissipate a spin up or spin down accumulation. We therefore choose to model the IP magnetised layer as being an ideal spin sink to OOP spin. In terms of the material parameters this corresponds to setting the spin-flip scattering rate $r \to +\infty$ in the IP layer. Any spin accumulation of thermal electrons in the IP layer is quenched as this effectively sets $\mu_s = 0$ within the IP magnetised layer. More specifically $\mu_s(z_{\mathrm{IP}}, t) = 0$.

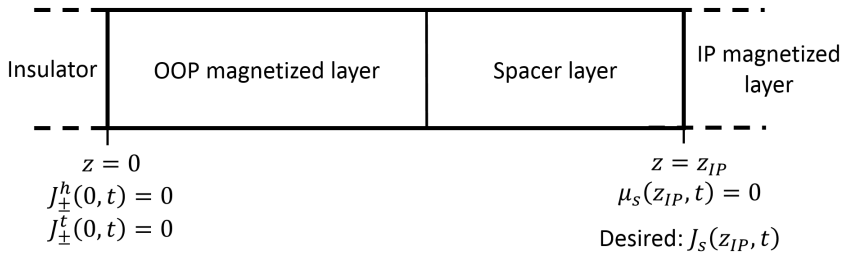

Figure 2.10: Working region of the spin-dynamics model applied to a typical model model of an experiment. The out of plane coordinate z on the horizontal axis. At $z = 0$ the interface with an insulating layer provides an insulating boundary condition, while at $z = z_{\mathrm{IP}}$ the IP magnetic layer being an ideal spin sink gives a zero spin accumulation boundary condition. Applying the presented model on such a system to find the excitation of the magnetic precession of the IP layer, we are ultimately interested in the spin current into the IP layer over time, $J_s(z_{\mathrm{IP}}, t)$.

We will tend to model the OOP magnetic layer to be sandwiched between the spacer and an insulator. The position of the interface between the insulator and OOP layer is chosen as $z = 0$. The insulator will give an insulating boundary condition at $z = 0$, and the IP layer being a perfect spin sink gives a boundary condition on $z = z_{\mathrm{IP}}$. This restricts the region where the spin dynamics have to be simulated to $0 < z < z_{\mathrm{IP}}$. This region contains the OOP magnetic layer and the spacer between the magnetic layers.

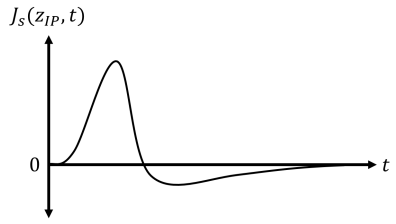

Figure 2.11: Sketch of the spin current into the IP magnetised layer over time after the multilayer experiencing laser excitation.

At this point the proposed model can be used for calculating the spin current into the IP magnetised layer over time. Figure 2.11 gives a rough sketch of what this spin current pulse could look like. In the case of hot electron effects causing the spin current, the flow of hot electrons would cause a spin current. The spin depletion caused by the excitation of these hot electrons would also cause a diffusion current with opposite sign, giving the two lobes with opposite signs sketched in the figure. When an *s-d* source is considered, the ultrafast demagnetisation inject a large spin accumulation which will diffuse into the IP layer to give a positive spin current. The following remagnetisation would extract spin from the thermal electrons, giving a spin depletion and a diffusion current with opposite sign, potentially giving a second lobe. The figure draws the two lobes as being distinct to clarify that multiple effects contribute to the spin current, which manifest at different times. This does not have to be the case in reality. The duration of the spin current pulse in question would have roughly have a ps duration, owing to the laser pulse used for excitation lasting some 100 fs, and the various processes contributing to the spin current equilibrating in similar time scales.

We still need some way to relate the calculated spin current over time to the thing we are actually measuring; the out-of-plane magnetic component corresponding to the magnetic precession of the in-plane magnetised layer. Because the initial canting is small, the canting process and the subsequent precession are approximately linear. We also neglect the dampening of the precession during excitation. The excitation amplitude A_ω of a magnetic precession mode with angular frequency ω, excited by a time-dependent spin current $J_s(z_{\mathrm{IP}}, t)$ into the magnetic layer can then be calculated using

$$A_\omega = \int_{-\infty}^{+\infty} \mathrm{d}t \, J_s(z_{\mathrm{IP}}, t) \, e^{i\omega t}. \tag{2.32}$$

The spin current $J_s(z_{\mathrm{IP}}, t)$ is the rate at which the IP magnetisation is canting at time t, while $e^{i\omega t}$ is the phase of this contribution. This A_ω contains both the amplitude and phase of the excitation. Taking the absolute value of it will extract purely the amplitude of excitation, which is the quantity we can relate to experiments. The current formulation of the model for ultrafast spin dynamics could already be applied to experiments, but we will refrain from doing so until approximations discussed in later chapters vastly simplify the problem.

2.6 Alternative parameterisations

To parameterise the state of the thermal electron system it is most straight-forward to use $\{N_+^t, N_-^t\}$ (or similarly $\{\mu_{0,+}, \mu_{0,-}\}$). While this works, there are alternative parameterisations that will have their use. In Chapter 3 we will change the model by requiring the charge to be zero everywhere, putting a constraint on the state of the thermal electron system. Using a parameterisation in terms of ρ will complement this constraint, so in Section 3.4 we will make use of the parameterisations introduced below.

Specifying the state of the thermal electrons in terms of the charge density ρ, the remaining degree of freedom can conveniently be specified by the spin accumulation μ_s or the thermal spin density N_s^t. The first gives a parameterisation in terms of $\{\mu_s, \rho\}$, while the second parameterisation would use $\{N_s^t, \rho\}$. Both of these alternative parameterisations can be interpreted as the thermal electron system consisting out of a spin and charge degree of freedom, the dynamics of which are interconnected. The transformations between $\{N_+^t, N_-^t\}$, $\{\mu_s, \rho\}$ and $\{N_s^t, \rho\}$ are one-to-one as long as the densities of state $D_\pm$ are both finite, so no information is lost by such a change in parameterisation.

Using (2.25) we can already calculate the time evolution of μ_s and N_s^t. The time evolution of the spin accumulation μ_s becomes

$$\frac{\partial}{\partial t}\mu_s = -\frac{\mu_s}{\tau} + S\frac{D_{\text{tot}}}{D_+D_-} - \frac{J_+^{t\,\prime}}{D_+} + \frac{J_-^{t\,\prime}}{D_-} - \frac{R_+}{D_+} + \frac{R_-}{D_-}, \qquad \tau = \frac{D_+D_-}{rD_{\text{tot}}}. \tag{2.33}$$

Here we introduced the spin-flip time scale τ. From (2.25) the time evolution of the thermal spin density N_s^t must be

$$\frac{\partial}{\partial t}N_s^t = -2r\mu_s + 2S - J_s^{t\prime} - R_+ + R_-. \tag{2.34}$$

In both Equation (2.33) and Equation (2.34) there is a term corresponding to spin flips, a term for the transport contribution, and the excitation or decay of hot electrons. To use (2.34) in practice, we would have to calculate μ_s from N_s^t using the cross transformation between the parameterisations provided below. This makes this parameterisation slightly awkward, but N_s^t does more clearly relate to continuity equations, in particular conservation of spin by transport.

To transform between the two parameterisations, we have the transformation from spin density to spin accumulation

$$\mu_s = \frac{1}{2}\frac{D_+ - D_-}{D_+D_-}\left(\rho/e + N^h\right) + \frac{1}{2}N_s^t\frac{D_{\text{tot}}}{D_+D_-}, \tag{2.35}$$

and the transformation from spin accumulation to spin density

$$N_s^t = -\left(\rho/e + N^h\right)\frac{D_+ - D_-}{D_{\text{tot}}} + 2\frac{D_+D_-}{D_{\text{tot}}}\mu_s. \tag{2.36}$$

The density of states is required to transform between units of energy and units of number density. Note that μ_s and N_s^t are in general not simply proportional. If the density of states changes (as happens in multilayers) the local density of state changes and the proportionality factor depends on the position z. Also, a term proportional to $\rho/e + N^h = -N^t$ with a correction for density of states also makes an additive contribution. These relations do show that $2\frac{D_+D_-}{D_{\text{tot}}}$ relates a change in μ_s to a change in N_s^t, so this factor can informally be thought of as an effective spin density of states. This factor appeared in Equation (2.33) too, where it could also be interpreted as an effective spin density of states.

This chapter introduced a model for the conducting electrons relevant for ultrafast spin currents, based on the Valet-Fert model. We discussed how the model and the various processes it describes are related to the studied experiments. Furthermore we showed some results relating to conservation laws in the model, and useful parameterisations of its state.

In principle, given the external processes driving spin currents, the model as it is presented can be implemented numerically to study the experiments under consideration. However, as is made clear by using one of the paramerisations of Section 2.6, this model includes both spin and charge dynamics. The charge dynamics complicates interpretation and implementation of the model, while we are only interested in the spin dynamics. The next chapter will provide an approximation to the model presented here with charge dynamics eliminated, making the model better suited for its intended application.

Chapter 3

Strong screening approximation

The model described in Chapter 2 includes both spin dynamics and charge dynamics. As the charge dynamics occurs on much faster time scales than the studied spin processes, we wish to remove these charge dynamics from the model. This would simplify further derivations, enable further intuition to be formed and improve performance of its numerical implementation. This chapter provides an approximation to the previously introduced model but with charge dynamics removed.

Section 3.1 will introduce and motivate the modification we make to the model. Section 3.2 will build on this modification to derive the related equation describing the currents of thermal electrons, with Section 3.3 using these to give equations for the spin currents. The strong screening approximation has simplified the equations for the thermal electron currents, which makes it interesting to revisit the time evolution of the thermal electron system state. This is done in Section 3.4.

3.1 The Strong screening approximation

The model proposed in Chapter 2 models both the accumulation of charge and the accumulation of spin, the charge and spin current and how all of these evolve over time. We are purely interested in the spin dynamics, so the charge dynamics is somewhat of a nuisance. Furthermore, the charge dynamics occur on much shorter time scales than the spin dynamics. This would be particularly inconvenient for numerical implementations of the model, as the numerical time step would have to be on the order of the charge dynamics time scales.

As the charge dynamics happen on substantially shorter time scales than the other processes contained in the model, during these other processes the charge dynamics is capable of nearly restoring its equilibrium. The charge dynamics would exactly be in equilibrium if there is zero local charge density at every position. The charge dynamics occurring at short time scales can then alternatively be put as any deviation of the charge ρ from 0 inducing an electric current that quickly (compared to time-scales of spin dynamics) restores $\rho \approx 0$. If we would approximate the charge dynamics as being instantaneous, this would give the stronger requirement of the system always having zero local charge density; $\rho = 0$.

The charge density being zero at all positions and times is not satisfied by the model described earlier, even if the system is prepared with $\rho = 0$. Movement of hot electrons carries charge, potentially producing a non-zero charge density. Even when no hot electrons are present charge can

build up in this model. If the spin specific conductivities at some point are different and a gradient in spin accumulation exists, a nett thermal electron current will arise, changing the accumulation of electrons. Interfaces between different materials with different conductivity provide another opportunity for the charge density to become non-zero.

While screening is fast, the screening time is finite as a non-zero charge density ρ is required for the E-field to become non-zero, which causes the screening. To have $\rho = 0$ exactly at all positions and times, the screening must be instantaneous; the E-field must screen charge before ρ deviates from 0. To do this, we should modify the behaviour of the E-field to work in an "active" instead of "reactive" manner. A natural step would be to replace the electric field equation $E' = \rho/\epsilon_0$ with a different specification of the E field, while keeping the remainder of the model unchanged. It turns out that keeping the remainder of the model and the exactly zero charge requirement uniquely specifies the E-field for any system state. Note that keeping the remaining equations of the model, we still have $V' = -E$ relating the electric field to the electric potential V. The electric potential V will still contribute to the electrochemical potentials $\mu_\pm$ in a non-trivial way, making $\mu_\pm$ substantially different than $\mu_{0,\pm}$. In fact, this contribution is exactly the screening.

From conservation of electrons as described in Equation (2.31), $\rho = 0$ implies that the total electron current J is constant[1]. Furthermore, the multilayers in the experiments we attempt to describe have an insulating boundary condition, fixing this electron current to $J = 0$[2]. This zero electron current will serve as the foundation of the strong screening approximation.

Note that imposing zero current stops the discussed model from being a generalisation of the Valet-Fert model, as the giant magnetoresistance measurements clearly have a non-zero out of plane current flowing through the multilayer.

3.2 Thermal electron currents

We wish to calculate the spin specific thermal electron currents $J^t_\pm$. Equation (2.9) states that these are described by

$$J^t_\pm = -\sigma_\pm \left(\mu'_{0,\pm} + eE\right). \tag{3.1}$$

Now that we are in the strong screening approximation, the electric field E is no longer specified by Gauss' law. Instead, we now require no total electron current, $J = 0$, which implies $J^t_+ + J^t_- = -J^h$. With above equation this requires the electric field to conform to

$$eE = \frac{J^h - \sigma_+\mu'_{0,+} - \sigma_-\mu'_{0,-}}{\sigma_{\text{tot}}}. \tag{3.2}$$

This is our new equation for calculating the electric field, replacing Gauss' law. Substituting this into (3.1) gives

$$J^t_\pm = -\frac{\sigma_\pm}{\sigma_{\text{tot}}}\left(\sigma_{\text{tot}}\,\mu'_{0,\pm} + J^h - \sigma_+\,\mu'_{0,+} - \sigma_-\,\mu'_{0,-}\right). \tag{3.3}$$

Writing the equation for both spin + and − and simplifying shows that the spin specific thermal electron currents $J^t_\pm$ are specified by

$$J^t_\pm = \mp\sigma_{\text{diff}}\,\mu'_s - \frac{\sigma_\pm}{\sigma_{\text{tot}}}J^h, \qquad \sigma_{\text{diff}} = \frac{\sigma_+\sigma_-}{\sigma_{\text{tot}}}. \tag{3.4}$$

[1] In turn $J' = 0$ implies ρ is constant in time, so enforcing $J' = 0$ and neutral charge in the initial state is sufficient to satisfy the constraint $\rho = 0$.

[2] More-over, there is an interface with air which definitely does not conduct electrons to a meaningful extent.

The thermal currents are composed of two terms, the first is a diffusion current proportional to μ_s' through the "spin diffusion conductivity" σ_{diff}. Other work refers to this material property as the "spin averaged conductivity" or the "effective conductivity". The spin + diffusion current is equal and opposite to the spin − diffusion current, so non-zero diffusion will never move charge but always move spin. The second term is the screening of the hot electron current J^h. The fraction of spin + screening electrons to spin − screening electrons is simply the ratio of spin specific conductivities σ_+/σ_-.

It is interesting to see that the diffusion term depends on the state of the thermal system $\mu_{0,\pm}$ only through μ_s. To see why this happened, write $\mu_{0,\pm}$ in an even and odd (under change of spin label) component; $\mu_{0,\pm} = \frac{1}{2}(\mu_{0,+} + \mu_{0,-}) \pm \frac{1}{2}\mu_s$. In Equation (3.1) the spatial derivative of the even term contributes to both $J_\pm^t$ exactly as an electric field would, and it being non-zero would contribute to the total charge current. However, we choose the electric field such that no total charge current exists; the electric field will perfectly cancel any contribution of the even term. Put differently, $[\mu_{0,+} + \mu_{0,-}]' \neq 0$ attempts to move charge but is overruled by strong screening.

Moreover, the diffusion term only depends on the material properties $\sigma_\pm$ through σ_{diff}. This will be convenient in the important special case of the model where no hot electrons are present, so only diffusive processes remain. We have actually seen σ_{diff} appear in such a situation earlier; the spin diffusion length λ as was given in Equation (2.6) can be written as

$$\lambda = \sqrt{\frac{\sigma_{\text{diff}}}{r}}. \tag{3.5}$$

3.3 Spin currents

Combining both versions of Equation (3.4) gives the full thermal contribution to the spin current as

$$J_s^t = -2\,\sigma_{\text{diff}}\,\mu_s' - \frac{\sigma_+ - \sigma_-}{\sigma_{\text{tot}}} J^h, \tag{3.6}$$

and the total spin current

$$J_s = -2\,\sigma_{\text{diff}}\,\mu_s' + J_+^h - J_-^h - \frac{\sigma_+ - \sigma_-}{\sigma_{\text{tot}}} J^h, \tag{3.7}$$

where we see that spin current is caused by three contributions. In the order of appearing in above equation; diffusion of thermal electrons, flow of hot electrons, and flow of thermal electrons to screen the hot electrons. Diffusion and screening are contained in J_s^t, while hot electron flow is contained in J_s^h. We can choose to to combine the hot electron and screening terms in a term called J_s^*, giving

$$J_s = -2\,\sigma_{\text{diff}}\,\mu_s' + J_s^*, \qquad J_s^* = 2\frac{\sigma_- J_+^h - \sigma_+ J_-^h}{\sigma_{\text{tot}}}. \tag{3.8}$$

We can calculate J_s^* using only $J_\pm^h$, so not requiring any knowledge of the state of the thermal system through μ_s. Note that J_s^* may be substantially different from J_s^h, it can even have a different sign. This approach of grouping the spin current contributions will become particularly convenient when studying the steady state solution of the model as will be done in Chapter 5.

3.4 Time evolution

Before imposing strong screening, the thermal electron system had $N_\pm^t$ as mutually independent electron densities, with $J_\pm^t$ as the associated electron current densities. When strong screening was enforced, the constraints $\rho = 0$, $J = 0$ dropped one degree of freedom in the system of thermal electrons. The thermal electron model is reduced from two interacting populations, + and −, to effectively a single spin density population with the associated thermal spin current [3]. Parameterising the thermal electron system in terms of $N_\pm^t$ under the strong screening constraint is therefore somewhat inconvenient. As is done in Lagrangian mechanics, it is often more convenient to deal with constraints by using a different parameterisation in which the constraint is simpler to enforce. In this case either of the parameterisations introduced in 2.6 parameterise the thermal electron system in therms of ρ, making it easier to enforce $\rho = 0$. Using these, the remaining degree of freedom is either μ_s or N_s^t. The time evolution associated with these were shown in (2.33) and (2.34). Now that we have derived Equation (3.4) providing $J_\pm^t$ under the strong screening approximation we can rewrite the time derivative of the spin accumulation and the time derivative of the thermal spin density as

$$\frac{\partial}{\partial t}\mu_s = -\frac{\mu_s}{\tau} + S\frac{D_{\text{tot}}}{D_+ D_-} + \left[\sigma_{\text{diff}}\,\mu_s'\right]'\frac{D_{\text{tot}}}{D_+ D_-} - \frac{R_+}{D_+} + \frac{R_-}{D_-} + \frac{J^{h\prime}}{\sigma_{tot}}\left(\frac{\sigma_+}{D_+} - \frac{\sigma_-}{D_-}\right) + J^h\frac{\sigma_{\text{diff}}}{\sigma_{\text{tot}}}\left(\frac{\sigma_+'}{\sigma_+} - \frac{\sigma_-'}{\sigma_-}\right)\frac{D_{\text{tot}}}{D_+ D_-}, \quad (3.9)$$

$$\frac{\partial}{\partial t}N_s^t = \underbrace{-2\,r\,\mu_s + 2\,S}_{\text{A}} \quad \underbrace{+2\left[\sigma_{\text{diff}}\mu_s'\right]'}_{\text{B}} \quad \underbrace{-R_+ + R_-}_{\text{C}} \quad \underbrace{+J^{h\prime}\frac{\sigma_+ - \sigma_-}{\sigma_{\text{tot}}}}_{\text{D}} \quad \underbrace{+2J^h\frac{\sigma_{\text{diff}}}{\sigma_{\text{tot}}}\left(\frac{\sigma_+'}{\sigma_+} - \frac{\sigma_-'}{\sigma_-}\right)}_{\text{E}}. \quad (3.10)$$

If we choose to parameterise the system in terms of the spin density N_s^t, we would still need to calculate the spin accumulation μ_s using Equation (2.35) with $\rho = 0$ to evaluate the system evolution. These equations show the five effects that may contribute to the time evolution of the thermal electron system. The various terms in Equations (3.9) and (3.10) are explained in more detail below, but briefly stating what these terms represent; (A) captures spin-flips of thermal electrons, either driven by μ_s or by the external spin source S. (B) describes diffusion of spin in the thermal electron system. (C) gives the contribution of excitation (respectively, decay) of hot electrons, which removes (adds) electrons and their spin from (to) the thermal electron system, changing the spin accumulation and spin density. Finally, (D) and (E) are related to transport of hot electrons which induces screening currents in the thermal electron system. More specifically, (D) describes the effect of screening currents in bulk material. When the conductivity changes on material interfaces an additional contribution (E) appears.

Note that all terms in Equation (3.9) contain a factor of the density of states (internalized in the case of τ) which is required to translate from the rate of change of the number density to the rate of change in chemical potential [4]. In contrast Equation (3.10) does not mention density of states, but when calculating μ_s from N_s^t the density of states needs to be used.

Spin flips (A) and spin diffusion (B) are the only processes that are mostly "internal" to the thermal electron system, as the terms (C), (D) and (E) stem from interactions with hot electrons.

[3] This is related to the importance of $\sigma_\pm$ in calculating $J_\pm^t$. In Equation (3.1) $\sigma_\pm$ were important, but strong screening reducing the thermal electrons to effectively a single population, a single combined conductivity σ_{diff} appeared in (3.4).

[4] The opposite effect of this is that in steady state the rate of change of both the number density and chemical potential must be 0, so the density of states becomes unimportant. This will become clear in Chapter 5.

If the hot electron system is disabled by setting $R_\pm = 0$, $J^h_\pm = 0$ to only study s-d spin current sources, we are left with (A) and (B) and the model reduces to

$$\frac{\partial}{\partial t}\mu_s = -\frac{\mu_s}{\tau} + S\frac{D_{\text{tot}}}{D_+ D_-} + [\sigma_{\text{diff}}\,\mu_s']'\,\frac{D_{\text{tot}}}{D_+ D_-}, \tag{3.11}$$

$$\frac{\partial}{\partial t}N_s^t = \underbrace{-2\,r\,\mu_s + 2\,S}_{\text{A}} \quad \underbrace{+2\,[\sigma_{\text{diff}}\,\mu_s']'}_{\text{B}}. \tag{3.12}$$

These equations closely resemble the standard diffusion equation $\frac{\partial \phi}{\partial t} = \text{source} + \frac{\partial}{\partial x}[D\frac{\partial \phi}{\partial x}]$ with a source term, but the density of states present a crucial difference. Only where D_{tot}/D_+D_- is constant in space we can pull it through a spatial derivative to get the diffusion coefficient

$$D = \sigma_{\text{diff}}\frac{D_{\text{tot}}}{D_+ D_-}, \tag{3.13}$$

where technically the diffusion coefficient D may still change with z if σ_{diff} does. This approach breaks down on material interfaces, where D_{tot}/D_+D_- will in general change over z, so only within uniform layers the diffusion equation can be used. In uniform layers we get a new relation for the spin diffusion length in terms of the diffusion coefficient as defined by Equation (3.13)

$$\lambda = \sqrt{\tau D}, \tag{3.14}$$

which is the standard equation for the mean free path in diffusive transport. A sketch of the diffusive processes within a single homogeneous layer is shown in Figure 3.1. The figure shows a spatially varying spin accumulation. The gradients cause a diffusive spin current, drawn as horizontal arrows representing the movement of spin. Also, the spin accumulation will drive spin flips, which are drawn as vertical arrows representing the decrease of the local spin accumulation by these local spin flips. If the spin accumulation shown in Figure 3.1 are translated back to the underlying spin accumulations, Figure 2.6 would be reproduced.

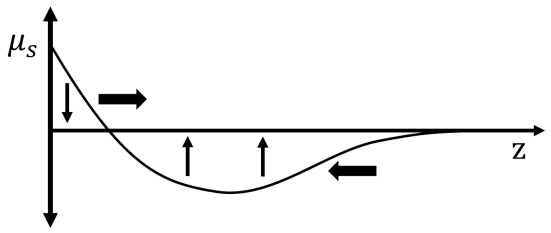

Figure 3.1: Spin flips and diffusion in the strong screening model. On the vertical axis the spin accumulation μ_s, and position z on the horizontal axis. The horizontal arrows represent diffusive spin currents, transporting spin from large to small spin accumulation. The vertical arrows represent spin flips from the $-2\,r\,\mu_s$ term, working to reduce the local spin accumulation. This figure conveys the same processes as shown in figure 2.6. Instead of the separate spin + and spin − populations shown in that figure, the strong screening has reduced these to effectively a single population.

The hot electron system can be thought of as providing additional source terms to the thermal system, either by adding or removing spin, or imposing thermal electron currents through screening. Adding or removing spin is caused by hot electron excitation and decay, as captured by (C) in Equations (3.9) and (3.10). Through screening, a hot electron current will cause a thermal electron current. Figure 3.2 shows an example of a hot electrons current causing a screening current. Change in the spin accumulation and spin density can be caused by a difference in the in-flow of thermal electrons compared to the out-flow. The figure shows two ways in which this can happen; a change in hot electron current or a change in material properties. A change in hot electron current happens at the initial and final positions of the hot electron. At the initial position of the hot electron, there is a screening current in-flow without out-flow. At the final position there is no in-flow but a finite out-flow. These contributions to the time evolution of the spin accumulation and spin density are contained in (D) of Equations (3.9) and (3.10).

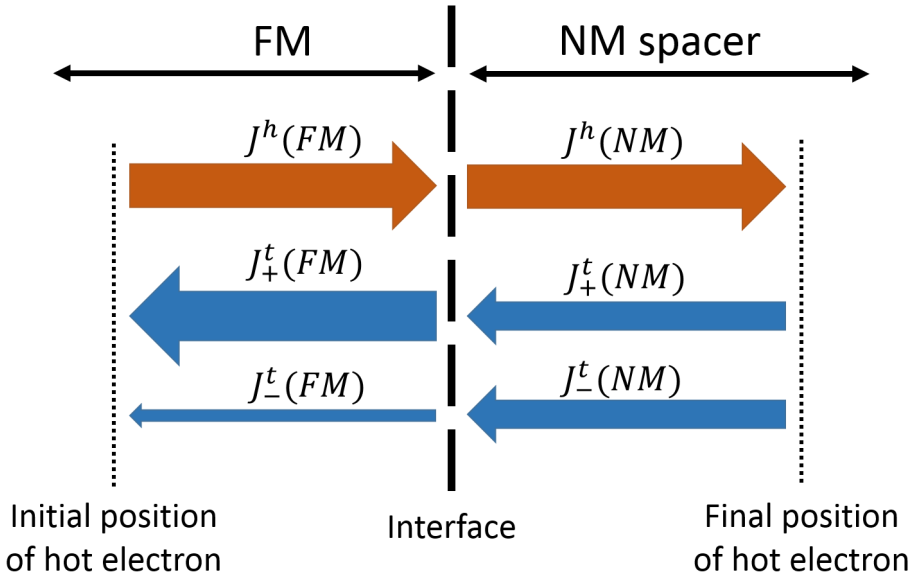

Figure 3.2: A hot electron current (orange) and the spin specific screening currents (blue) associated with it. z on the horizontal axis. The left half of the figure represents a ferromagnetic material, while the right is a nonmagnetic metal. At every position the screening currents must exactly compensate the hot electron current. The spin composition of the screening currents depends on the spin-specific conductivity, so the spin-specific screening currents will change over material interfaces.

At the interface between the ferromagnetic and nonmagnetic layer, the spin polarisation of in-flow screening current differs to that of the out-flow. In this example more spin + electrons flow away from the interface than towards it, and more spin − flow in than out. This allows screening currents to change the spin density and spin accumulation at material interfaces, which is described by the (E) term of Equations (3.9) and (3.10).

The strong screening approximation has substantially simplified the model of thermal electrons. Where the model initially consisted of two thermal electron populations and dynamics on screening time-scales, we now have effectively a single population changing on spin diffusion time-scales. Writing a numerical implementation of the model becomes much more tractable. Also the model has become less complex to interpret. In particular, because motion of hot electron now directly modifies the thermal electrons instead of indirectly through electric fields, their effect has become clearer. While we are set to calculate spin current profiles, realise that the measurements from experiments we are studying do not provide spin currents, but only the tilting of a magnetisation. In the next chapter we show how this measurement process allows further simplification of the model in the context of the experiments under consideration.

Chapter 4

Zero phase approximation

In Chapters 2 and 3 a model was build up that can be used to calculate spin currents in the context of ultrafast spin dynamics. In the experiments under consideration these spin currents cause the canting and subsequent precession of a magnetisation, which is the effect that is measured. It turns out that the spin current causing the canting is effectively instantaneous compared to the period of the precession. As will be expanded on in Section 4.1 this causes only the total amount of spin injected to be of relevance to the experimental observations. Realising that we are not interested in the spin current over time, but just its integral over time allows the model to be simplified even further. This simplification will be discussed in Section 4.2.

4.1 Excitation of magnetic precessions

One of the main goals of the model derived in Chapters 2 and 3 was to study ultrafast spin currents exciting a magnetic precession in experiments such as [11, 12, 13]. How the presented model would be applied to these was discussed in Section 2.5. Equation (2.32) stated that the amplitude A_ω of a mode with angular frequency ω by a time-dependent spin current $J_s(z_{\mathrm{IP}}, t)$ into the in-plane magnetic layer can be calculated as

$$A_\omega = \int_{-\infty}^{+\infty} \mathrm{d}t \, J_s(z_{\mathrm{IP}}, t) \, e^{i\omega t}. \tag{4.1}$$

It is interesting to compare the time-scale of $J_s(z_{\mathrm{IP}}, t)$ with the time scale of the magnetic precessions, captured in $e^{i\omega t}$. In experiments studying homogeneous magnetic precessions, these precessions have a frequency in the order of 10 GHz giving a period of some 100 ps [11]. Regarding the duration of spin current pulses, the slowest process in our model is remagnetisation driving spin flips through S, which tends to be of picosecond time scale. This suggests that spin currents should be much shorter than the magnetic precessions they excite. The experimental observations seem to verify this, as the MOKE measurements in the first tens of ps are already well described by the fit to a damped oscillation.

As the period is much longer than the spin current, so $e^{i\omega t}$ is approximately constant during the period when $J_s(z_{\mathrm{IP}}, t)$ is non-negligible. Approximating $e^{i\omega t}$ as being constant during the spin

current pulse, we can approximate Equation (4.1) as

$$A_\omega \approx e^{i\phi} \int_{-\infty}^{+\infty} \mathrm{d}t \, J_s(z_{\mathrm{IP}}, t), \tag{4.2}$$

where ϕ gives the phase related to the center of the spin current pulse. Luckily, the magnitude of excitation can be calculated without requiring knowledge of the phase. In conclusion, to find the magnitude of excitation we can approximately solve the problem by just finding the total spin transfer;

$$|A_\omega| \approx \int_{-\infty}^{+\infty} \mathrm{d}t \, J_s(z_{\mathrm{IP}}, t). \tag{4.3}$$

To find the magnitude of excitation $|A_\omega|$ we could go through the process of using the model for ultrafast spin currents to calculate the spin current into the absorbing layer $J_s(z_{\mathrm{IP}}, t)$ to plug this result into Equation (4.3). Because we are ultimately interested in calculating $|A_\omega|$ we might as well compose these steps into a single larger one. The next section will show that this combined step can be simplified substantially.

So far this section only discussed homogeneous magnetic precessions with frequencies of the order 10 GHz. However, in similar experiments inhomogeneous spin wave modes have been observed. These have much higher frequencies, up to THz [13], giving periods as short as ps. These periods are potentially similar to the spin current pulse duration, so the validity of using the zero-phase approximation to these experiments is less clear. Still, it is quite possible that the spin currents pulses have a duration of few tens of ps, which would give a big enough margin for the zero-phase approximation to hold. In the experiment of [13] the excitation efficiency seems fairly constant for the observed range of frequencies, from 0.5 THz to 1.2 THz. This would suggest that the driving spin current pulse has little Fourier components in this frequency range, giving some hope that the spin current pulse could be short enough to use the zero-phase approximation when studying these experiments[1].

4.2 Relation with linear time invariance of the model

The models derived earlier are linear time invariant (LTI); both before and after the strong screening approximation was applied. Time invariance of a system means that shifting the moment labeled as $t = 0$ does not affect the model. Linearity of a system S means that given two inputs I_1, I_2 and the related system responses $O_1 = S[I_1], O_2 = S[I_2]$, the response of the input $I_1 + I_2$ is $S[I_1 + I_2] = O_1 + O_2$. Also, scaling an input will give a scaling of the output $S[\alpha I] = \alpha S[I]$. In the model described in the previous chapters, external influences of the *s-d* spin source or hot electron dynamics would be the input. The output we are most interested in is the spin current into the spin absorbing layer over time. As above section showed that its time integral relates to the measured precession amplitude.

[1] Even if slower processes contribute to the spin current pulse, these contributions being slow would prevent them from efficiently contributing to the excitation. In that case, removing these processes from the spin current pulse would barely change the excitation. For example, suppose that the remagnetisation gives a slow *s-d* contribution while the other processes are plenty short. We could cheat by removing remagnetisation from the model, barely affecting excitation of magnetic precessions, and afterwards use the zero-phase approximation on the short spin current pulse that remains.

For a moment we keep the discussion more abstract and discuss any LTI system where we want to study the integral of its output signal over all time, $\int_{-\infty}^{+\infty} \mathrm{d}t\, O(t)$. To keep the discussion simple, we will take the input as being a real valued function of time. We can then decompose the input into Dirac delta functions

$$I(t) = \int_{-\infty}^{+\infty} \mathrm{d}t'\, I(t')\, \delta_{t'}(t) \tag{4.4}$$

where $\delta_{t'}$ is the Dirac delta peaking at t'; $\delta_{t'}(t) = \delta(t - t')$. In this section primes are used as part of the variable name instead of a spatial derivative. If we now calculate the integral of the related output, above decomposition works well with the linearity of the system. Furthermore using time-invariance and a change of variables we find

$$\begin{aligned}
\int_{-\infty}^{+\infty} \mathrm{d}t\, O(t) &= \int_{-\infty}^{+\infty} \mathrm{d}t\, S[I](t) \\
&= \int_{-\infty}^{+\infty} \mathrm{d}t\, S\left[\int_{-\infty}^{+\infty} \mathrm{d}t'\, I(t')\delta_{t'}\right](t) \\
&= \int_{-\infty}^{+\infty} \mathrm{d}t'\, I(t') \int_{-\infty}^{+\infty} \mathrm{d}t\, S\left[\delta_{t'}\right](t) \\
&= \int_{-\infty}^{+\infty} \mathrm{d}t'\, I(t') \int_{-\infty}^{+\infty} \mathrm{d}t\, S\left[\delta_0\right](t - t') \\
&= \left(\int_{-\infty}^{+\infty} \mathrm{d}t'\, I(t')\right) \left(\int_{-\infty}^{+\infty} \mathrm{d}t''\, S\left[\delta_0\right](t'')\right).
\end{aligned} \tag{4.5}$$

This can be thought of as saying that to find the area under the output curve given some input, we can multiply the area under the input curve by the area under the output curve corresponding to a Dirac delta input. The result now depends on the system only through the response to a delta input. We can further simplify the factor containing the system. Using time invariance to shift the moment of evaluation to 0, using linearity of the system and evaluating an integral over a delta function we get

$$\int_{-\infty}^{\infty} \mathrm{d}t\, S[\delta_0](t) = \int_{-\infty}^{\infty} \mathrm{d}t\, S[\delta_{-t}](0) = \left(\int_{-\infty}^{\infty} \mathrm{d}t\, S[\delta_{-t}]\right)(0) = S\left[\int_{-\infty}^{\infty} \mathrm{d}t\, \delta_{-t}\right](0) = S\left[C_1\right](0), \tag{4.6}$$

where C_a stands for the function that returns a regardless of the input; $C_a(t) = a$. As we are feeding a constant function into the system, it immediately follows that $S[C_1]$ is a system in steady state. This potentially makes the problem much simpler to solve than the dynamic we started with. Inserting this into Equation (4.5) and rewriting gives the final result

$$\int_{-\infty}^{+\infty} \mathrm{d}t\, O(t) = S\left[C_{\int_{-\infty}^{+\infty} \mathrm{d}t\, I(t)}\right](0). \tag{4.7}$$

Informally, this derivation shows that in LTI systems (with real valued input and output functions) we may change an integral over the output to an integral over the input, making the new input function constant in time. As the input is steady the entire system must be in steady state, potentially hugely simplifying the equations to be solved and interpreted. In fact, Equation (4.7)

holds in the much more general setting where the input and output functions may be in vector-valued function spaces $I : \mathbb{R} \to V$ and $O : \mathbb{R} \to W$ [2]. The derivation of this more general result is performed in Appendix B. Note that the integral we are moving from output to input has dimensions of time. This means that every property of the state has picked up a dimension time. For example, starting with Equation (4.5) the output of S was the spin current, which we needed to integrate over time to get the total transferred spin. In Equation (4.7) the output of the steady-state S is the total transferred spin.

Connecting this abstract result to ultrafast spin dynamics, Equation (4.3) showed that we are interested in the integral of a spin current. The thermal electron system is linear with combination of the spin source S and hot electron system behaviour $R_\pm$, $J^h_\pm$ as input. These inputs are in function spaces, so we can use the generalized result to justify using the virtual steady state perspective.

The derivation above was based on the abstract property of the model in consideration being LTI. It is also possible to algebraically perform this change in perspective by integrating the equations governing the system over time and rearranging the result. As an example, we perform this change in perspective for the thermal electron model with S, $R_\pm$ and $J^h_\pm$ as input. First, take the integral over the local thermal spin current given by (3.6) over all time

$$\int \mathrm{d}t\, J^t_s(z,t) = -2\,\sigma_{\text{diff}}(z)\left[\int \mathrm{d}t\,\mu_s(z,t)\right]' - \frac{\sigma_+(z)-\sigma_-(z)}{\sigma_{\text{tot}}(z)}\int \mathrm{d}t\, J^h(z,t). \tag{4.8}$$

Notice the prime indicating that we take the spatial partial derivative of the therm in square brackets. Similarly, integrate the evolution of the local thermal spin density as given by (2.34) over all time [3]

$$\begin{aligned} N^t_s(z,t=+\infty) - N^t_s(z,t=-\infty) \;=\; -\,2\,r(z)\int \mathrm{d}t\,\mu_s(z,t) - \left[\int \mathrm{d}t\, J^t_s(z,t)\right]' + \\ \int \mathrm{d}t\,\big(2S(z,t) - R_+(z,t) + R_-(z,t)\big). \end{aligned} \tag{4.9}$$

At time $t = -\infty$ the system is prepared in an equilibrium state. At some time the experiment is performed and after waiting an infinitely long time the system will return to this equilibrium. From this $N^t_s(z,t=+\infty) - N^t_s(z,t=-\infty) = 0$. If we write an overline as the integral over all time of the variable under it, for example $\bar{J}_s(z) = \int \mathrm{d}t\, J_s(z,t)$, the two equations above can be written as

$$0 = -2\,r\,\bar{\mu}_s - \bar{J}^{t\,\prime}_s + 2\bar{S} - \bar{R}_+ + \bar{R}_-, \qquad \bar{J}^t_s = -2\,\sigma_{\text{diff}}\,\bar{\mu}'_s - \frac{\sigma_+ - \sigma_-}{\sigma_{\text{tot}}}\bar{J}^h. \tag{4.10}$$

This looks exactly like the equations we started with, but all time-dependent quantities picking up an overline and a dimension time, and the time evolution was removed by setting $\bar{N}^{t\,\prime}_s = 0$ [4]. If the

[2] The vector spaces V and W are allowed to be of infinite dimensionality, so V and W may even be function spaces.

[3] While we use the equation for $J^t_\pm$ under the strong screening approximation, the same can be done with the original equation (2.2) and a longer derivation. It turns out the result of such a derivation will be the same as found here, as will become clear in Section 5.1.

[4] This derivation shows a similarity between this approach of reducing a time dependent model to a steady state one with the more common quasi-static approximation, which has the same effect of transforming a dynamic model to a stationary one. The quasi-static approximation effectively approximates the change in local accumulation as negligible compared to flow terms. In the approach presented here we were able to integrate the equations governing the model over all time. The initial state is the same as the final state, so the total change in local accumulation must be 0, and in the time-integrated model all terms corresponding to changes in accumulation vanish. In short, in the quasi-static approximation in-flow and out-flow approximately cancel each other in every instant, but when studying a time-integrated LTI model with the same initial as final state, the total in-flow and cancels the total out-flow.

external processes acting on the thermal system ($\bar{S}$, $\bar{R_\pm}$ and $\bar{J^h_\pm}$) are known, we can use this as a coupled differential equation to solve for $\bar{\mu_s}$ and $\bar{J^t_s}$. Adding the time integrated hot electron spin current we have found the total spin transfer into the absorbing layer $\int \mathrm{d}t\, J_s(z_{\mathrm{IP}}, t) = \bar{J}_s(z_{\mathrm{IP}}) = \bar{J}^t_s(z_{\mathrm{IP}}) + \int \mathrm{d}t\, J^h_s(z_{\mathrm{IP}}, t)$. The zero phase approximation showed that the total spin transfer equals the excitation of the magnetic precession, $\bar{J}_s(z_{\mathrm{IP}}) = A_\omega$, which is exactly what we wanted to know. In this process we have avoided calculating the time-dependent J_s or μ_s and having to deal with the partial differential equations governing them.

Again, note that the steady state system we have changed perspective to has added a dimension time to every parameter. If we are interested in the total spin transfer into the IP layer of the dynamic model, $\int \mathrm{d}t\, J_s(z_{\mathrm{IP}}, t)$, that means we are interested in the virtual spin current of the steady-state model $\bar{J}_s(z_{\mathrm{IP}})$. This extra unit time appearing through the model makes it clear that the "virtual steady state solution" in this new perspective (the right side of Equation (4.7) or $\bar{\mu_s}$, $\bar{J^t_s}$ in (4.10)) does not represent a state that will physically materialize at some time during the studied process. Rather, it represents the combination of all transient states. Some transient states may show substantially different behaviour than this integral. For example, consider hot electrons temporarily moving a lot of spin out of a magnetic layer, but shortly afterwards much of the spin diffuses back. The dynamic model would show a brief spin depletion in the magnetic layer. Experimentally such a temporal depletion could be measured by MOKE as part of the demagnetisation. The steady-state perspective would provide little information on such effects. Instead, performing the time integral will cause the hot electron spin current and diffusive spin current to overlap, showing the net spin transfer to be marginal. This example shows that spin transport causing a demagnetisation signal does not need to imply a net spin transfer. The original paper introducing superdiffusive spin transport[9] was concerned with demagnetisation in the first few hundred femtoseconds. The net spin transfer is a related but different effect, making our study of superdiffusive spin transport largely orthogonal to its original treatment.

Besides the model having to be LTI, a major constraint is calculating the relevant inputs of the model without need of the internal state of the model. As a concrete and important example; one might model the external spin source S to depend on the spin accumulation μ_s already present in the thermal electrons. We would have to calculate the time-dependent spin accumulation in order to calculate the time-dependent external spin source. If the contribution of μ_s to S is LTI we could potentially resolve the problem by studying a larger LTI model that describes the combination of thermal electrons, the external spin source and their interaction. This larger model also being LTI, the presented abstract proofs show that this model can also be analysed from a steady-state perspective.

In this chapter, we showed that the process of observing the spin currents through an excited magnetic precession implies that we often only need to know the total spin transfer. In turn, only being interested in the total spin transfer allows the transient dynamics to be "forgotten", and a simpler model that appears like a steady state model provides enough information to calculate the excitation of magnetic precessions. The next chapter will discuss this simpler model in more depth.

Chapter 5

Steady-state

Chapter 4 showed that some experimental observations can be studied using a virtual steady-state system, governed by the same equations as the dynamic model with all time derivatives set to 0. We can use this approach to use the model presented in this thesis, but as we are looking for a steady state solution the model can be simplified substantially. This chapter will discuss the these simplified equations governing solutions in steady state.

Section 5.1 will discuss the relation between the steady-state constraint and the strong screening approximation. The equations governing the steady state case are shown in Section 5.2. The steady-state requirement makes the system a lot simpler, the governing equations are a lot shorter and steady-state makes conservation laws much more restrictive. Section 5.3 will use this to give some insights into the behaviour of the steady-state model. The spin diffusion length is an important parameter emerging from the underlying material properties. Section 5.4 will discuss some of the intuition related to it.

While the governing equations of steady state and "virtual steady state" are the same, they describe different functions. For example spin currents in the "virtual steady state" correspond to the total spin transfer, i.e. time integrated spin current of the dynamic model. While the virtual steady state is used for interpreting experiments, in this chapter we will write everything as the dynamic model being in steady state. That the results regarding steady state spin currents can be applied to time integrated spin currents of the dynamic model is understood implicitly.

5.1 Relation to strong-screening approximation

Reminding ourselves of conservation of electrons as given by Equation (2.31) it is obvious that in steady state J must be a constant. Because we study multi-layers with air interfaces and non-conducting substrates this constant is fixed as $J = 0$. This is exactly the assumption that the steady state approximation given in Chapter 3 was built on top of, so in steady state the equations for $J^i_\pm$ derived under the steady state approximation have become exact. Alternatively this can be thought of as the model from Chapter 2 and its modification from Chapter 3 reducing to the same model once being in steady-state is imposed.

5.2 Governing system of differential equations

The obvious way of finding the equations governing the steady state solution is to take the equations for the time evolution, Equation (3.9) or (3.10), and simply set the time derivative to 0. This is valid and the interpretation of effects related to their terms remain useful, but the resulting differential equation of the spin accumulation or spin density are fairly involved [1]. Also, we are ultimately not interested in the spin accumulation μ_s or spin density N_s^t themselves, but in the resulting total spin current J_s.

Being in steady state, the conservation of spin as stated in Equation (2.30) becomes much more restrictive. Combined with Equation (3.8) we get the system of differential equations

$$0 = -J_s' - 2\,r\,\mu_s + 2\,S, \qquad J_s = -2\,\sigma_{\text{diff}}\,\mu_s' + J_s^* \tag{5.1}$$

that given some boundary conditions and the "inputs" S and J_s^* uniquely fix J_s and μ_s. Alternatively this system of equations can be written as a second order differential equation describing the thermal electron state in terms of μ_s by taking the spatial derivative of the right equation to eliminate J_s' from the left equation. This gives

$$2\,r\,\mu_s - 2\,\left[\sigma_{\text{diff}}\,\mu_s'\right]' = 2\,S - J_s^{*\prime}. \tag{5.2}$$

Once a solution μ_s is found, Equation (3.8) can be used to find the corresponding spin current. Similarly we can take the first derivative of the left equation in (5.1) to eliminate μ_s and get a second order equation in the total spin current J_s, as

$$\sigma_{\text{diff}}\left[\left(J_s' - 2\,S\right)/r\right]' = J_s - J_s^*. \tag{5.3}$$

The hot electron system affects the thermal electron system through excitation, decay and screening, but above equations show that in steady-state these mechanisms only act on the thermal electron system through the screened hot electron spin current J_s^*. In particular Equation (5.2) shows that J_s^* acts on the thermal system exactly like some spin source would. From the perspective of the thermal electron system the only thing the hot electron system does is removing spin at one position and placing it elsewhere. To calculate the total spin current we also do not need more knowledge of the hot electron system than J_s^*.

A reason these equations are convenient is that we were able to combine the influences of the hot electron system, $R_\pm$ and $J_\pm^h$, into J_s^*, combining excitation and transport of both spins. Unfortunately such a formulation is impossible in the dynamic case. The fundamental reason for this is that in the time-dependent system excitation and transport of hot electrons may occur at different moments, so rate of excitation and transport are decoupled. This prevents us from being able to say something about the excitation rate solely on hot electron currents. In steady state the continuity equation for hot electrons as written in (2.26) becomes strong enough that a given hot electron current $J_\pm^h$ uniquely fixes the related excitation rate $R_\pm = J_\pm^{h\prime}$.

The model was initially constructed as an extension of the Valet-Fert[6] model to include time dependence, driven spin flips and hot electrons. Because we are back to steady state, we have lost the time dependence. This makes it interesting to compare the presented model with Valet-Fert

[1] Observe that (3.9) involves the density of states $D_\pm$. To use (3.10) we would have to use transformation (2.35), also containing the density of states. It is not obvious how these equations can be rewritten to remove them, but this section will show that the density of states turns out to be mostly unimportant if we are looking for a steady-state solution.

once again. Both of these models include spin diffusion driven by gradients in the spin accumulation μ_s' and spin flips driven by the spin accumulation itself μ_s. The combination of these gives the spin-diffusion length-scale λ. The fundamental difference between the models is that our model has S and J_s^* driving the spin-accumulation, but in constraining ourselves to samples with a metal-air interface we have imposed no current flow through $J = 0$. The Valet-Fert model does not provide S and J_s^*, instead the combination $J \neq 0$ with spatial differences in spin specific conductivity creates a non-zero spin accumulation[2]. Comparing the processes contained in the two models, the Valet-Fert model allows two independent currents $J_\pm$, which can alternatively be written as an electron current J and a spin current J_s. The model proposed here is constrained by $J = 0$, so there is effectively only a single degree of freedom to the current in the thermal electrons.

Note that in this formulation we have lost any direct dependence on the density of states, which is also one of the improvements regarding simplicity. In the dynamic case these were really prominent and crucial to satisfy conservation laws. We can think of the density of states as the number of electron states that need to be filled for the chemical potential to change one unit, in that sense describing how much time it takes for some transfer of electrons (spin) to change the local chemical potential (spin accumulation). In the steady state such time-scales are irrelevant so the need for the density of states for finding the spin accumulation disappears[3].

In relating to other work performed in dynamic settings we are bothered by the existence of the density of states. In the dynamic case it is common to quantify material properties using the spin-flip time τ and the spin diffusion coefficient D, which in our discussion emerged in Equations (2.33) and (3.13). Our fundamental material properties for the same processes are r and σ_{diff}. These are related to τ and D through the density of states, more specifically, the factor D_+D_-/D_{tot} appearing in both equations. This factor can be thought of as an effective density of states, as justified by (2.36). To use values of τ and D given in literature we therefore need to use the density of states to calculate r and σ_{diff}. However, equation (3.14) showed that we can compute the spin diffusion length $\lambda = \sqrt{\sigma_{\text{diff}}/r} = \sqrt{\tau D}$ from τ and D without using the density of states.

5.3 Conservation of spin and spin currents

Section 2.5 described how the model at that point could be applied to experiments. In Chapter 4 we showed how this can be changed to an interest in $J_s(z_{\text{IP}})$ in a steady-state setting. Now that we have the equations governing this steady state worked out in a convenient way, lets investigate some immediate consequences of the steady state model applied to the experiments we are interested in.

The left equation of (5.1) represents conservation of spin. Working in the context of experiments as was described in Section 2.5, we can integrate this from the interface with the insulator at $z = 0$ to the interface into the IP magnetised layer at $z = z_{\text{IP}}$. As the insulator at $z = 0$ prevents current at this place $J_s(0) = 0$, so conservation of spin gives the spin current into the IP layer as

$$J_s(z_{\text{IP}}) = \int_0^{z_{\text{IP}}} \mathrm{d}z \, \left(-2\, r(z)\, \mu_s(z) + 2\, S(z)\right). \tag{5.4}$$

This simply states that any spin flowing into the IP layer must come from a spin flip between $z = 0$ and $z = z_{\text{IP}}$. Comparing the *s-d* model to hot electron based models, if the spin current

[2]To emphasize this, if we were to impose $J = 0$ in the Valet-Fert model the solution would be trivial. In particular the spin accumulation and spin current would vanish; $\mu_s = 0$, $J_s = 0$.

[3]If we would care about finding $\mu_{0,\pm}$ we would still need to know the density of states despite being in steady state.

is driven by an external spin source S, the spin source itself provides the spin flips. Any spin flips on $0 < z < z_{\mathrm{IP}}$ driven by the spin accumulation μ_s will reduce the amount of spin left to contribute to $J_s(z_{\mathrm{IP}})$. The situation is opposite when studying spin currents caused by hot electron currents. While transporting spin, hot electron excitation, transport and decay do not flip spin by themselves. Excitation of electrons does however cause a depletion region, as can be seen from the right side of Equation (5.2). This depletion region causes spins to flip. As Equation (5.4) shows, the more spin-flip events, the larger $J_s(z_{\mathrm{IP}})$ will become. This gives an interesting contrast between spin currents as predicted by the *s-d* and hot electron models of spin transport. For external spin sources S to give a large spin current we want few spin flips driven by the spin accumulation, but for screened hot electron transport J_s^* to give a large spin current the spin accumulation must cause many spin flips.

To make this relation more concrete we consider some multilayer and compare the spin current created by an external spin source S localized at z_S to one caused by a constant [4] screened hot electron current J_s^* originating from z_S. We again work in the context as introduced in Section 2.5, which requires $0 < z_S < z_{\mathrm{IP}}$. We write the source as

$$S(z) = \frac{\alpha}{2}\delta(z - z_S), \qquad J_s^*(z) = \beta\,\Theta(z - z_S). \tag{5.5}$$

Here Θ is the Heaviside theta and δ the Dirac delta distribution. The factor $1/2$ in the source term for spin flips is chosen to compensate for our conventions allowing 1 spin flip to contribute 2 to the spin transfer; the up electron moving one way and the down electron oppositely. α and β represent to what extend spin flips or screened electron currents are the cause of the spin current. By introducing them we can put both sources in the same system at the same time, and after finding a solution change α and β to select if we are considering S or J_s^* as driving the spin current. If we use Equation (5.2) to describe the state of the thermal electrons, these will give a combined source term to the thermal spin accumulation of

$$2\,S(z) - J_s^{*\prime}(z) = (\alpha - \beta)\,\delta(z - z_S). \tag{5.6}$$

This essentially states that the spin accumulation caused by a spin source at z_S gives is precisely opposite to the spin depletion caused by the excitation and screening currents corresponding to a screened spin current originating from the same position. As the differential equation is linear, this also implies that the spin accumulation over space must also precisely be opposite when comparing these cases. This is illustrated in Figure 5.1.

If we provide some material properties and boundary conditions for the system under consideration we can now solve the differential equation to find μ_s. Because the differential equation we are solving is linear we can find some dimensionless constant ϕ such that for all α and β

$$\mu_s'(z_{\mathrm{IP}}) = -\frac{\phi\,(\alpha - \beta)}{2\,\sigma_{\mathrm{diff}}(z_{\mathrm{IP}})}. \tag{5.7}$$

We can use this with Equation (5.1) to calculate the total spin current into the IP magnetised layer as

$$J_s(z_{\mathrm{IP}}) = \phi\,(\alpha - \beta) + \beta = \phi\,\alpha + \beta\,(1 - \phi). \tag{5.8}$$

[4] The constraint for J_s^* to be constant is troublesome. Even if we choose to model hot electrons as non-decaying, they might traverse different materials, such that the screening currents will carry different amounts of spin. In those cases we can use linearity to write $J_s^*(z) = \Sigma_{n=1}^{N}\beta_n\Theta(z - z_{S,n})$ and use the superposition principle to find the spin transfer caused by the total, but multiple spin sources to the thermal electrons will emerge.

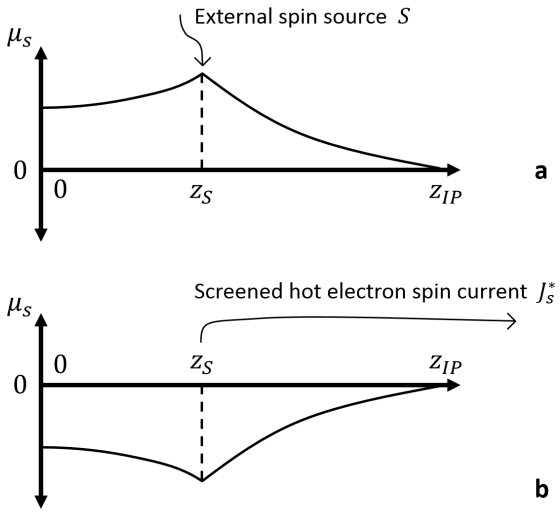

Figure 5.1: Comparison of a spin accumulation profile caused by an external spin source (a), and a screened hot electron spin current (b) of the same magnitude. On the vertical axis the spin accumulation μ_s, on the horizontal axis z. Equation (5.6) shows that the source term to the thermal spin accumulation is the same but opposite sign. As the differential equation governing the spin accumulation is linear, the spin accumulation and spin current in (a) and (b) also only differ in sign. In particular the diffusive spin current into the IP layer is equal and opposite.

$J_s(z_{\mathrm{IP}})$ is the rate of spin flowing into the IP magnetised layer, while α represents the rate of spin being injected by an external source and β is the rate of spin moved into the IP magnetised layer by a screened hot electron current.

Switching off the screened hot electron current by setting $\beta = 0$ gives $J_s(z_{\mathrm{IP}}) = \phi\,\alpha$, so ϕ can be interpreted as the efficiency for an *s-d* source at z_S to transport the introduced spin to z_{IP} where it contributes to the spin current $J_s(z_{\mathrm{IP}})$. Similarly, switching off the external spin source by setting $\alpha = 0$ gives $J_s(z_{\mathrm{IP}}) = \beta\,(1-\phi)$. From this, $1-\phi$ is the efficiency for a screened hot electron spin current originating from z_S to contribute to $J_s(z_{\mathrm{IP}})$. The efficiency is different from 1 because the screened hot electron current creates a depletion region that will diffuse to the IP layer. Equation (5.6) shows that this depletion is similar to that of an *s-d* spin source, so will have efficiency ϕ, but giving a contribution of opposite sign. This shows that in such a configuration the efficiency of spin injection by hot electrons is exactly opposite to the efficiency of spin injection by a spin source. If one is efficient the other is not, and the other way around.

This highlights a big difference between the *s-d* and hot electron based model of ultrafast spin currents. *s-d* and hot electron driven spin currents behave quite differently because *s-d* sources are a spin source while hot electron related processes are not. The *s-d* spin source therefore competes with with equilibrating spin flips r, which in this case acts as a spin sink. Hot electron driven spin currents need nonzero r to make the transferred spin. This principle is based on the conservation law of spin, so while this exposition was done in the virtual steady state setting, it does not depend on it. In cases where changing to a virtual steady state perspective is not allowed this difference between *s-d* and superdiffusive sources will therefore remain relevant.

5.4 Spin diffusion lengths

The observation of the previous section is interesting, but not having any indication of the value of ϕ is not that satisfying[5]. In general one would have to solve a differential equation to find it but we can give a little intuition regarding its behaviour. Equation (5.8) shows that ϕ is the fraction of injected spin (from either an *s-d* source or screened hot electrons) that diffuses to z_{IP}. The only other thing that can happen to this spin is being dissipated through a spin flip. This means that ϕ can also be thought of as comparing how much spin is transported out of a region to how much is lost to spin flips in that region. This is closely related to the spin diffusion length $\lambda = \sqrt{\sigma_{\text{diff}}/r}$. Within homogeneous systems it can be thought of as "how far spin will diffuse before flipping".

In totally homogeneous space the spin diffusion length completely specifies how far spin is able to diffuse, and ϕ will just be the exponential decay $\phi = \frac{1}{2}e^{(z_S - z_{\text{IP}})/\lambda}$. However, by setting an insulating boundary condition at $z = 0$ and an ideal spin sink at $z = z_S$ we already made the system inhomogeneous. Despite this, within the individual layers of the system the spin diffusion length specifies how far spin will diffuse.

When studying spin diffusion in multilayers, this makes it tempting to look at the spin diffusion lengths of the constituent layers to estimate how efficient diffusion is in the multilayer. Here the spin diffusion lengths of the constituent layers can paint a misleading picture of the relative efficiency of spin diffusion and spin flips in the combined system. As an example, think of a multilayer consisting of alternating layers of materials A and B, with all layers having the same thickness and many repeats on a distance of 1 unit length. Material A has material properties $\sigma_{\text{diff}} = 10$, $r = 10$, giving $\lambda = 1$. Material B has properties $\sigma_{\text{diff}} = 0.1$, $r = 0.1$, also giving it a spin diffusion length of $\lambda = 1$. One might expect the multilayer to behave similarly to a material with $\lambda = 1$ in regards to how the efficiency of spin diffusion and spin flips compare. In reality, spin diffusion will be limited by material B, giving an effective $\sigma_{\text{diff}} \approx 0.2$, and spin flips are dominated by material A such that effectively $r \approx 5$ [6]. These combine to give an effective spin diffusion length of $\lambda \approx \sqrt{0.2/5} = 1/5$, substantially smaller than $\lambda = 1$ of the constituent layers. While this example concerns many layers, similar effects can even arise when just two layers and a single interface is present. Next chapter will present an example of this in Section 6.2.1.

In this chapter the consequences of enforcing steady state on the proposed model were explored, with the results being useful to understand dynamic experiments through the results from Chapter 4. The governing equations were presented, and we discussed the various changes making it more convenient to use than dynamic model. The simpler governing equations allowed some behaviour of the model to be better understood. This chapter concludes the mathematical infrastructure presented in this thesis. The following chapter will apply what has been build up to the experiments that motivated this work.

[5] Other than ϕ being between 0 and 1, as spin flips and diffusion can only dissipate spin, and it can dissipate no more spin than was injected.

[6] The factor 2 or 1/2 appears in both cases because in the multilayer material A and B take up half the thickness.

Chapter 6

Application to Experiments

In the previous chapters we derived and simplified a model for studying the experiments performed in [11, 12, 13]. This chapter will use the final simplification of the "virtual steady state" described in the previous chapter to build models of the experiments we are trying to better understand. The measurement most relevant to this discussion is from [11], where the efficiency of excitation of the magnetic precession is measured for different spacer thicknesses.

Section 6.1 will describe how the proposed model will be applied to this experiment. With this set up done, Section 6.2 will study how spin currents stemming from an *s-d* would behave in this experiment. Section 6.3 will study spin currents driven by hot electron dynamics. For both processes driving spin currents, the respective results will be compared to the measurements of [11] to attempt to find out which of the processes gives the spin transfer observed in this experiment.

6.1 Model of experiments

How to apply the proposed model to the experiments under consideration was introduced in Section 2.5. This section will briefly recap the setup and make it more specific. The direction of spin up is chosen along the OOP direction. An insulator is modeled at $z < 0$, giving an insulating boundary conditions at $z = 0$. The IP magnetised layer is positioned at $z > z_{\mathrm{IP}}$, which is modeled to act as an ideal spin sink for OOP spin. This gives a no spin accumulation boundary condition; $\mu_s(z_{\mathrm{IP}}) = 0$. These boundary conditions cause that only the range $0 < z < z_{\mathrm{IP}}$ needs to be studied. Working in the virtual steady state perspective makes the state of the model constant in time, and the spin current into the IP magnetised layer $J_s(z_{\mathrm{IP}})$ represents the excitation of the magnetic precession.

In this chapter we choose to model the region of interest $0 < z < z_{\mathrm{IP}}$ as consisting of the OOP magnetic layer and a spacer layer, both of which are internally homogeneous. The OOP layer will be labeled with subscript 1, while the spacer layer has subscript 2. This setup is sketched in Figure 6.1. The figure shows the OOP coordinate on the horizontal axis, divided into the separate relevant layers of the sample. Furthermore, the boundary conditions at interfaces between the various layers are shown below these interfaces.

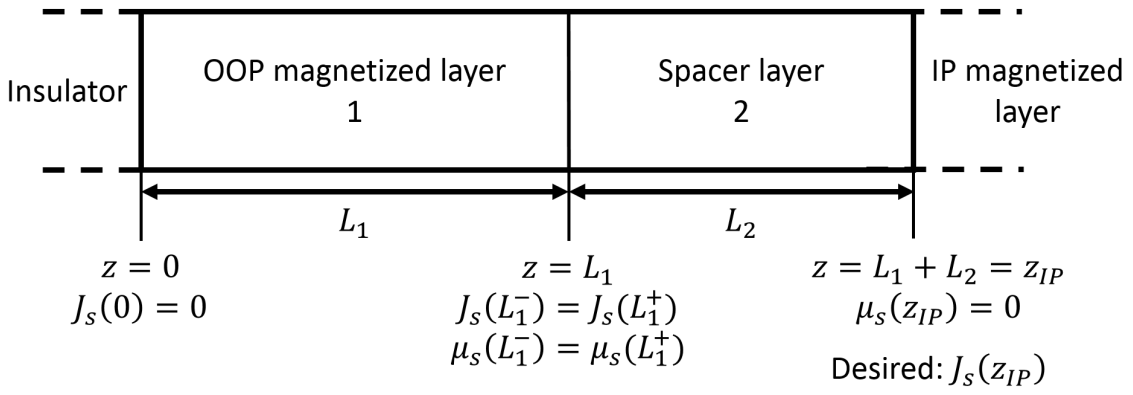

Figure 6.1: Sketch of the multilayer and the relevant boundary conditions we will be considering in this chapter. The horizontal axis corresponds to the out-of-plane coordinate z.

6.2 s-d source

First we study *s-d* spin sources as the cause of spin currents. The hot electron system is disabled by setting $J_s^* = 0$, so only the external spin source S will cause a spin current to exist. This external spin source was related to conservation of spin angular momentum during ultrafast demagnetisation, the spin from localised electrons being transferred to the itinerant, i.e. thermal electrons. As we are working in the virtual steady state picture, S represents the total amount of spin injected locally into the thermal electrons system. For this reason, this external spin source S is nonzero only in the OOP magnetised layer, where we model it to be uniform[1].

In Section 6.2.2 a fairly general solution will be given, but the derivation is involved and it turns out that the spin accumulation inside the OOP magnetised layer is not that important to much of the behaviour. For this reason we will first restrict ourselves to the limiting case of an infinitesimal OOP layer, such that the internal state of the OOP layer is effectively removed. Even this limiting case will be introduced by showing special cases before discussing the more general infinitesimal OOP layer problem. Spin flips in the spacer layer and spin flips in the OOP magnetic layer are switched off in turn. After these results the infinitesimal OOP solution is shown, which is interpreted in terms of the special cases. Finally the case of finite OOP layers is discussed, which is interpreted by comparison to the solution to the infinitesimal OOP layer problem.

6.2.1 Infinitesimal OOP layer

We consider a system with an infinitesimal OOP magnetised layer, corresponding to a limit $L_1 \downarrow 0$. We will write 0^+ for this limit to 0 from the positive side, so the OOP magnetised layer spans $0 < z < 0^+$ and the spacer layer spans $0^+ < z < z_{\mathrm{IP}}$ [2]. The OOP layer being shrunk to thickness

[1]This will allow us to write S both for the function it referred to previously and the constant value it takes in the OOP magnetised layer. Which of the two is used in equations will be clear from context.

[2]Because the OOP layer is infinitesimal we have simply $z_{\mathrm{IP}} = L_2$. In anticipation for studying the case with finite OOP magnetised layer we will use L_2 where the thickness of the spacer is relevant, and z_{IP} when evaluating functions at the interface with the IP magnetised layer.

0 prevents it from having any internal state. Instead it will act as a boundary condition to the spin accumulation in the spacer layer, which we will derive now. If we integrate the left equation in (5.1) (conservation of spin) from $z = 0$ to $z = 0^+$, we get

$$J_s(0^+) - J_s(0) = -2 \int_0^{0^+} \mathrm{d}z\, r_1(z)\, \mu_s(z) + 2 \int_0^{0^+} \mathrm{d}z\, S(z). \tag{6.1}$$

Informally, because the distance between $z = 0$ and $z = 0^+$ is infinitesimal we take μ_s to be constant over this region. This motivates us to simplify above integrals by introducing $\tilde{S}$ and $\tilde{r}$ as[3]

$$\tilde{r}\, \mu_s(0^+) = \int_0^{0^+} \mathrm{d}z\, r_1(z)\, \mu_s(z), \qquad \tilde{S} = \int_0^{0^+} \mathrm{d}z\, S(z). \tag{6.2}$$

Using this with the no current boundary condition on the interface with the insulator $J_s(0) = 0$ gives

$$J_s(0^+) = 2\,\tilde{S} - 2\,\tilde{r}\, \mu_s(0^+), \tag{6.3}$$

which will serve as the boundary condition on the state of the spacer layer on the interface with the FM layer. Note that a single spin flip contributes two to the spin current into the spacer[4]. With this, the maximum spin current reachable with source $\tilde{S}$ is $J_s(z_{\mathrm{IP}}) = 2\tilde{S}$.

The boundary condition of the spacer layer at its interface with the IP magnetised layer is $\mu_s(z_{\mathrm{IP}}) = 0$, by modeling the IP layer to be an ideal spin sink. Now we need to solve the differential equation of the spin accumulation in the spacer layer with the boundary conditions stated above. We will use Equation (5.2) and the right-hand side of Equation (5.1). Within the spacer layer these reduce to

$$r_2\, \mu_s = \sigma_{\mathrm{diff},2}\, \mu_s'', \qquad J_s = -2\, \sigma_{\mathrm{diff},2}\, \mu_s', \tag{6.4}$$

where r_2 and $\sigma_{\mathrm{diff},2}$ are positive real numbers. This sets up the problem of spin currents caused by an *s-d* source in infinitesimal OOP magnetised layers.

No spin flips in OOP layer

First we consider the special case when no spin flips occur in the OOP layer, which means $\tilde{r} = 0$. From (6.4), the solution of μ_s in the spacer layer can be written as

$$\mu_s(0^+ < z < z_{\mathrm{IP}}) = \mu^+ e^{+z/\lambda_2} + \mu^- e^{-z/\lambda_2} \tag{6.5}$$

where $\mu^\pm$ are real numbers parameterising the solution and $\lambda_2 = \sqrt{\sigma_{\mathrm{diff},2}/r_2}$ is the spin diffusion length of the spacer layer. The boundary condition on the interface with the IP magnetised layer is $\mu_s(z_{\mathrm{IP}}) = 0$, while $\tilde{r} = 0$ reduces the boundary condition with the OOP layer as given in (6.3) to $J_s(0^+) = 2\tilde{S}$. This gives a system of equations that can be used to solve for $\mu^\pm$, which can be used to calculate the spin current into the IP magnetised layer as

$$J_s(z_{\mathrm{IP}}) = \frac{4\tilde{S}}{e^{+L_2/\lambda_2} + e^{-L_2/\lambda_2}}. \tag{6.6}$$

[3]Mathematically, this step should be thought of as taking the limit $0^+ \downarrow 0$, with r and S increasing to keep $\tilde{S}$ and $\tilde{r}$ constant. Ultimately though, the main justification of this approach is that its result agrees with a limiting case of the model with finite OOP layer, which will be discussed in Section 6.2.2.

[4]Every spin-flip, a spin is removed and an electron with opposite spin is inserted. Both the removed and injected spin will contribute, giving the factor 2.

We see that on changing the spacer thickness L_2, the only relevant length-scale is the spacer spin diffusion length λ_2. The behaviour of $J_s(z_{\mathrm{IP}})$ on changing L_2 is shown in Figure 6.2. We see in the equation and figure that setting the spacer thickness to 0 will give $J_s(z_{\mathrm{IP}}) = 2\tilde{S}$, so all injected spin diffuses into the IP magnetised layer. On the other hand, in the limit of large spacer thickness, $\lim_{L_2\to\infty} J_s(z_{\mathrm{IP}}) = 0$, so all spin is dissipated by flips in the spacer layer.

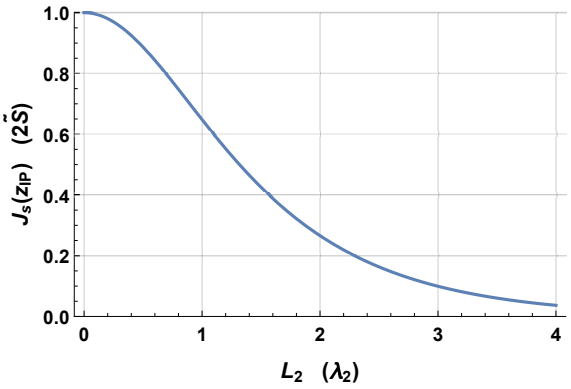

Figure 6.2: $J_s(z_{\mathrm{IP}})$ as function of L_2 in the limiting case $\tilde{r} \to 0$; no spin flips occur in the OOP magnetised layer. Vertical axis in units $2\,\tilde{S}$, horizontal axis in units λ_2.

No spin flips in spacer layer

Now we discuss the special case of infinitesimal OOP magnetised layers where no spin flips occur in the spacer layer. Any spin injected into the OOP layer can either dissipate in the OOP layer itself or diffuse into the IP magnetised layer. Mathematically, disabling spin flips in the spacer layer amounts to setting $r_2 = 0$. This makes the differential equation in the spacer, the left side of Equation (6.4), reduce to $\mu_s'' = 0$. The solution of μ_s within the spacer layer can then be written as

$$\mu_s(0^+ < z < z_{\mathrm{IP}}) = \mu_s(0) - \frac{J_s}{2\,\sigma_{\mathrm{diff},2}} z. \tag{6.7}$$

Using this with the right side of Equation (6.4) gives the spin current in the spacer being constant; $J_s(0^+ < z < z_{\mathrm{IP}}) = J_s$, justifying the notation. With the boundary condition with the IP layer $\mu_s(z_{\mathrm{IP}}) = 0$, and Equation (6.3) as the boundary condition for the interface with the OOP layer we get a system of equations that can be solved for $\mu_s(0)$ and J_s. With these we can derive the spin current into the IP layer to be

$$J_s(z_{\mathrm{IP}}) = \frac{2\tilde{S}}{1 + L_2/\gamma}, \qquad \gamma = \sigma_{\mathrm{diff},2}/\tilde{r} \tag{6.8}$$

Now, changing the spacer layer thickness L_2 will affect the spin current through the newly introduced length scale γ. Figure 6.3 shows the behaviour of $J_s(z_{\mathrm{IP}})$ when changing L_2. As in the previous case, the limit of $L_2 \downarrow 0$ makes all injected spin diffuse to the IP layer, and the limit $L_2 \to \infty$ prevents any spin from diffusing into the IP layer.

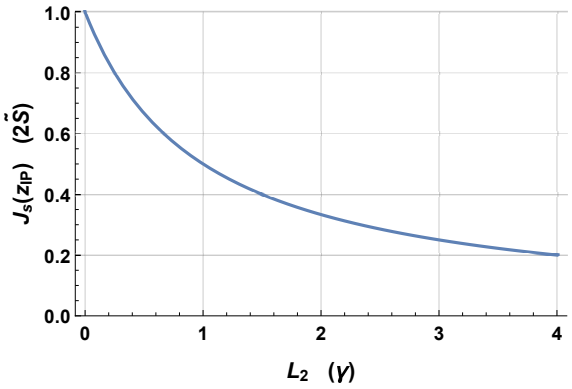

Figure 6.3: $J_s(z_{\mathrm{IP}})$ as function of L_2 in the limiting case $r \to 0$; no spin flips in the spacer layer. Vertical axis in units of $2\,\tilde{S}$, horizontal axis in units of γ.

This is the simplest example that shows that on changing L_2, we might see behaviour at quite different length scales than the spin-diffusion length of the spacer layer[5]. The cause is the interplay between the different layers, which is clear by γ comparing the rate of spin decay through the OOP layer ($\tilde{r}$) with diffusion through the spacer layer ($\sigma_{\mathrm{diff},2}$). The use of $\tilde{r}$ (which only exists in a non-physical limit of infinitesimal OOP layers) in the equation for γ makes it hard to give an estimate on what order of magnitude γ may be. This problem will be solved when studying finite OOP layers as will be done in Section 6.2.2.

General infinitesimal OOP layer case

Now that we have studied the special cases of only allowing spin flips in the spacer layer or the OOP magnetised layer, we are set for the more general case of spin flips allowed in both layers. Still, we are dealing with infinitesimal OOP layers. The derivation of this problem largely follows those of the special cases discussed before. The spin current into the IP layer turns out to be

$$J_s(z_{\mathrm{IP}}) = \frac{4\,\tilde{S}}{e^{+L_2/\lambda_2} + e^{-L_2/\lambda_2} + \frac{\lambda_2}{\gamma}\left(e^{+L_2/\lambda_2} - e^{-L_2/\lambda_2}\right)}, \qquad \gamma = \sigma_{\mathrm{diff},2}/\tilde{r}. \tag{6.9}$$

In the limit $\gamma \to +\infty$ the right part of the denominator is killed, and the solution reduces to that of the special case where no spin-flips occur in the OOP layer as given by Equation (6.6). In the limit $\lambda_2 \to +\infty$ we can expand the exponents to first order to recover the solution to the special case where no spin-flips occur in the spacer layer, given by Equation (6.8).

$J_s(z_{\mathrm{IP}})$ depends on L_2, λ_2 and γ. Because all three are in units of length, effectively there are only two independent degrees of freedom. In Figure 6.4 the behaviour of $J_s(z_{\mathrm{IP}})$ is sketched. We see that if λ_2 and γ are substantially different, the solution will closely resemble the limiting case of the larger of the two tending to infinity. Put differently, the shortest of λ_2 and γ will dominate the behaviour of $J_s(z_{\mathrm{IP}})$ with changing spacer thickness L_2.

[5] In setting $r_2 \downarrow 0$ we have effectively set $\lambda_2 \to \infty$.

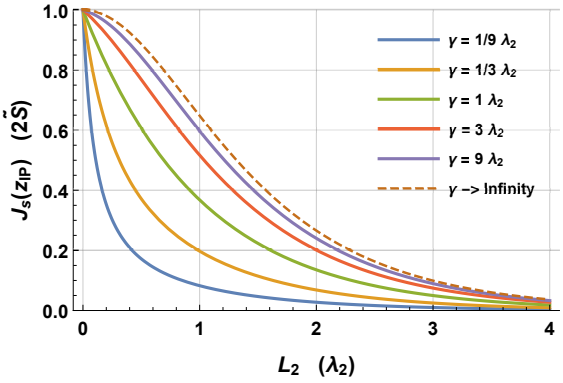

(a) $J_s(z_{\mathrm{IP}})$ depending on L_2 and γ, both in units of λ_2. Including the limiting case $\gamma \to \infty$ as described by Equation (6.6).

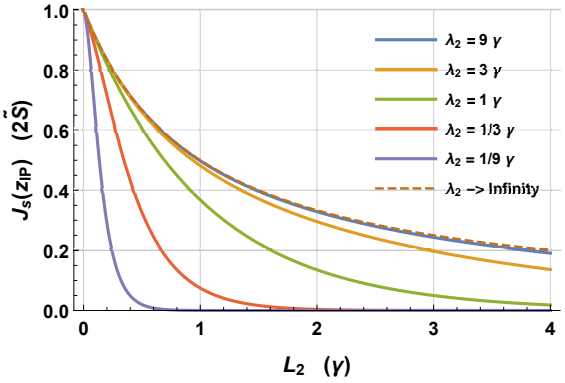

(b) $J_s(z_{\mathrm{IP}})$ depending on L_2 and λ_2, both in units of γ. Including the limiting case $\lambda_2 \to \infty$ as described by Equation (6.8).

Figure 6.4: The behaviour of spin current flowing into the IP magnetised layer as given by Equation (6.9), depending on L_2, λ_2 and γ. On the vertical axes $J_s(z_{\mathrm{IP}})$ in units of $\tilde{S}$. On the horizontal axis the spacer thickness L_2. Note that the non-limiting solutions (solid curves) are the same in both figures ($\lambda_2 = a\gamma$ corresponds to $\gamma = 1/a\,\lambda_2$), but the curves appear different because the horizontal axis has different units.

6.2.2 Finite FM layers

Now that the limiting case of infinitesimal OOP layers is discussed we are prepared to study finite OOP layers. The derivation mostly follows the steps in the derivations above, but the derivation has become substantially larger because we now have to consider the internal state of the OOP layer besides the internal state of the spacer layer dealt with previously. Here we will only state the result, the derivation of which can be found in Appendix C.1. In the case of finite OOP magnetised layers in virtual steady state, the spin current into the IP layer is

$$J_s(z_{\mathrm{IP}}) = \frac{4\,S\,T}{e^{+L_2/\lambda_2} + e^{-L_2/\lambda_2} + \frac{\lambda_2}{\gamma}\left(e^{+L_2/\lambda_2} - e^{-L_2/\lambda_2}\right)}, \qquad \gamma = \frac{\sigma_{\mathrm{diff},2}}{r_1\,T}, \qquad T = \lambda_1\,\tanh(L_1/\lambda_1) \tag{6.10}$$

where the quantities T and γ in units of length were introduced. The behaviour of $J_s(z_{\mathrm{IP}})$ on changing λ_2, γ and L_2 is identical to that in case of an infinitesimal OOP layer case. This justifies the new equation for γ as a generalisation of the γ of the infinitesimal OOP layer case and allows us to carry over much of the intuition formed when studying the infinitesimal OOP layer. In particular Figure 6.4 carries over exactly to finite OOP layers[6]. The limiting cases of $\gamma \to \infty$ and $\lambda_2 \to \infty$ as discussed for the infinitesimal OOP layer case also have their counterparts as

$$\lim_{\gamma\to\infty} J_s(z_{\mathrm{IP}}) = \frac{4\,S\,T}{e^{+L_2/\lambda_2} + e^{-L_2/\lambda_2}}, \qquad \lim_{\lambda_2\to\infty} J_s(z_{\mathrm{IP}}) = \frac{2\,S\,T}{1 + L_2/\gamma}. \tag{6.11}$$

The behaviour of these on changing L_2 is exactly like their counterparts in the infinitesimal OOP layer case, which were plotted in Figures 6.2, 6.3 and 6.4.

[6]Where the vertical axis is now in units of $S\,T$.

The only differences between the finite and infinitesimal OOP layer case are the replacements of $\tilde{S}$ becoming $S\,T$ in the equation for $J_s(z_{\mathrm{IP}})$, and $\tilde{r}$ becoming $r_1\,T$ in the new definition of γ. Remind that in Equation (6.2) the symbols $\tilde{S}$ and $\tilde{r}$ were defined as integrals of S, respectively r_1, over the OOP layer. With T being of unit length and $\tilde{S} \sim S\,T$, $\tilde{r} \sim r_1\,T$, we can think of T as the thickness of the region in the OOP that contributes spin to the spin current into the IP layer. The definition of T also conforms to what one might expect under such an interpretation of it. In the limiting case $L_1 << \lambda_1$ we get $T = L_1$; the OOP layer is much smaller than its spin diffusion length so the entire layer contributes. The other extreme $\lambda_1 << L_1$ gives $T = \lambda_1$; only the region closer than one spin flip length from the spacer will contribute to J_s. In general T is approximately the shortest of λ_1 and L_1.

In the limiting case of infinitesimal OOP layer we were not able to give reasonable estimates of γ as it depended on the non-physical $\tilde{r}$, but now we can attempt to estimate it. The equation for γ provided in Equation (6.10) can be rewritten using the definition of T and λ_1, giving alternatively

$$\gamma = \lambda_1 \frac{\sigma_{\mathrm{diff},2}}{\sigma_{\mathrm{diff},1}} / \tanh(L_1/\lambda_1). \tag{6.12}$$

As an example, based on a stack consisting of a Co/Pt OOP magnetised layer and a Cu spacer and the material properties of these materials specified in [16], in Appendix D we estimate that we would expect γ to be between 15 nm and 80 nm. In contrast, [16] provides the spin diffusion length of the copper as 400 nm. While we can not give much confidence in any value of γ, is seems likely that γ is substantially shorter than λ_2 in this material system. This would make the resulting behaviour of $J_s(z_{\mathrm{IP}})$ on changing the spacer thickness L_2 reasonably described by the right of (6.11).

6.2.3 Relation to experimental observations

In the MOKE measurements used to study experiments the most accessible way of quantifying the spin transfer is the efficiency, as the MOKE is sensitive of the out-of-plane magnetisation of the entire stack. The study of [11] varied the spacer thickness to measure the spin transfer efficiency. This measurement is shown in Figure 6.5. The model presented above will be used to interpret the measurements in this paper.

We will write the efficiency of spin diffusing to the IP layer relative to the injected spin as ϕ. To calculate the efficiency of spin transfer, we need to divide the spin transfer given by Equation (6.10) by the total amount of injected spin, $2\,S\,L_1$. As the *s-d* model states that the spin lost by demagnetisation equals the spin injected into the thermal electron, this justifies the relation between the calculated ϕ and the efficiency observed in experiment. This gives

$$\phi = \frac{2\,T/L_1}{e^{+L_2/\lambda_2} + e^{-L_2/\lambda_2} + \frac{\lambda_2}{\gamma}(e^{+L_2/\lambda_2} - e^{-L_2/\lambda_2})}, \tag{6.13}$$

While it is difficult to calculate γ in the experiment in question, we can observe from Figure 6.5 that the change of ϕ with L_2 is on much shorter length-scales than the spin diffusion length of the copper spacer of some 400 nm. Assuming the proposed model is correct would therefore imply that $\gamma << \lambda_2$. This allows us to use the $\lambda_2 \to \infty$ limit, which simplifies the spin transfer efficiency to

$$\phi = \frac{T/L_1}{1 + L_2/\gamma}. \tag{6.14}$$

Fitting this to the measurements with γ and T/L_1 as fitting variables gives $\gamma = 7.6\,\text{nm}$ and $T/L_1 = 0.024$, though a substantial range of other values would fit the measurements fairly well. The fit to the measurement data is shown in Figure 6.5, together with the exponential decay fit as used in the original paper.

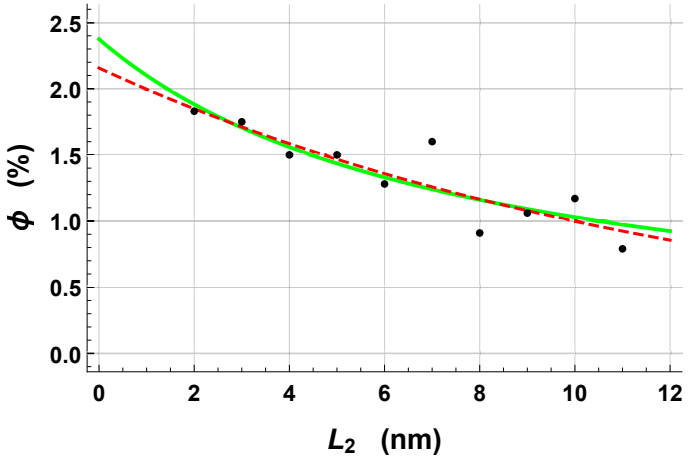

Figure 6.5: For various spacer thicknesses the efficiency of spin transfer, i.e. the spin absorbed by the in-plane magnetised layer relative to the demagnetisation of the out-of-plane magnetised layer. In black the measurement data from [11]. The red, dashed curve is the exponential fit as used in the original paper, with a length-scale of 13 nm. The green curve is the fit of Equation (6.14) to the measurement data, with fitting variables $\gamma = 7.6\,\text{nm}$ and $T/L_1 = 0.024$.

Using the definition of T to write T/L_1 as

$$T/L_1 = \frac{\lambda_1}{L_1} \tanh\left(\frac{L_1}{\lambda_1}\right) \tag{6.15}$$

shows that $T/L_1 = 0.024$ would approximately imply $\lambda_1/L_1 = 0.024$. Knowing that the OOP layer of the experiments has a thickness of $L_1 = 3.2\,\text{nm}$ this would give an impossibly short spin diffusion length of the OOP layer of $\lambda_1 = 0.08\,\text{nm}$. The fit value of γ also seems implausibly short. These discrepancies give some problems for using the *s-d* model as used here to describe the experiment in question.

An important difference with the stack as modelled here compared to the stack used in the experiment of [11] is the platinum layer adjacent to the OOP layer, where we have modelled an insulating interface. Platinum is a heavy metal, so it does conduct electrons and its large mass causes it to relatively quickly dissipate spin. This layer would give a third place for spin to be dissipated, besides the previously mentioned spin flips in the spacer layer and OOP magnetised layer. It seems sensible that such an additional spin dissipation channel would lower the spin transfer efficiency relative to the model presented here, explaining the implausibly small fit value of T/L_1 when not including the Pt layer. Also, if $r\,T \sim \tilde{r}$ can be interpreted as the effectiveness of spin to be flipped before reaching the spacer layer, it seems plausible that the added spin sink would give an effective increase in $\tilde{r}$. This might in turn result in a decrease in the length-scale $\gamma = \sigma_{\text{diff},2}/\tilde{r}$, explaining the small value obtained in the fit to the experimental data. Finally, including the effect

of interfacial conductivities between the several layers might change the behaviour of the model, potentially acting as an additional cause for the small observed spin transfer efficiency in comparison to above model. It seems plausible that such modifications would significantly improve the ability of the *s-d* of reproducing the behaviour observed in the studied measurements, but a lack of time has prevented these modifications from being studied further.

6.3 Hot electrons

Having discussed the *s-d* effect as a source of spin currents, we now switch our attention to hot electron excitation and transport as the cause of spin currents. Here we disable the external spin source by setting $S = 0$ everywhere in the multilayer, while the screened hot electron current J_s^* can now be non-zero.

We will keep the discussion limited to infinitesimal OOP layers. This substantially simplifies the problem, but it discards potentially interesting behaviour caused by the screening currents in the OOP layer having a different spin polarisation than that in the spacer layer[7]. The approach of introducing the infinitesimal OOP magnetised layers is the same as was done in the *s-d* case. The boundary condition related to the interface between the OOP layer and spacer layer, as given by Equation (6.3) in the *s-d* case, now becomes

$$J_s(0^+) = -2\,\tilde{r}\,\mu_s(0^+). \tag{6.16}$$

In the *s-d* case, the spin current into the IP layer was purely the diffusive current. Now we both have a diffusive spin current and the screened hot electrons themselves contributing to the spin transfer.

Initially we will discuss the special case where no hot electron decay occurs in the spacer layer. Afterwards we will include hot electron decay, but only in the limiting cases when either no spin flips occur in the OOP magnetised layer ($\tilde{r} \to 0$), or no spin flips occur in the space layer ($r_2 \to 0$).

6.3.1 No hot electron decay

First considering the simple case when hot electrons do not decay. Every hot electron leaving the OOP magnetised layer reaches the IP magnetised layer. This makes the screened hot electron current J_s^* constant over the spacer layer. This constant will be written as $J_s^*(0^+)$ in anticipation to the case when hot electron decay will be included. It represents the screened hot electron spin current leaving the OOP magnetised layer both here and when hot electron decay will be included.

When calculating the spin transfer into the IP magnetised layer, the screened hot electron current contribution will be $J_s^*(z_{\mathrm{IP}}) = J_s^*(0^+)$. The diffusive contribution to the spin current can be derived by a similar derivation as the one related to *s-d* driven spin currents in infinitesimal spacer layers. In fact we can use the result described there with the result of Section 5.3 where we

[7]Electron excitation and the screening current of hot electron transport cause a spin depletion region. Depending on the spin polarisation of the screening currents in the OOP layer, this spin depletion region could either be where electrons are excited, or on the OOP layer - spacer layer interface where the spin polarisation of the screening current changes. In the extreme case of spin neutral screening currents in the OOP layer, the spin polarisation does not change over the interface so there is no interfacial spin accumulation. On the other hand, if the screening current in the OOP layer is as spin polarised as the hot electron current, in the OOP layer the screened hot electron current will have 0 spin polarisation; $J_s^* = 0$. In that case the spin depletion region would exist at the OOP layer - spacer layer interface.

showed how in the case of constant J_s^*, spin currents as predicted by the *s-d* model are related to those predicted by a hot electron model. The derivation shows that the spin transfer caused by a constant screened hot electron current is

$$J_s(z_{\mathrm{IP}}) = J_s^*(0^+)\left(1 - \frac{2}{e^{+L_2/\lambda_2} + e^{-L_2/\lambda_2} + \frac{\lambda_2}{\gamma}\left(e^{+L_2/\lambda_2} - e^{-L_2/\lambda_2}\right)}\right), \qquad \gamma = \sigma_{\mathrm{diff},2} \,/\, \tilde{r}. \quad (6.17)$$

Like in the *s-d* case, the spin current into the IP magnetised layer depends on the spacer thickness L_2 and the length-scales λ_2 and γ. We also have the limiting cases of no spin flips in the OOP layer ($\gamma \to \infty$) and no spin flips in the spacer layer ($\lambda_2 \to \infty$) carrying over

$$\lim_{\gamma\to\infty} J_s(z_{\mathrm{IP}}) = J_s^*(0^+)\left(1 - \frac{2}{e^{+L_2/\lambda_2} + e^{-L_2/\lambda_2}}\right), \qquad \lim_{\lambda_2\to\infty} J_s(z_{\mathrm{IP}}) = J_s^*(0^+)\left(1 - \frac{1}{1 + L_2/\gamma}\right). \quad (6.18)$$

The behaviour of $J_s(z_{\mathrm{IP}})$ on varying L_2, λ_2 and γ, including the limiting cases, is shown in Figure 6.6.

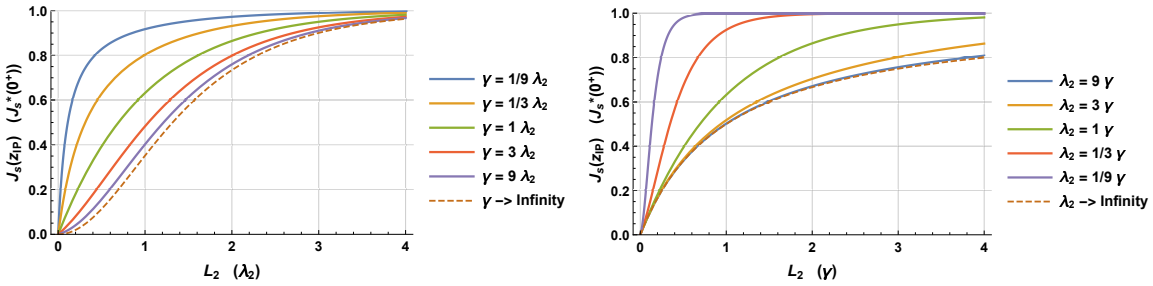

(a) $J_s(z_{\mathrm{IP}})$ depending on L_2 and γ, both in units of λ_2. Including the limiting case $\gamma \to \infty$ as described by left equation of (6.18).

(b) $J_s(z_{\mathrm{IP}})$ depending on L_2 and λ_2, both in units of γ. Including the limiting case $\lambda_2 \to \infty$ as described by the right equation of(6.18).

Figure 6.6: The behaviour of spin current flowing into the IP magnetised layer as given by Equation (6.17), depending on L_2, λ_2 and γ. On the vertical axes $J_s(z_{\mathrm{IP}})$ in units of $J_s^*(0^+)$. On the horizontal axis the spacer thickness L_2. Note that the non-limiting solutions (solid curves) are the same in both figures ($\lambda_2 = a\,\gamma$ corresponds to $\gamma = 1/a\,\lambda_2$), but the curves appear different because the horizontal axis has different units.

Again, λ_2 is the length scale related to spin flips in the spacer layer, while γ is the length-scale related to spin flips in the OOP layer. If the spacer layer thickness L_2 is smaller than both of these, spin will not flip in the OOP layer nor in the spacer layer. Instead a diffusive current from the IP layer will compensate the spin depletion caused by excitation and screening of hot electrons. This diffusive spin current exactly compensates the screened hot electron spin current, causing the total spin current to be small when the spacer is small; $\lim_{L_2\to 0} J_s(z_{\mathrm{IP}}) = 0$, as visible in Figure 6.6.

On the other hand, if the spacer thickness L_2 is larger then one of λ_2 or γ, the process related to it is capable of dissipating the spin-depletion caused by the screened hot electron current. This causes the diffusion current flowing back to the depletion region to be small. In the extreme case the diffusion current flowing out of the IP magnetised layer is zero, achieving the largest possible spin injection of $J_s^*(0^+)$. From this, the shortest of λ_2 and γ dictated the length scale of $J_s(z_{\mathrm{IP}})$ when changing the spacer thickness L_2, as happened in the *s-d* case.

This can also be observed in Figure 6.6. Subfigure 6.6a shows that the rise of of spin transfer with increasing spacer thickness is at the length scale λ_2 or faster. On the other hand, Subfigure 6.6b shows this rise being at the scale of γ or more quickly. As these are the only length scales involved, this shows that the shortest of λ_2 and γ must dictates the length scale at which the spin transfer rises.

Not having hot electrons decay is an unrealistic modelling choice, but it does show an important contrast to the *s-d* source of spin currents. Firstly that hot electron induced spin currents in combination with having a tiny spacer would prevent a net spin transfer to take shape. In this situation, increasing the number of spin flips in the OOP magnetised layer or the spacer layers actually causes an increase of the total spin current. This makes the length-scales related to spin-flips, λ_2 and γ, to now be a length-scales related to the spin transfer $J_s(z_{\mathrm{IP}})$ increasing with spacer thickness L_2. However for sufficiently thick spacer layers the assumption of hot electrons not decaying becomes problematic. The next section will investigate how hot electron decay changes the behaviour.

6.3.2 Hot electron decay

We now allow hot electrons to decay. To keep the derivations and their solutions simple, we choose an exponential decay of the screened hot electron current J_s^* over z with a characteristic length-scale λ_h, subscript h for "hot". This makes the screened hot electron current follow

$$J_s^*(0^+ < z < z_{\mathrm{IP}}) = J_s^*(0^+)\, e^{-z/\lambda_h}. \tag{6.19}$$

In the limit $\lambda_h \to \infty$ hot electrons will not decay, reproducing J_s^* being constant as was investigated above. The limit $\lambda_h \to 0$ will make hot electrons decay before traveling any meaningful distance, such that $J_s^* = 0$. This gives a trivial limiting case $\lim_{\lambda_h \to 0} J_s(z_{\mathrm{IP}}) = 0$.

Hot electron decay will change the spin transfer into the IP magnetised layer in two ways. The most obvious way is the screened hot electron current $J_s^*(z_{\mathrm{IP}})$ into the IP layer now decreasing with growing spacer thickness L_2. Somewhat more hidden, the decay of hot electrons in the spacer will inject a spin accumulation into the spacer layer. This spin accumulation can contribute to the diffusive spin current into the IP magnetised layer.

We already saw in the case of no hot electron decay that λ_2 and γ are length scales related to $J_s(z_{\mathrm{IP}})$ increasing with the spacer thickness L_2. In contrast, the hot electron length scale λ_h is a length scale related to the decrease of $J_s(z_{IP})$ with increasing L_2.

Working with infinitesimal OOP magnetised layers and hot electron decay is still fairly difficult, so we will not give a general solution including both spin flips in the OOP magnetised layer and in the spacer layer. Instead we present the limiting cases of disabling spin flips in the OOP layer or the spacer layer.

No spin flips in OOP magnetised layer

In this case, no spin flips are allowed in the OOP magnetised layer, corresponding to the limit $\tilde{r} \to 0$, or alternatively $\gamma \to \infty$. We have the screened hot electron current causing a spin depletion at the OOP layer, transporting this spin either to the IP magnetised layer or letting it decay somewhere in the spacer layer. The spin accumulation in the spacer will potentially cause a diffusive contribution to the spin current into the IP layer. The derivation corresponding to this problem is given in

Appendix C.2, the solution gives the spin current into the IP layer as

$$J_s(z_{\mathrm{IP}}) = J_s^*(0^+)\frac{\lambda_h^2}{\lambda_h^2-\lambda_2^2}\left(e^{-L_2/\lambda_h}\left(1+\frac{\lambda_2}{\lambda_h}\cdot\frac{e^{+L_2/\lambda_2}-e^{-L_2/\lambda_2}}{e^{+L_2/\lambda_2}+e^{-L_2/\lambda_2}}\right)-\frac{2}{e^{+L_2/\lambda_2}+e^{-L_2/\lambda_2}}\right). \tag{6.20}$$

While non-obvious, this function seems to be continuous when $\lambda \approx \lambda_h$. The behaviour of $J_s(z_{\mathrm{IP}})$ on changing L_2, λ_2 and λ_h is shown in Figure 6.7. The figure shows that having spacers much smaller than the spin diffusion length ($L_2 << \lambda_2$) prevents a spin spin current from being formed, as happened before introducing hot electron decay[8]. Due to hot electrons decaying, having spacer thickness larger than the hot electron decay length ($\lambda_h << L_2$) will now also prevent a net spin current from taking shape. Given some material parameters λ_2 and λ_h there now is some spacer thickness that maximises the total spin current into the IP layer.

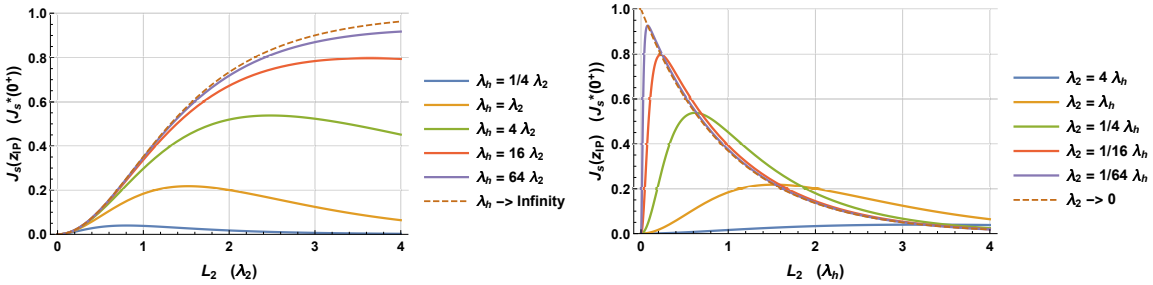

(a) $J_s(z_{\mathrm{IP}})$ depending on L_2 and λ_h, both in units of λ_2. Including the limiting case $\lambda_h \to \infty$ as described by the left of Equation (6.18). The spin diffusion length λ_2 is a length scale related to the increase of $J_s(z_{\mathrm{IP}})$ with spacer thickness L_2.

(b) $J_s(z_{\mathrm{IP}})$ depending on L_2 and λ_2, both in units of λ_h. Including the limiting case $\lambda_2 \to 0$, where $\lim_{\lambda_2\to 0} J_s(z_{\mathrm{IP}}) = J_s^*(z_{\mathrm{IP}})$. The hot electron decay length scale λ_h is related to a decrease of $J_s(z_{\mathrm{IP}})$ with spacer thickness L_2.

Figure 6.7: The behaviour of spin current flowing into the IP magnetised layer as given by Equation (6.20), depending on L_2, λ_2 and λ_h. On the vertical axes $J_s(z_{\mathrm{IP}})$ in units of $J_s^*(0^+)$. On the horizontal axis the spacer thickness L_2. Note that the non-limiting solutions (solid curves) are the same in both figures ($\lambda_h = a\,\lambda_2$ corresponds to $\lambda_2 = 1/a\,\lambda_h$), but the curves appear different because the horizontal axis has different units.

Besides the limits of $\lambda_h \to 0$ ($\lambda_h << L_2$) and $\lambda_2 \to \infty$ ($L_2 << \lambda_2$) causing no spin to flow into the IP layer, the solution has two more interesting limiting cases. The limit $\lambda_h \to \infty$ implies no hot electron decay. As we also imposed no spin flips in the OOP layer this limit reproduces the left of Equation (6.18). The last limit we can take is $\lambda_2 \to 0$, corresponding to the spacer layer being an ideal spin sink. This prevents any diffusive spin currents to contribute to $J_s(z_{\mathrm{IP}})$, leaving only the screened hot electron current contribution; $\lim_{\lambda_2\to 0} J_s(z_{\mathrm{IP}}) = J_s^*(z_{\mathrm{IP}})$. Even when not in this limit, the decay of spin transfer with increasing spacer thickness closely resembles the decay of hot electrons in this case.

[8] More specifically, in the case without hot electron decay and no spin flips in the spacer; the limit $\gamma \to \infty$.

No spin flips in spacer layer

If no spin is able to flip in the spacer layer, continuity requires the nett spin current to be constant over the spacer layer. Hot electron decay will still inject spin into the spacer layer, which must diffuse to either the OOP or IP magnetised layer to be dissipated. This gives a fairly interesting situation. The derivation related to this case is given in Appendix C.3, with the solution for the spin current into the IP layer being

$$J_s(z_{\mathrm{IP}}) = J_s^*(0^+)\frac{\lambda_h\left(1-e^{-L_2/\lambda_h}\right)}{\gamma + L_2}, \qquad \gamma = \sigma_{\mathrm{diff},2}\,/\,\tilde{r}. \tag{6.21}$$

Now, $J_s(z_{\mathrm{IP}})$ depends on L_2, γ and λ_h. Its behaviour is plotted in Figure 6.8. Again, γ is related to a spin-flip process, so gives a length-scale at which $J_s(z_{\mathrm{IP}})$ increases with spacer thickness L_s. In the case $L_2 << \gamma$ this prevents a spin current from reaching the IP magnetised layer. The hot electron decay length λ_h again acts as a length-scale related to the decrease of spin transfer with increasing spacer thickness, so $\lambda_h << L_2$ causes $J_s(z_{\mathrm{IP}}) = 0$. Because of these effects, again there is a specific spacer thickness that maximises $J_s(z_{\mathrm{IP}})$ given material properties γ and λ_h.

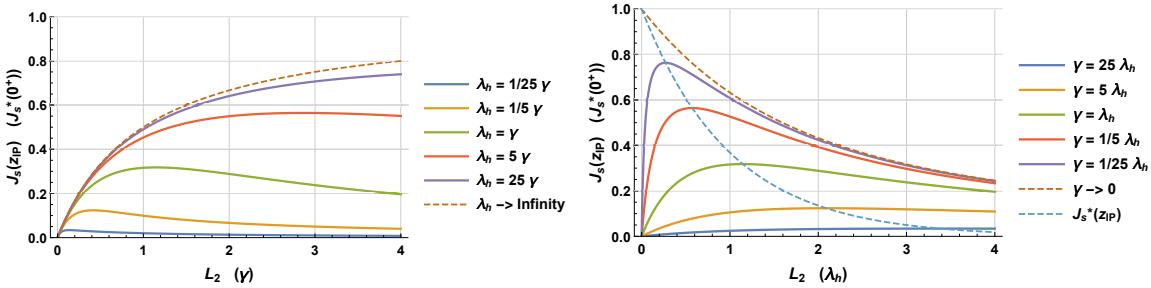

(a) $J_s(z_{\mathrm{IP}})$ depending on L_2 and λ_h, both in units of γ. Including the limiting case $\lambda_h \to \infty$ as described by the right of Equation (6.18). γ is a length scale related to the increase of $J_s(z_{\mathrm{IP}})$ with the spacer thickness L_2.

(b) $J_s(z_{\mathrm{IP}})$ depending on L_2 and γ, both in units of λ_h. Including the limiting case $\gamma \to 0$ as described by the Equation (6.22), and the screened hot electron current into the IP magnetised layer, $J_s^*(z_{\mathrm{IP}})$. The hot electron decay length scale λ_h is related to a decrease of $J_s(z_{\mathrm{IP}})$ with spacer thickness L_2.

Figure 6.8: The behaviour of spin current flowing into the IP magnetised layer as given by Equation (6.21), depending on L_2, γ and λ_h. On the vertical axes $J_s(z_{\mathrm{IP}})$ in units of $J_s^*(0^+)$. On the horizontal axis the spacer thickness L_2. Note that the non-limiting solutions (solid curves) are the same in both figures ($\lambda_h = a\,\gamma$ corresponds to $\gamma = 1/a\,\lambda_h$), but the curves appear different because the horizontal axis has different units.

Note that the decrease in spin transfer with increasing spacer thickness is substantially slower than the hot electron decay, as can be seen in Figure 6.8b. The difference stems from hot electron decay in the spacer layer, which will contribute to the spin accumulation in the spacer layer. Part of this will diffuse to the IP layer. Especially as we are considering a case where spin flips in the spacer layer are not modelled, so any spin deposited by hot electrons will have to diffuse to either the OOP or IP magnetised magnetic layer.

Of the two other limiting cases, the limit $\lambda_h \to \infty$ removes hot electron decay, reproducing the right of Equation (6.18). The remaining limit of $\gamma \to 0$ is an interesting one. It is related to $\tilde{r} \to \infty$,

such that the OOP magnetised layer becomes an ideal spin sink. It results in the spin current into the IP layer following

$$\lim_{\gamma \to 0} J_s(z_{\mathrm{IP}}) = J_s^*(0^+) \frac{\lambda_h}{L_2} \left(1 - e^{-L_2/\lambda_h}\right). \tag{6.22}$$

This limit is shown in Subfigure 6.8b. Like the solutions with finite γ, this solution has a quite different behaviour than the screened hot spin current into the IP magnetised layer, $J_s^*(z_{\mathrm{IP}})$.

6.3.3 Relation to experimental observations

Like we did for spin currents driven by the *s-d* process, we will compare the behaviour of $J_s(z_{\mathrm{IP}})$ changing with the spacer thickness L_2 to the behaviour observed in [11], as was shown in Figure 6.5. We are looking for a good fit of the models with realistic values of the spacer spin diffusion length λ_2, the hot electron decay length λ_h, and the length-scale comparing diffusion through the spacer to spin flips in the OOP layer, γ.

The spacer used in the experiments is a copper layer, such that the spin diffusion length is of order $\lambda_2 = 400\,\mathrm{nm}$ [16]. This is much larger than the thickness of the studied spacers, which range from 2 to 11 nm. This should make spin flips in the spacer layer a small contribution, so we will approximate the problem has having no spin flips in the spacer layer and use the result derived in Section 6.3.2. The dependence of $J_s(z_{IP})$ on the spacer thickness L_2 is given by Equation (6.21), which depends only on λ_h and γ. We will fit this relation to the experimental measurements, including a free vertical scaling[9]. It turns out that a good fit is achieved for a substantial range of values of γ, so two extremes of this range are explored. These fits are shown in Figure 6.9.

As was discussed before, γ is related to how quickly $J_s(z_{\mathrm{IP}})$ increases with spacer thickness, while λ_h relates to the rate of decay. The measurements showing no indication of an increase of spin transfer with increasing spacer thickness makes the fit is fairly insensitive to the value of γ. The only constraint is γ being small enough to provide a sufficiently strong dissipation of spin. This spin dissipation must be strong enough for the corresponding increase of spin transfer with layer thickness to be finished before $L_2 = 2\,\mathrm{nm}$, the smallest measured spacer thickness. While we can not give accurate estimates of γ based on the material properties and other experiments, it seems that $\gamma < 0.7\,\mathrm{nm}$ is an order of magnitude too small to be realistic. It seems more sensible for γ to be on the order of 20 nm, which would cause the spin transfer to substantially increase when increasing spacer thicknesses in the studied range.

In infinitesimal OOP layers, γ is the sole parameter determining the rate of spin decay. γ would then have to be small for the related spin decay to dissipate the spin depletion caused by hot electron excitation. However in finite OOP layers, the spin depletion caused by hot electron excitation and transport could take shape further away from the spacer layer. This would reduce the spin diffusion current out of the OOP layer and increase the rate of spin-flips. Also, the samples have a platinum layer adjacent to the OOP magnetised layer, which would further aid the rate of spin-flips. This enhances the spin decay, potentially allowing the true value of γ to be substantially larger than the values suggested by the fit of infinitesimal OOP layer models, explaining the discrepancy between its fit value and realistic values of it.

In contrast to the wide range of γ that fit to the measurements, the hot electron decay length is fit to a relatively tight range of $3.6\,\mathrm{nm} < \lambda_h < 5.4\,\mathrm{nm}$, as it must fit the gradual decrease of

[9]The vertical scaling is required because the presented hot electron model provides the amplitude of excited precessions, while the measurement data show an efficiency spin transfer in relation to a demagnetisation that this model does not provide.

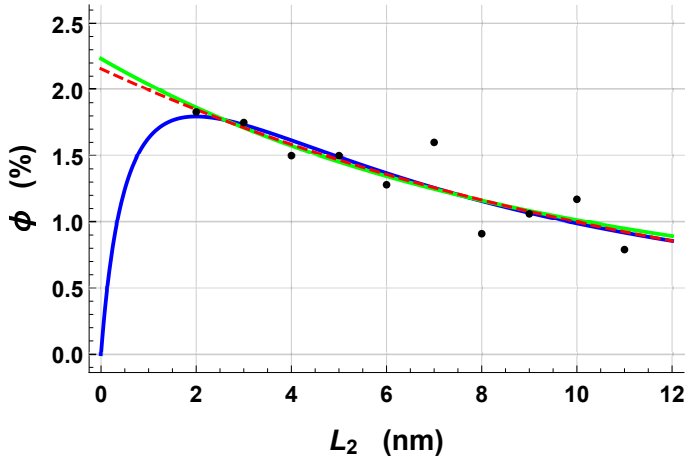

Figure 6.9: For various spacer thicknesses the efficiency of spin transfer, i.e. the spin absorbed by the in-plane magnetised layer relative to the demagnetisation of the out-of-plane magnetised layer. In black the measurement data from [11]. The red, dashed curve is the exponential fit as used in the original paper, with a length-scale of 13 nm. The green and blue curves both are fits of Equation (6.22) with a fitted vertical scaling. The green fit has $\gamma = 0$ imposed, giving a fit value of $\lambda_h = 5.4\,\text{nm}$. The Blue curve has $\gamma = 0.7\,\text{nm}$, giving a fit value of $\lambda_h = 3.6\,\text{nm}$.

$J_s(z_{\text{IP}})$ with increasing spacer thickness L_2 seen in the measurements. This range of hot electron decay lengths is considerably shorter than the 13 nm length-scale of the exponential decay fit. This difference arises because the hot electrons decaying in the spacer may still diffuse to the IP layer, making the total spin current $J_s(z_{\text{IP}})$ behave quite different than its screened hot electron component $J_s^*(z_{\text{IP}})$. This discrepancy was also visible in Figure 6.8b, where it is clear that regardless of γ the screened hot electron current into the IP layer, $J_s^*(z_{\text{IP}})$, decreases with spacer thickness much more quickly than the total spin current $J_s(z_{\text{IP}})$ that we fit to the measurements.

These values of the hot electron decay length λ_h seem to conflict with other measurements on hot electron decay in copper. Other experiments show hot electrons in copper to have life times in the order of 40 fs [18]. As Fermi velocities typically are of order 1 nm/fs, the z component of velocity of hot electrons would be some 0.5 nm/fs. This would suggest hot electron decay lengths in the order of 20 nm, a factor four larger than proposed hot electron model applied to the studied measurements would suggest. This discrepancy is a major problem when interpreting the measurements in terms of hot electrons.

The choice of the screened hot electron current J_s^* following an exponential decay was introduced fairly ad-hoc, without substantial basis in models of hot electron dynamics. Certainly the superdiffusive model of hot electrons, including multiple generations of hot electrons and a spin-dependent decay length, would behave substantially different from a simple exponential decay. This difference might be the cause of the discrepancy between the fit value of λ_h and its interpretation in terms of hot electron decay lengths. However, it still seems implausible that modelling multiple generations of hot electrons would lead to an effective decay length as short as the fit value of λ_h.

In this chapter we studied spin transfer in models of experiments. Both for spin currents driven by the *s*-*d* effect and hot electrons, we derived closed form expressions for spin transfer as a function of the spacer layer thickness and relevant material properties. These results were compared to measurements of spin transfer depending on spacer thickness, checking if the studied models are able to reproduce the behaviour observed in experiments. Both models could give a good fit to the data, but also in both cases the fitting variables seemed somewhat too unrealistic to trust these fits as being physical. In the case of the *s*-*d* model a possible explanation for the discrepancy was proposed. The model based on hot electron currents was plagued by hot electrons having to decay after unrealistically short lengths to be able to reproduce the measured behaviour. This seems to be an insurmountable problem for using hot electrons to describe the studied spin transfer process, making spin diffusion caused by an *s*-*d* source a more plausible explanation for the observed spin transfer.

Chapter 7

Conclusion and discussion

The goal of this thesis was to study ultrafast spin currents caused by optical excitation of thin-film magnetic layer. In particular to provide a model of ultrafast spin currents. This model was constructed as a generalisation of the Valet-Fert model to include time-dependence, hot electrons, and external spin sources. Including both hot electron transport and external spin sources would make this model useful for comparing these two possible causes of spin currents on an equal footing. Specifically, the relative contribution of these effects to experiments measuring spin currents through the excitation of a magnetic precession.

In the first chapter of this thesis, the proposed model was set up. Later chapters would modify the model to simplify its use in the context of the studied experiments. The strong screening approximation was able to remove charge dynamics from the model, simplifying understanding of the various effects that might occur and make subsequent calculations easier. Furthermore this step would improve stability and ease of implementation of numerical implementations of the model.

The observation that the ultrafast spin current pulses have a much shorter duration than the magnetic precession they induce in studied experiments inspired the zero-phase approximation. Only the total amount of spin injected into the absorbing magnetic layer would be of relevance to the measured signal. Linear-time-invariance of the spin dynamics model allowed the calculation of the total spin transfer to be simplified tremendously. While this approach is limited to the specific experiments of our interest, it made it feasible for the experimentally observed behaviour to be studied in an analytical manner. Also, the simplified equations following from it would immediately give further insight into behaviour of experimental signals allowed by the model.

With the model simplified and adapted to the experiments under investigation, the model was applied to these experiments. The measurements of spin transfer depending on spacer thickness were the main focus of the study. These experiments show interesting behaviour by the efficiency of spin transfer decreasing quite quickly with increasing spacer thickness, more quickly than one might expect. Also, as only the spacer thickness is varied between measurements, the data points can be compared in a relatively fair way. Spin currents driven by *s-d* induced spin accumulations where studied separately from spin currents caused by hot electron excitation and motion.

s-d induced spin currents were able to give a potential explanation for the quick decrease in efficiency with increasing spacer thickness. This model applied to study the modelled experiment suggests that most of the spin flips that decrease the spin transfer occur in the out-of-plane magnetised layer. In comparison, the amount of spin flips in the spacer layer would be negligible. The

spin flips in the out-of-plane magnetised layer could plausibly be the effect that makes spin transfer decrease with spacer thickness as quickly as is observed, though it is hard to check if the fit values of the model correspond to realistic material properties. The low spin transfer efficiency measured in experiments was not reproduced by the model driven by the *s*-*d* effect. The lack of modeling a platinum layer present in the experimental samples might be the reason for this discrepancy between model and measurements. The used model not including finite interfacial conductivities between the spacer layer and magnetised layers might also substantially affect the efficiency of spin transfer and its relation to spacer thickness. Including the platinum layer and finite interfacial conductivities to the model would therefore be an interesting next step.

Regarding spin transfer caused by hot electrons, the model showed the importance of having an efficient spin sink channel for the spin depletion associated with the excitation of spin polarised hot electrons. In fact, to reproduce the measurements, this spin sink channel would need to be so efficient that it seems not to be realistic. Also, the model shows that spacer layers being much thinner than their spin diffusion length would cause the spin deposited by decaying hot electrons to diffuse out of the spacer layer. This effect would enable hot electron currents to cause spin currents through substantially larger spacers than the hot electron decay length. Together with the spin transfer quickly decreasing with spacer thickness, this requires the hot electrons to decay on length scales much shorter than other experiments indicate. This makes it seem unrealistic for the measured spin transfer to stem from hot electrons as they are modeled in this thesis.

Appendix A

Hot electron model

This appendix will give a model of hot electrons, which complements the model of thermal electrons given in Section 2.1 to make a complete model for ultrafast spin dynamics. Like the superdiffusive model for hot electrons, this model treats hot electrons as moving on ballistic trajectories. However, unlike the superdiffusive model, the model presented here does not include electron-electron scattering, allowing hot electrons to excite other electrons to a hot state.

All electron excitation is optical, effectively only describing first generation hot electrons as modelled in the superdiffusive model[9]. The rate of electrons with spin $\pm$ moving from thermal to the hot system, $R_\pm$, is composed of a rate of excitation $R_{ex,\pm}$ and rate of decay $R_{dc,\pm}$

$$R_\pm = R_{ex,\pm} - R_{dc,\pm}. \tag{A.1}$$

When a laser excites the multilayer, it provides energy according to the distribution $p(z,t)$. We model this energy to be absorbed by electrons, exciting them to hot states. Any excitation takes up the photon energy E_p, such that the excitation rate is $R_{ex} = p/E_p$. We introduce the parameters $E_\pm$ to specify the fraction that is excited to spin + or spin −. With this, the spin specific excitation rate is

$$R_{ex,\pm} = \frac{p}{E_p}\frac{E_\pm}{E_{tot}}, \quad E_{tot} = E_+ + E_-. \tag{A.2}$$

On excitation, new hot electrons are assigned a random 3-d velocity of which is uniformly distributed over the sphere with the Fermi velocity v_f as radius. We model the hot electrons as ballistic, such that they maintain their velocity during their lifetime. However, they will experience specular reflection on metal-air interfaces. Hot electrons have a chance of decaying to the thermal system that depends on the spin and material, which will be encoded in the hot electron life-time $\tau_\pm(z)$. The hot electron state is a distribution in the $z, v, \pm$ space. At time t, the density of hot electrons at position z with velocity v and spin $\pm$ is $n_\pm(z,v,t)$. This is related to the density of hot electrons $N^h_\pm$ through

$$N^h_\pm(z,t) = \int_{-\infty}^{+\infty} \mathrm{d}v\, n_\pm(z,v,t). \tag{A.3}$$

The hot electron system evolution is described by the Boltzmann equation

$$n_{\pm}(z+v\Delta t, v, t+\Delta t) = n_{\pm}(z,v,t)\, e^{-\Delta t/\tau_{\pm}(z)} + \int_t^{t+\Delta t} \mathrm{d}\tilde{t}\, \frac{\Theta(v_f+v)\Theta(v_f-v)}{2\, v_f} R_{ex,\pm}\left(z+v\left(\tilde{t}-t\right),\tilde{t}\right) e^{-\left(t+\Delta t-\tilde{t}\right)/\tau_{\pm}(z)}, \tag{A.4}$$

where Θ is the Heaviside theta function. Hot electrons in the state $n_{\pm}(z,v,t)$ will after time Δt either decay or with probability $e^{-\Delta t/\tau_\sigma}$ move to $n_\sigma(z+v\Delta t, v, t+\Delta t)$, explaining the first term. To derive the contribution of excitation, realize that for a hot electron to reach $z+v\Delta t, v, t+\Delta t$ it must be excited to velocity v, so the time and position of excitation $\tilde{z}, \tilde{t}$ are linked via $\tilde{z} = z + v(\tilde{t}-t)$, with $\tilde{t} \in [t, t+\Delta t]$. To add all contributing excitation events, we integrate over $\tilde{t}$, taking into account the excitation rate at $\tilde{z}, \tilde{t}$, the probability density for an excited electron to get a velocity v (being uniformly distributed on a sphere gives $\Theta(v_f+v)\Theta(v_f-v)/2v_f$), and the probability for the electron to decay before reaching $z+v\Delta t, v, t+\Delta t$. This gives the right term. Observing that velocities do not change and hot electrons can only be excited to velocities $|v| < v_f$, it follows immediately that $|v| > v_f$ implies $n_\sigma(z,v,t) = 0$. Taking the derivative with respect to Δt and evaluating at $\Delta t = 0$ gives

$$\frac{\partial}{\partial t} n_{\pm}(z,v,t) = -\frac{n_\sigma(z,v,t)}{\tau_{\pm}(z)} - v\frac{\partial}{\partial z} n_{\pm}(z,v,t) + \frac{R_{ex,\pm}(z,t)}{2v_f}\Theta(v_f+v)\Theta(v_f-v). \tag{A.5}$$

The left side of the equation is the time evolution. The first term on the right side represents the hot electron decay contribution, the second therm the transport contribution and the third term electron excitation. To find the local decay rate, we just need to integrate the decay term from the previous equation over all velocities, giving

$$R_{dc,\pm}(z,t) = \int_{-v_f}^{v_f} \mathrm{d}v\, \frac{n_{\pm}(z,v,t)}{\tau_{\pm}(z)} = \frac{N^h_{\pm}(z,t)}{\tau_{\pm}(z)}. \tag{A.6}$$

This model of hot electrons provides two ways in which the hot electron current can be spin-polarized, which makes them contribute to the spin current we are ultimately interested in. On excitation, $E_+ \neq E_-$ will cause a different number of spin up electrons than spin down electrons to be excited. Transport is independent of spin, but the decay rate depends on spin through $\tau_\pm$. In the paper on superdiffusive demagnetisation this difference is the main cause of the hot electrons being spin polarized [9].

Appendix B

Derivation generalized change to steady state perspective

In Section 4.2 we showed a derivation concluding with Equation (4.7). This derivation concerned a system S which transformed time-dependent real valued signals to other such signals, in a manner that is linear-time-invariant. It was claimed that the result in the form

$$\int_{-\infty}^{\infty} \mathrm{d}t\, S\left[f\right](t) = S\left[C_{\int_{-\infty}^{\infty} \mathrm{d}t\, f(t)}\right](0) \tag{B.1}$$

would also apply in a much more general case, where the input and output signals of S are vector-valued functions. Here we show the derivation of this result.

We have the two vector spaces V and W over $\mathbb{R}$ (finite-dimensionality of the vector spaces is not required, so these vector spaces may contain function spaces). The domain of system S is the function space $\mathbb{R} \to V$, while the codomain is the function space $\mathbb{R} \to W$. Alternatively; $S : (\mathbb{R} \to V) \to (\mathbb{R} \to W)$. The function spaces $\mathbb{R} \to V$, $\mathbb{R} \to W$ are themselves vector spaces by pointwise addition and multiplication: $(f+g)(x) = f(x) + g(x)$, $(a\, f)(x) = a\, f(x)$.

S is linear time invariant. Linearity gives that for all $f, g \in \mathbb{R} \to V$ and all $\alpha \in \mathbb{R}$

$$S[f+g] = S[f] + f[g], \qquad S[\alpha\, f] = \alpha\, S[f]. \tag{B.2}$$

Introducing the time shift operator T_τ, defined as $(T_\tau(f))(t) = f(t-\tau)$. In therms of this, the time invariance of S implies

$$T_\tau(S[f]) = S\left[T_\tau(f)\right]. \tag{B.3}$$

Having set up this context we can start with the derivation. Given an input $f \in \mathbb{R} \to V$, we are interested in the system output $S[f]$ integrated over all time. First we use linearity and time

invariance properties of S to change the integral over the output to an integral over the input

$$\begin{aligned}
\int_{-\infty}^{\infty} \mathrm{d}t\, S\left[f\right](t) &= \int_{-\infty}^{\infty} \mathrm{d}t\, \left(T_{-t}\left(S\left[f\right]\right)\right)(0) && \text{Definition of time shift operator} \\
&= \int_{-\infty}^{\infty} \mathrm{d}t\, \left(S\left[T_{-t}(f)\right]\right)(0) && \text{Time invariance of } S \\
&= \left(\int_{-\infty}^{\infty} \mathrm{d}t\, \left(S\left[T_{-t}(f)\right]\right)\right)(0) && \text{Pointwise adition of functions} \\
&= \left(S\left[\int_{-\infty}^{\infty} \mathrm{d}t\, T_{-t}(f)\right]\right)(0) && \text{Linearity of } S \\
&= S\left[\int_{-\infty}^{\infty} \mathrm{d}t\, T_{-t}(f)\right](0). && \text{Brackets can be dropped}
\end{aligned}$$

At this point, just looking at the input function to S

$$\begin{aligned}
\int_{-\infty}^{\infty} \mathrm{d}t\, T_{-t}(f) &= \tilde{t} \mapsto \int_{-\infty}^{\infty} \mathrm{d}t\, \left(T_{-t}(f)\right)(\tilde{t}) && \text{Introducing arrow notation; } f = x \mapsto f(x) \\
&= \tilde{t} \mapsto \int_{-\infty}^{\infty} \mathrm{d}t\, f(t+\tilde{t}) && \text{Definition of time shift operator} \\
&= \tilde{t} \mapsto \int_{-\infty}^{\infty} \mathrm{d}t\, f(t) && \text{Change of integration variable} \\
&= C_{\int_{-\infty}^{\infty} \mathrm{d}t\, f(t)}. && \text{Introduction of the constant function}
\end{aligned}$$

The constant function C_a was introduced in the last line. It is defined by $C_a(x) = a$. Combining this with the previous result gives in conclusion

$$\int_{-\infty}^{\infty} \mathrm{d}t\, S\left[f\right](t) = S\left[C_{\int_{-\infty}^{\infty} \mathrm{d}t\, f(t)}\right](0). \tag{B.4}$$

The one step of this derivation that was not formal was the use of linearity of S to justify moving the integral from the output of S to the input of S. More abstractly this step can be written as

$$\int_{-\infty}^{+\infty} \mathrm{d}x\, S[f_x] = S\left[\int_{-\infty}^{+\infty} \mathrm{d}x\, f_x\right]. \tag{B.5}$$

This is a known result in the field of vector measures[19][page 123], as long as a sufficient level of continuity is met. Intuitively this step can be made plausible by defining the integral as a Riemann sum for some sufficiently small step size h. In this case the linearity of S is sufficient to rewrite

$$\int_{-\infty}^{+\infty} \mathrm{d}x\, S[f_x] = \sum_{n=-\infty}^{+\infty} h\, S[f_{hn}] = S\left[\sum_{n=-\infty}^{+\infty} h\, f_{hn}\right] = S\left[\int_{-\infty}^{+\infty} \mathrm{d}x\, f_x\right]. \tag{B.6}$$

Unfortunately we can not do this in the limit $\lim_{h\to 0}$, as we would need some appropriate continuity to move this limit through S.

Appendix C

Derivations model applied to experiments

This appendix contains the derivations from Chapter 6 that were too large to show in the main text. The set up of these derivations will only succinctly be recited here, and the results derived here are discussed in the main text.

C.1 Derivation diffusion model of multilayer

Here we show the derivation relevant to Section 6.2.2, of which the main text used the result in Equation (6.10). To simplify the derivation we use a slightly different convention for the position of the layers than is used in the main text. Here the finite OOP magnetic layer spans $-L_1 < z < 0$, while the spacer spans $0 < z < L_2$.

On $z = -L_1$ we have an insulator, so $J_s(-L_1) = 0$ as boundary condition, while at $z = L_2$ an ideal spin sink imposes $\mu_s(L_2) = 0$. On the interface between the FM layer and the spacer layer, at $z = 0$, the boundary conditions are continuity of μ_s and J_s. The differential equations within both layers are based on Equation (5.2), but simplified by being in the absence of hot electrons ($J_s^* = 0$) and the material being uniform within the layer

$$r\,\mu_s - \sigma_{diff}\,\mu_s'' = S, \qquad J_s = -2\,\sigma_{diff}\,\mu_s'. \tag{C.1}$$

In the FM layer, S is constant while it is zero in the spacer layer, so as abuse of notation we will use S both as the label for the spin source function and the scalar that represents the function's magnitude in the FM layer. Also, because this derivation only uses diffusive conductivities we will write $\sigma_{diff,1} = \sigma_1$ and $\sigma_{diff,2} = \sigma_2$ in this section. The homogeneous solution to above differential equation in a homogeneous layer would be

$$\mu_s(z) = \mu^+ e^{+z/\lambda} + \mu^- e^{-z/\lambda} + S/r, \tag{C.2}$$

with as usual $\lambda = \sqrt{\sigma_{diff}/r}$. We use this to write the solution of the spin accumulation in the OOP layer as

$$\mu_s(-L_1 < z < 0) = \mu_1^+ e^{+z/\lambda_1} + \mu_1^- e^{-z/\lambda_1} + S/r_1, \tag{C.3}$$

while the spin accumulation in the spacer layer is

$$\mu_s(0 < z < L_2) = \mu_2^+ e^{+z/\lambda_2} + \mu_2^- e^{-z/\lambda_2}. \tag{C.4}$$

Here we paramaterised the solution by the four real numbers $\mu_1^\pm$, $\mu_2^\pm$. We will now fix these.

The relevant boundary conditions are no spin current at $z = -L_1$, giving $J_s(-L_1) = 0$. At $z = L_2$ we have zero spin accumulation, $\mu_s(L_2) = 0$. On the interface between the OOP layer and spacer layer we have continuity of spin accumulation and spin current, giving $\mu_s(0^-) = \mu_s(0^+)$ and $J_s(0^-) = J_s(0^+)$. In terms of $\mu_1^\pm$ and $\mu_2^\pm$, these boundary conditions impose the following constraints; $J_s(-L_1) = 0$ gives

$$\mu_1^+ e^{-L_1/\lambda_1} = \mu_1^- e^{+L_1/\lambda_1}, \tag{C.5}$$

$\mu_s(L_2) = 0$ gives

$$\mu_2^+ e^{+L_2/\lambda_2} + \mu_2^- e^{-L_2/\lambda_2} = 0, \tag{C.6}$$

$\mu_s(0^-) = \mu_s(0^+)$ gives

$$\mu_1^+ + \mu_1^- + S/r_1 = \mu_2^+ + \mu_2^-, \tag{C.7}$$

and $J_s(0^-) = J_s(0^+)$ gives

$$\frac{\sigma_1}{\lambda_1}(\mu_1^+ - \mu_1^-) = \frac{\sigma_2}{\lambda_2}(\mu_2^+ - \mu_2^-). \tag{C.8}$$

Equation (C.5) can be used to eliminate μ_1^+ through $\mu_1^+ = \mu_1^- e^{2L_1/\lambda_1}$. Equation (C.6) is used to eliminate μ_2^- using $\mu_2^- = -\mu_2^+ e^{2L_2/\lambda_2}$. The remaining system of equations is

$$\begin{cases} \mu_1^-(1 + e^{2L_1/\lambda_1}) + S/r_1 & = \mu_2^+(1 - e^{2L_2/\lambda_2}) \\ \frac{\sigma_1}{\lambda_1}\mu_1^-(-1 + e^{2L_1/\lambda_1}) & = \frac{\sigma_2}{\lambda_2}\mu_2^+(1 + e^{2L_2/\lambda_2}) \end{cases} \tag{C.9}$$

We eliminate μ_1^- (as $\mu_2^\pm$ is more interesting if we want to know $J_s(L_2)$) using the second equation written as

$$\mu_1^- = \mu_2^+ \frac{\lambda_1}{\lambda_2}\frac{\sigma_2}{\sigma_1}\frac{e^{2L_2/\lambda_2} + 1}{e^{2L_1/\lambda_1} - 1}. \tag{C.10}$$

Plugging this into the first gives μ_2^+ as

$$\mu_2^+ = \frac{S/r_1}{(1 - e^{2L_2/\lambda_2}) - \frac{\lambda_1}{\lambda_2}\frac{\sigma_2}{\sigma_1}\frac{e^{+L_1/\lambda_1} + e^{-L_1/\lambda_1}}{e^{+L_1/\lambda_1} - e^{-L_1/\lambda_1}}(1 + e^{2L_2/\lambda_2})}. \tag{C.11}$$

Using the benefit of hindsight we can already introduce γ in this equation, rewriting it as

$$\mu_2^+ = \frac{S/r_1}{(1 - e^{2L_2/\lambda_2}) - \frac{\gamma}{\lambda_2}(1 + e^{2L_2/\lambda_2})}, \qquad \gamma = \lambda_1 \frac{\sigma_2}{\sigma_1} / \tanh(L_1/\lambda_1). \tag{C.12}$$

We can now calculate $J_s(L_2)$ using

$$J_s(L_2) = -2\sigma_2 \mu_s'(L_2) = -2\frac{\sigma_2}{\lambda_2}(\mu_2^+ e^{+L_2/\lambda_2} - \mu_2^- e^{-L_2/\lambda_2}) = -4\frac{\sigma_2}{\lambda_2}\mu_2^+ e^{+L_2/\lambda_2}. \tag{C.13}$$

This gives

$$J_s(L_2) = 4\frac{\sigma_2}{\lambda_2}\frac{S}{r_1}\frac{1}{e^{+L_2/\lambda_2} - e^{-L_2/\lambda_2} + \frac{\gamma}{\lambda_2}(e^{+L_2/\lambda_2} + e^{-L_2/\lambda_2})}. \tag{C.14}$$

We then Multiply the numerator and denominator by λ_2/γ

$$J_s(L_2) = 4\,\sigma_2 \frac{S}{r_1}\frac{1}{\gamma}\frac{1}{e^{+L_2/\lambda_2} + e^{-L_2/\lambda_2} + \frac{\lambda_2}{\gamma}(e^{+L_2/\lambda_2} - e^{-L_2/\lambda_2})}, \tag{C.15}$$

and write out $1/\gamma$ using $\sigma_1/r_1 = \lambda_1^2$

$$J_s(L_2) = \frac{4\,S\,\lambda_1\,\tanh(L_1/\lambda_1)}{e^{+L_2/\lambda_2} + e^{-L_2/\lambda_2} + \frac{\lambda_2}{\gamma}(e^{+L_2/\lambda_2} - e^{-L_2/\lambda_2})}. \tag{C.16}$$

Taking the limit of $\lambda_2 \to +\infty$ (with σ_2 fixed) shows that the value of γ we had anticipated is correct.

To write this in the form used in the main text, Equation (6.10), we introduce T as

$$T = \lambda_1 \tanh(L_1/\lambda_1), \tag{C.17}$$

which allows us to write $J_s(L_2)$ and γ as

$$J_s(L_2) = \frac{4\,S\,T}{e^{+L_2/\lambda_2} + e^{-L_2/\lambda_2} + \frac{\lambda_2}{\gamma}(e^{+L_2/\lambda_2} - e^{-L_2/\lambda_2})}, \qquad \gamma = \frac{\sigma_2}{r_1 T}. \tag{C.18}$$

C.2 Hot electrons, no spin flips in OOP layer

This section will show the derivation relevant to Section 6.3.2, the result was used in Equation (6.20). We use the differential equation as presented in Equation (5.3). As we have $S = 0$ and no differences in material properties in the region we are interested in, this reduces to

$$\lambda_2^2\, J_s'' = J_s - J_s^*, \tag{C.19}$$

where λ_2 is the spin diffusion length of the spacer layer. The screened hot electron current J_s^* is imposed as

$$J_s^*(z) = J_s^*(0^+)e^{-z/\lambda_h}. \tag{C.20}$$

The solution of the total spin current in the spacer layer can then be written in the functional form

$$J_s(0^+ < z < L_2) = j^+ e^{+z/\lambda_2} + j^- e^{-z/\lambda_2} + c\, e^{-z/\lambda_h}, \tag{C.21}$$

where $j^\pm$ and c are real numbers parameterising the solution. Inserting this into Equation (C.19) gives c as

$$c = J_s^*(0^+)\frac{\lambda_h^2}{\lambda_h^2 - \lambda_2^2}. \tag{C.22}$$

The two other parameters $j^\pm$ are fixed by the boundary conditions. The first of these is a zero spin current boundary condition into the OOP layer, giving $J_s(0^+) = 0$. Using this with Equation (C.21) gives

$$j^+ + j^- + c = 0. \tag{C.23}$$

The second boundary condition is zero spin accumulation at the interface with the IP magnetised layer, $\mu_s(L_2) = 0$. Using the left side of Equation (5.1) this can alternatively be written as $J_s'(L_2) = 0$. With Equation (C.21) this gives

$$\frac{1}{\lambda_2}\left(j^+ e^{+L_2/\lambda_2} - j^- e^{-L_2/\lambda_2}\right) - \frac{c}{\lambda_h} e^{-L_2/\lambda_h} = 0. \tag{C.24}$$

These two equations can be used to solve for $j^\pm$. We use the first to write $-j^- = j^+ + c$. Using this to eliminate j^- gives j^+ as

$$j^+ = c\frac{\frac{\lambda_2}{\lambda_h} e^{-L_2/\lambda_h} - e^{-L_2/\lambda_2}}{e^{+L_2/\lambda_2} + e^{-L_2/\lambda_2}}. \tag{C.25}$$

Now we will can use the found substitutions to calculate $J_s(L_2)$, as

$$\begin{aligned}
J_s(L_2) &= j^+ e^{+L_2/\lambda_2} + j^- e^{-L_2/\lambda_2} + c\, e^{-L_2/\lambda_h} \\
&= j^+ e^{+L_2/\lambda_2} - (j^+ + c)\, e^{-L_2/\lambda_2} + c\, e^{-L_2/\lambda_h} \\
&= j^+ \left(e^{+L_2/\lambda_2} - e^{-L_2/\lambda_2}\right) + c\, e^{-L_2/\lambda_h} - c\, e^{-L_2/\lambda_2} \\
&= c\left(\left(\frac{\lambda_2}{\lambda_h} e^{-L_2/\lambda_h} - e^{-L_2/\lambda_2}\right)\frac{e^{+L_2/\lambda_2} - e^{-L_2/\lambda_2}}{e^{+L_2/\lambda_2} + e^{-L_2/\lambda_2}} + e^{-L_2/\lambda_h} - e^{-L_2/\lambda_2}\right) \\
&= J_s^*(0^+)\frac{\lambda_h^2}{\lambda_h^2 - \lambda_2^2}\left(\left(\frac{\lambda_2}{\lambda_h} e^{-L_2/\lambda_h} - e^{-L_2/\lambda_2}\right)\frac{e^{+L_2/\lambda_2} - e^{-L_2/\lambda_2}}{e^{+L_2/\lambda_2} + e^{-L_2/\lambda_2}} + e^{-L_2/\lambda_h} - e^{-L_2/\lambda_2}\right).
\end{aligned} \tag{C.26}$$

With a bit of rewriting, this can be changed to

$$J_s(z_{IP}) = J_s^*(0^+)\frac{\lambda_h^2}{\lambda_h^2 - \lambda_2^2}\left(e^{-L_2/\lambda_h}\left(1 + \frac{\lambda_2}{\lambda_h}\frac{e^{L_2/\lambda_2} - e^{-L_2/\lambda_2}}{e^{L_2/\lambda_2} + e^{-L_2/\lambda_2}}\right) - \frac{2}{e^{+L_2/\lambda_2} + e^{-L_2/\lambda_2}}\right), \tag{C.27}$$

which was used in the main text.

C.3 Hot electrons, no spin flips in spacer layer

Here we perform the derivation related to Section 6.3.2, in particular the derivation of Equation (6.21). Here there are no spin flips in the spacer layer. Continuity (left hand side of Equation (5.1)) then requires that the spin current is constant in the spacer layer. This makes the derivation in this section substantially different from those in the previous sections. We again impose zero spin accumulation at the interface with the IP layer; $\mu_s(L_2) = 0$. The boundary condition to the infinitesimal layer is $J_s(0^+) = -2\,\tilde{r}\,\mu_s(0^+)$, from a derivation similar to the one performed in Section 6.2.1.

We use the right hand side of Equation (5.1) adapted to this case,

$$J_s = -2\,\sigma_{diff,2}\,\mu_s'(z) + J_s^*(z). \tag{C.28}$$

This way of writing made it explicit that J_s and $\sigma_{diff,2}$ are real numbers, independent of z. Integrating this from $z = 0^+$ to $z = L_2$ gives

$$L_2\, J_s = -2\,\sigma_{diff,2}\left(\mu_s(L_2) - \mu_s(0^+)\right) + \int_{0^+}^{L_2} \mathrm{d}z\, J_s^*(z) \tag{C.29}$$

We have imposed the boundary conditions $\mu_s(L_2) = 0$ and $J_s = -2\,\tilde{r}\mu_s(0^+)$, so we can eliminate both times the spin accumulation is mentioned. Furthermore, we have set $J_s^*(z) = J_s^*(0^+)\,e^{-z/\lambda_h}$, so the integral related to it can be performed. This gives

$$L_2\,J_s = -\sigma_{diff,2}\,J_s\,/\,\tilde{r} - J_s^*(0^+)\,\lambda_h\,\left(e^{-L_2/\lambda_h} - 1\right). \tag{C.30}$$

Rearranging to solve for J_s and introducing γ gives the result

$$J_s = J_s^*(0^+)\,\lambda_h \frac{1 - e^{-L_2/\lambda_h}}{\gamma + L_2}, \qquad \gamma = \sigma_{diff,2}/\tilde{r}. \tag{C.31}$$

Appendix D

Estimate of gamma

In Section 6.2.2 we studied spin transfer in systems with finite OOP magnetised layer. An important variable of dimension length, γ, emerged. One of the equations for it is

$$\gamma = \lambda_1 \frac{\sigma_{diff,2}}{\sigma_{diff,1}} / \tanh(L_1/\lambda_1). \tag{D.1}$$

We would like to have an estimate to give a realistic order of magnitude that γ may have in the multilayers studied in experiments. We will make use of the material properties given in [16].

To use above equation for γ, we need the spin diffusion length of the OOP magnetised layer, and the diffusive conductivity of both the OOP layer and the spacer layer. The spin diffusion length of the listed materials is specified, but the spin diffusive conductivity σ_{diff} used in our treatment of spin diffusion is not. However, the total conductivity is given. We can write $\sigma_{\pm}$ in terms of the total conductivity σ_{tot} and a spin polarization q as

$$\sigma_+ = q\,\sigma_{tot}, \quad \sigma_- = (1-q)\,\sigma_{tot} \tag{D.2}$$

Using this to calculate σ_{diff} gives

$$\sigma_{diff} = \frac{\sigma_+\sigma_-}{\sigma_{tot}} = q\,(1-q)\,\sigma_{tot} \tag{D.3}$$

In the spacer we have symmetry so $q = 0.5$. The spin polarization in the out of plane magnetised layer is q_1. This gives γ as

$$\gamma = \frac{\lambda_1}{4\,q_1\,(1-q_1)} \frac{\sigma_{tot,2}}{\sigma_{tot,1}} / \tanh(L_1/\lambda_1). \tag{D.4}$$

Now that we have this adapted equation for γ, we can use this with the given material properties. Considering a Co/Pt magnetic multilayer and a Cu spacer, [16] gives the material properties $\lambda_1 = 1\,\text{nm}$, $\sigma_{tot,1} = 2.3 \cdot 10^6\,\Omega^{-1}\,\text{m}^{-1}$, $\sigma_{tot,2} = 39 \cdot 10^6\,\Omega^{-1}\,\text{m}^{-1}$. As we usually have $L_1 > 1\,\text{nm}$, we have approximately $\tanh(L_1/\lambda_1) \approx 1$. Plugging these in Equation (D.4) gives

$$\gamma = \frac{4.24\,\text{nm}}{q_1\,(1-q_1)}. \tag{D.5}$$

We have no way to estimate q_1 using this data, but as long as the current is not extremely spin polarized, the estimate of γ is fairly insensitive to it. The value of γ for various values of q_1 are listed in Table D.1.

q_1	γ
0.5	17 nm
0.6	18 nm
0.7	20 nm
0.8	27 nm
0.9	47 nm
0.95	89 nm
0.975	174 nm
0.99	428 nm

Table D.1: Estimates for γ, for various values of q_1.

With q_1 approaching 1 (or 0) γ diverges. For somewhat moderate spin polarizations having the value of γ being in the order of 15 to 80 nm would be expected. More importantly, we should compare γ to the spin diffusion length of copper. Provided as $\lambda_2 = 400$ nm this is probably substantially larger than γ. Comparing this relative difference with the behaviour of Equation (6.10), it seems that the mechanism related to γ would be dominant in such samples.

Bibliography

[1] Brajesh Kumar Kaushik et al. *Next Generation Spin Torque Memories*. Jan. 2017. ISBN: 978-981-10-2719-2. DOI: 10.1007/978-981-10-2720-8.

[2] Vinod Kumar Joshi. "Spintronics: A contemporary review of emerging electronics devices". In: *Engineering Science and Technology, an International Journal* 19.3 (2016), pp. 1503–1513. ISSN: 2215-0986. DOI: https://doi.org/10.1016/j.jestch.2016.05.002. URL: https://www.sciencedirect.com/science/article/pii/S2215098615300501.

[3] J. M. D. Coey. *Magnetism and Magnetic Materials*. Cambridge University Press, 2010. DOI: 10.1017/CBO9780511845000.

[4] M. N. Baibich et al. "Giant Magnetoresistance of (001)Fe/(001)Cr Magnetic Superlattices". In: *Phys. Rev. Lett.* 61 (21 Nov. 1988), pp. 2472–2475. DOI: 10.1103/PhysRevLett.61.2472. URL: https://link.aps.org/doi/10.1103/PhysRevLett.61.2472.

[5] G. Binasch et al. "Enhanced magnetoresistance in layered magnetic structures with antiferromagnetic interlayer exchange". In: *Phys. Rev. B* 39 (7 Mar. 1989), pp. 4828–4830. DOI: 10.1103/PhysRevB.39.4828. URL: https://link.aps.org/doi/10.1103/PhysRevB.39.4828.

[6] T. Valet and A. Fert. "Theory of the perpendicular magnetoresistance in magnetic multilayers". In: *Phys. Rev. B* 48 (10 Sept. 1993), pp. 7099–7113. DOI: 10.1103/PhysRevB.48.7099. URL: https://link.aps.org/doi/10.1103/PhysRevB.48.7099.

[7] E. Beaurepaire et al. "Ultrafast Spin Dynamics in Ferromagnetic Nickel". In: *Phys. Rev. Lett.* 76 (22 May 1996), pp. 4250–4253. DOI: 10.1103/PhysRevLett.76.4250. URL: https://link.aps.org/doi/10.1103/PhysRevLett.76.4250.

[8] Gregory Malinowski et al. "Control of speed and efficiency of ultrafast demagnetization by direct transfer of spin angular momentum". In: *Nature Physics* 4 (Sept. 2008), pp. 855–858. DOI: 10.1038/nphys1092.

[9] Marco Battiato, Karel Carva, and Peter Oppeneer. "Superdiffusive Spin Transport as a Mechanism of Ultrafast Demagnetization". In: *Physical review letters* 105 (July 2010), p. 027203. DOI: 10.1103/PhysRevLett.105.027203.

[10] Alexey Melnikov et al. "Ultrafast Transport of Laser-Excited Spin-Polarized Carriers in Au / Fe / MgO (001)". In: *Physical review letters* 107 (Aug. 2011), p. 076601. DOI: 10.1103/PhysRevLett.107.076601.

[11] Adrianus Schellekens et al. "Ultrafast spin-transfer torque driven by femtosecond pulsed-laser excitation". In: *Nature communications* 5 (July 2014), p. 4333. DOI: 10.1038/ncomms5333.

[12] Gyung-Min Choi et al. “Spin current generated by thermally driven ultrafast demagnetization”. In: *Nature communications* 5 (July 2014), p. 4334. DOI: 10.1038/ncomms5334.

[13] M. L. M. Lalieu, P. L. J. Helgers, and B. Koopmans. “Absorption and generation of femtosecond laser-pulse excited spin currents in noncollinear magnetic bilayers”. In: *Phys. Rev. B* 96 (1 July 2017), p. 014417. DOI: 10.1103/PhysRevB.96.014417. URL: https://link.aps.org/doi/10.1103/PhysRevB.96.014417.

[14] M. L. M. Lalieu et al. “Deterministic all-optical switching of synthetic ferrimagnets using single femtosecond laser pulses”. In: *Phys. Rev. B* 96 (22 Dec. 2017), p. 220411. DOI: 10.1103/PhysRevB.96.220411. URL: https://link.aps.org/doi/10.1103/PhysRevB.96.220411.

[15] Erlend G. Tveten, Arne Brataas, and Yaroslav Tserkovnyak. “Electron-magnon scattering in magnetic heterostructures far out of equilibrium”. In: *Phys. Rev. B* 92 (18 Nov. 2015), p. 180412. DOI: 10.1103/PhysRevB.92.180412. URL: https://link.aps.org/doi/10.1103/PhysRevB.92.180412.

[16] Im-Hyuk Shin et al. “Ultrafast spin current generated by electron–magnon scattering in bulk of ferromagnets”. In: *Japanese Journal of Applied Physics* 57.9 (Aug. 2018), p. 090307. DOI: 10.7567/jjap.57.090307. URL: https://doi.org/10.7567/jjap.57.090307.

[17] Johannes Kimling and David G. Cahill. “Spin diffusion induced by pulsed-laser heating and the role of spin heat accumulation”. In: *Phys. Rev. B* 95 (1 Jan. 2017), p. 014402. DOI: 10.1103/PhysRevB.95.014402. URL: https://link.aps.org/doi/10.1103/PhysRevB.95.014402.

[18] M. Bauer, Alexander Marienfeld, and Martin Aeschlimann. “Hot electron lifetimes in metals probed by time-resolved two-photon photoemission”. In: *Progress in Surface Science* 90 (Aug. 2015). DOI: 10.1016/j.progsurf.2015.05.001.

[19] N. DINCULEANU. “CHAPTER II - INTEGRATION”. In: *Vector Measures*. Ed. by N. DINCULEANU. Vol. 95. International Series of Monographs on Pure and Applied Mathematics. Pergamon, 1967, pp. 82–286. DOI: https://doi.org/10.1016/B978-1-4831-9762-3.50005-6. URL: https://www.sciencedirect.com/science/article/pii/B9781483197623500056.